Spin-Orbit Coupled Bose-Einstein Condensates:Ground States, Dynamics and Topological Defects

李, 犇

https://doi.org/10.15017/1500760

出版情報：九州大学, 2014, 博士（理学）, 課程博士
バージョン：

Spin-Orbit Coupled Bose-Einstein Condensates:

Ground States, Dynamics, and Topological Defects

九州大学
KYUSHU UNIVERSITY

Ben LI

Department of Applied Science for Electronics and Materials,
Interdisciplinary Graduate School of Engineering Sciences,
Kyushu University

Thesis submitted for the degree of

Doctor of Philosophy

February 2015

I would like to dedicate this thesis to my loving
parents, **brother**, **wife** and **daughter**
for their love, encouragement and support.

Declaration

I hereby declare that except where specific references are made to the work of others, the contents of this dissertation are original and have not been submitted in whole or in part for consideration for any other degree or qualification in this, or any other university.

Ben LI
February 2015

Acknowledgements

I would like to express my great gratitude to my supervisor, Professor Hidetsugu Sakaguchi, for allowing me the opportunity to pursue this work and for invaluable advice, guidance and support during the course of these studies.

Many thanks to Professor Haruo Honjo for giving me the great research environment and for useful advice in life in Japan and career plan.

My grateful appreciation to Prof. Boris A. Malomed for productive discussion and collaboration during my Ph. D course.

I am very grateful to Dr. Hiroshi Miki and Dr. Yusuke Kageyama for their helps in managing computing environment and discussions in physics over years.

At last, I would like to express my especial thanks to other members and staff in Non-linear physics group for their advice, kind helps and friendship.

Abstract

The thesis focuses on the ground states, dynamics and topological defects of the spinor Bose-Einstein condensates (BECs) with two-dimensional (2D) Spin-Orbit (SO) coupling. We studied two different cases for the external trapping condition: the homogeneous case and optical lattices potential.

In solid-state physics, the SO coupling originated from the relativistic effects. It couples the particle's spin and its orbital degree of freedom. SO coupling plays the central role for the quantum spin Hall effect and the topological insulators. In recent years, as a great breakthrough, the synthetic SO coupled BEC has been realized in experiment. It enables us to investigate the certain issues related to the SO coupling in other fields, such as, solid-state physics and particle physics, as quantum simulator by using the cold atomic systems.

In the first part of my thesis, we studied the SO coupled BECs in optical lattices. Especially, we investigated the energy dispersion, spin textures, vortex-antivortex pair structures, and presented the ground-state phase diagram. First, the general method to solves the Gross-Pitevskii Equation (GPE) for the SO coupled spinor BEC in optical lattices is presented in numerical simulation and analytical calculation. We showed that: (1) The optical lattices will change dramatically the energy dispersion of a SO coupled BEC; (2) The SO coupling generates the spin textures in the ground states; (3) Vortex lattices appear in a certain parameter region. Second, a vortex–antivortex pair (VAP) appears spontaneously in a SO coupled spinor BEC. The wave functions for the spin-up and spin-down components are mirror symmetric with respect to the y-axis, because the GPE is invariant under the combined operation of the spin inversion and the mirror transformation. Third, the ground-state phase diagram for a SO coupled spinor BEC in an optical lattice is presented. We found that, as a result of the spontaneous symmetry breaking, there are six types of ground-state phases. Among them, the twofold vortex lattices and the lattices chain are predicted for the first time, they reflected the symmetry and topological properties of the system.

In the second part, we researched the SO coupled BECs in 2D free space. Es-

pecially, we focus on the stable soliton and half-quantum vortices in the system. We found that a new stable soliton emerge spontaneously in 2D free space in a SO coupled BEC. The general systems cannot hold stable solitons in 2D free space, because of the occurrence of the collapse. Our results showed that the SO coupling prevents the collapse, and stabilizes the solitons in the ground state. Furthermore, we confirmed that the stable solitons include the half-quantum vortices and the mixed modes, in which the half-quantum vortices coexist with its time-reversed partner.

Contents

List of figures

List of tables

Chapter 1

Introduction

In the chapter, we review the basics of superfluid ^{4}He, experiment and theoretical model of the ultracold gaseous Bose-Einstein condensate (BEC), and give the thesis layout in end of the chapter.

The theory of the BEC is predicted by Satyendra Nath Bose and Albert Einstein in 1924. In that time, Bose presented the quantum statistics of photons, and sent his paper to Einstein. Then, Einstein extended the theory to other particle with mass and integer spin, that is the Bose-Einstein statistics [9]. Meanwhile, Einstein believes that one can produce the BEC by cooling bosons to very low temperature, so that the bosons can condense to the lowest quantum state of the system.

At temperature T, for identical particles, the Bose-Einstein distribution function can be written as

$$f(\epsilon_\nu) = \frac{1}{e^{(\epsilon_\nu - \mu)/kT} - 1}, \tag{1.1}$$

where ϵ_ν indicates the energy of the single-particle quantum state ν, k denotes the Boltzmann constant, μ expresses the chemical potential for the system. The mean occupation number N_ν for the single-particle quantum state ν can be calculated by using the Bose-Einstein distribution, and the definition is as following,

$$N_\nu = f(\epsilon_\nu) g_\nu = \frac{g_\nu}{e^{(\epsilon_\nu - \mu)/kT} - 1}, \tag{1.2}$$

where g_ν denotes the degeneracy for the state ν. When the temperature is very low, most of particles in the system will fall into a lowest quantum state, and form the BEC.

There are two types of superfluid so far, the superfluid ^{4}He and the gaseous

BEC with ultracold atoms. However, it is difficult to explain the superfluidity of ^{4}He, because of the strong interaction in the liquid. In 1938, F. London presented the idea about the connection between the superfluid ^{4}He and the BEC of particles with weakly interaction [10, 11].

Around 70 years later from the born of the theory of BEC, the BEC of the dilute atomic gas was produced in 1995 by using Rubidium ^{87}Rb [12], Sodium ^{23}Na [13], followed by Lithium ^{7}Li [14, 15] based on the methods of laser cooling. Here, the laser cooling and trapping atoms are very informant for production of the BEC in experiment. Due to the great achievements in the field, Steven Chu, Claude Cohen-Tannoudji (theory) and William Phillips was warded the Nobel Prizes in physics in 1997 for laser cooling and trapping [16–18], and Carl Wieman, Eric Cornell and Wolfgang Ketterle was warded the Nobel Prizes in physics in 2001 for the achievement of BEC [19, 20].

1.1 Superfluid ^{4}He

The superfluid ^{4}He is the first superfluid with strong interaction between the particles we found in nature. Based on the studying of the superfluid ^{4}He, we got so many insights on the properties of quantum fluids. The superfluidity is discovered by measuring the flow of the viscosity of ^{4}He by Kapitza [21], Allen and Misener [22] in 1938, and the critical temperature for the appearance of superfluid is $2.17K$. The superfluid ^{4}He has some special properties, such as it can flow insistently around a loop because the viscosity is vanished. In 1941, Landau presented the two-fluid model to explain the superfluidity [23], based on the theory, the system includes two components, superfluid component without viscosity and the normal one, which component dominates the system is depending on the temperature of the system. When the temperature of the system approaches the critical value, the normal component will be the main part, and the density of the superfluid component will approach to zero.

However, it is difficult to get deep understanding on the BEC by researching the superfluid ^{4}He, because the interaction of particles in the system is strong, so it is required to find other system with weak interaction of particles. We will find that the atomic gaseous BEC is a good candidate in the rest part of the chapter.

1.2 Bose-Einstein Condensates

There are two types of particle in nature, i.e., fermions and bosons, based on their spin. The bosons have integer spin like photon, while the fermions have half-integer spin like electron. These two types of particles follow different statistics, Bose-Einstein statistics (Eq. (1.1)) and Fermi-Dirac statistics. The difference between the bosons and fermions can be seen from the Pauli-exclusion principle, for fermions, each quantum state only can be occupied by no more than one fermion, while for bosons, there is not limit for the number of particles to occupy a quantum state. As a result, the wave function of bosons have symmetric and the wave function of fermions have asymmetric. For instance, the two-particle wave functions for bosons and fermions can be written as

$$\Psi = \frac{1}{\sqrt{2}}[\psi(x_1, E_a)\psi(x_2, E_b) + \psi(x_2, E_a)\psi(x_1, E_b)] \tag{1.3}$$

$$\Psi = \frac{1}{\sqrt{2}}[\psi(x_1, E_a)\psi(x_2, E_b) - \psi(x_2, E_a)\psi(x_1, E_b)] \tag{1.4}$$

where x_1 and x_2 are the positions of the particles, E_a and E_b are the energies of the particles. From these wave functions, we can get some understanding on the Pauli-exclusion principle. To do that, we can consider the a special case, $E_a = E_b = E$, then for bosons, the wave function reduces to $\Psi = \sqrt{2}\psi(x_1, E)\psi(x_2, E)$, and for fermions the wave function is vanished. That indicates that bosons are allowed to occupy a same quantum state while fermions are not.

The forming process of BEC can be seen from Figure 1.1. There are two parameters, the thermal de Broglie wavelength and the distance between the particles. Among them, the thermal de Broglie wavelength can be written as

$$\lambda_{dB} = \sqrt{\frac{2\pi\hbar^2}{mkT}}, \tag{1.5}$$

where m is the mass of particle, T is the temperature. We can find the thermal de Broglie wavelength is increasing with decreasing of the temperature. On the other hand, the mean distance between the particles d is of the order of $n^{-1/3}$, where $n = N/V$ is the density of the particle number N, and V is the volume.

At room temperature, the system follows the classical mechanics, and each particle has its own velocity, the behavior of particles looks like ball, the thermal de Broglie wavelength is very small than the mean distance between the particles. Based on the formula of the thermal de Broglie wavelength, decreasing the

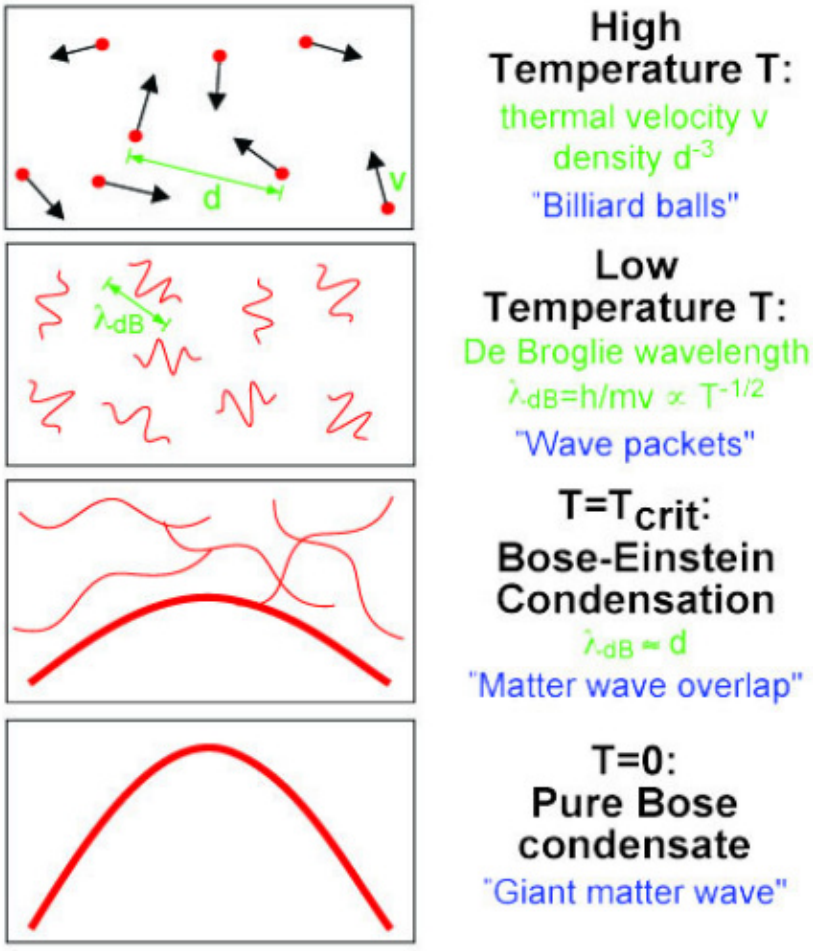

Fig. 1.1 Forming process of Bose-Einstein condensation. At high temperature, the system is controlled by classical physics, and the parameter is the distance between the paricles d, the particles can be seen as balls. When we decrease the temperature, then the quantum physics will take a main role in the system, the particles will have properties of wave, so the another parameter, wave length λ_{dB} will begin to takes roles. If the temperature approach to critical temperature, so that λ_{dB} is comparable with d, the BEC will take place. Finally, if the temperature decrease to zero, the pure BEC is formed, all the particles in the system will condense to a same quantum state to form a giant matter wave. The figure is cited from Ref. [1].

temperature will increases the value of the wavelength, and there is a critical value for the temperature in where λ_{dB} is comparable with the distance between the particles d, in the temperature, some particles condenses to the lowest quantum state, and the BEC takes place. At zero temperature, all the particles will contributes to form the giant matter wave, i.e., the pure BEC.

For BEC with non-interacting particles in three-dimensional (3D) uniform system, the critical condition is satisfied as $n\lambda_T^3 \ll \zeta(3/2)$ [24], where the Riemann zeta function $\zeta(3/2) \approx 2.612$. Meanwhile, the critical temperature can be written as,

$$T_c = \frac{2\pi\hbar^2}{mk}(\frac{n}{\zeta(3/2)})^{2/3}, \tag{1.6}$$

Below the critical temperature, the BEC will takes place. In the momentum space, all the particle occupy the zero momentum state when the pure BEC is produced, but, for the temperature (non-zero and below the T_c), the particles contributed to the BEC just a part of the total number of particles. The fraction of the particles for forming the BEC can be written as

$$N_0 = N\left[1 - (\frac{T}{T_c})^{3/2}\right], \tag{1.7}$$

where N_0 indicates the number of particles forming the BEC, and N expresses the total number of the particles.

In general, to produce a BEC, the harmonic trap is needed to confine the particles, the typical 3D trapping potential has the following form,

$$V(\mathbf{r}) = \frac{1}{2}m(\omega_x^2x^2 + \omega_y^2y^2 + \omega_z^2z^2), \tag{1.8}$$

where ω_i ($i = x, y, z$) is the oscillator frequency in i direction. Due to the presence of the trap, the critical temperature for the BEC transition in the condition of non-interacting will be changed to

$$T_c = \frac{\hbar\bar{\omega}}{k}(\frac{N}{\zeta(3)})^{1/3} \approx 0.94\hbar\bar{\omega}N^{1/3}, \tag{1.9}$$

where $\bar{\omega} = (\omega_x\omega_y\omega_z)^{1/3}$ denotes the mean oscillator frequency.

1.2.1 Realization of BEC in experiment

In general, at very low temperature, a gas will transits to solid state, but, for extreme dilute gas, it can be avoided. The density satisfied for the condition is of the order of $10^{13}/cm^3 - 10^{15}/cm^3$, while the density for common experiment is of the order $10^{19}/cm^3$. By using the formula of the critical temperature Eq. (1.6), the temperature according to the density is of the order of $10^{-6}K$. In the order of the temperature, only the s-wave scattering takes place, and the s-wave scattering length can be used to indicates the strength of the scattering. In 3D system, the density of the particles n and scattering length a_s have following relations,

$$a_s^3 n \ll 1. \tag{1.10}$$

In the theoretical treatment of BEC, such as in the Gross–Pitaevskii equation, we just consider the interactions induced by s-wave scattering length.

The first pure BEC was produced in experiment by Carl Wieman and Eric Cornell in 1995 by using rubidium atoms (^{87}Rb) [12]. Then the BEC with other series atoms, like sodium ^{23}Na is also realized by W. Ketterle's group at MIT [13]. The Nobel Prize in physics was awarded to Carl Wieman, Eric Cornell and Wolfgang Ketterle in 2001 for the achievement of BEC in dilute gases and the studying on the fundamental properties of the BEC. Fig. 1.2 shows the velocity distribution of the expanding rubidium atoms of BEC.

Up to now, following the first realization of BEC in experiment, so many groups reported their productions of BEC by using other atomic series including ^{4}He [25], ^{174}Yb [26], ^{133}Cs [27], ^{52}Cr [28], ^{84}Sr [29, 30], and so on.

1.2.2 Theoretical Model

When the temperature approaches to absolute zero, the BEC system can be described by the Gross-Pitaevskii equation (GPE). In the thesis, we will research some stationary and dynamical properties of the BEC with Spin-Orbit coupling, by using GPE, especially, focus on the solitons and vortices appeared in the system. In fact, for finite temperature, the GPE also can be used by making some changes.

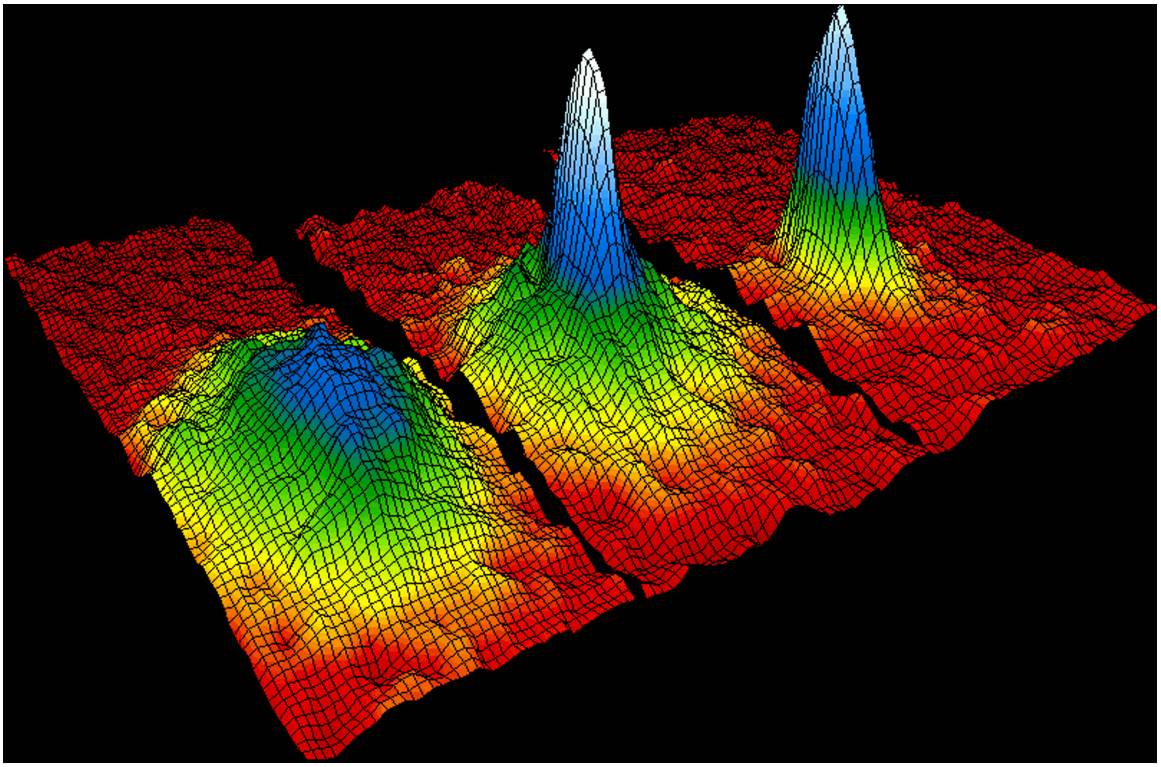

Fig. 1.2 Velocity-distribution of the rubidium atoms by expanding them in three temperatures, from right to light, $T > T_c$, $T \approx T_c$ and $T < T_c$, to confirm the production of BEC. The figure is cited from Ref. [2].

1.3 Thesis layout

The thesis includes 6 chapters, and divided to two parts.

The first part has three chapters, the aim of the part is to introduce the research basics of my work.

- The first chapter is a introduction of the superfluid ^{4}He and the gaseous BEC.
- Next, the second chapter will reviews the details of the theory of the Bose-Einstein condensates, includes mean-field treatment and different solutions for different conditions.
- In the third chapter, we focus on the Spin-Orbit Coupled Bose-Einstein condensates, give the introduction of the ground state phase diagram and the experimental details.

The next part is my research work during my doctoral course, it includes

- Chapter 4, Spin-Orbit Coupled Bose-Einstein condensates in free space,
- Chapter 5, Spin-Orbit Coupled Bose-Einstein condensates in optical lattices,
- Chapter 6, a conclusion of my work.

Finally, I would like to notice that

The first part (Chapters 1 - 3) ***is not*** *my original work, it is a review on the research background of the thesis work.*

The Chapters 4 - 5 ***are*** *our research works, the results have been published in [31–33]. These two chapters are re-writed based on these publications.*

Chapter 2

Theory of Bose-Einstein Condensates

In this chapter, we review the Mean-Field theory of Bose-Einstein Condensates (BECs) based on the text book and other references. At first, we intraduce the Mean-Field theory, and drive the Gross-Pitaevskii Equation (GPE) which can describes the BECs in two different methods. Then, we consider the physical meaning of the order parameter. Finally, the solutions of GPE will be presented both in free space and harmonic trap.

2.1 Mean-Field Theory and Gross-Pitaevskii Equation

At zero–temperature, all of atoms in dilute gas with weak interactions will occupy macroscopically the lowest energy level in momentum space and form the BECs. Generally, GPE which also called nonlinear Schrödinger equation (NLSE) as a common model, will be used to describes BECs. In order to describe multi-component condensates, this model can be trivially generalized to multi-component Gross–Pitaevskii equations (GPEs).

It has been proved that the GPE model is a good description for many static and dynamical properties both for single- and multi-component condensate systems [24, 34], even though fluctuations including thermal contributions and quantum one are not taken into account.

In this section, we give the details of driving GPE from two different ways, then the physical meaning of Order Parameter (OP) will be discussed.

2.1.1 Based on the First Quantization

We consider a system consist of particles with mass m and spin 0 in the following except specifying particularly.

A system formed from N interacting bosons can be described by an $N-$body wavefunction $\psi(\mathbf{r}_1, \mathbf{r}_2, \cdots, \mathbf{r}_N, t)$ where $\mathbf{r}_i$ is the position of atom i. This wavefunction obeys the well known Schrödinger equation as follows,

$$i\hbar\frac{\partial}{\partial t}\psi(\mathbf{r}_1, \mathbf{r}_2, \cdots, \mathbf{r}_N, t) = H\psi(\mathbf{r}_1, \mathbf{r}_2, \cdots, \mathbf{r}_N, t), \tag{2.1}$$

$$H \equiv -\frac{\hbar^2}{2m}\sum_{i=1}^{N}\nabla_i^2 + \sum_{i=1}^{N}U(\mathbf{r}_i, t) + \frac{1}{2}\sum_{i\neq j}^{N}V(\mathbf{r}_i - \mathbf{r}_j), \tag{2.2}$$

where $U(\mathbf{r}_i, t)$ is the external field dependent on the time, $V(\mathbf{r}_i - \mathbf{r}_j)$ is the two-body interaction, H is the system's Hamiltonian in coordinate basis.

For bosons, the wave fuction have a symmetry as follows,

$$\psi(\mathbf{r}_1, \cdots, \mathbf{r}_i, \cdots, \mathbf{r}_j, \cdots, \mathbf{r}_N, t) = \psi(\mathbf{r}_1, \cdots, \mathbf{r}_j, \cdots, \mathbf{r}_i, \cdots, \mathbf{r}_N, t). \tag{2.3}$$

In mean-field theory, we assume the N-body wave-function to be

$$\psi(\mathbf{r}_1, \mathbf{r}_2, \cdots, \mathbf{r}_N, t) = \prod_{i=1}^{N}\phi(\mathbf{r}_i, t), \tag{2.4}$$

here, $\phi(\mathbf{r}_i, t)$ is single-particle wave-function, it satisfies the Normalization condition,

$$\int d\mathbf{r}|\phi(\mathbf{r}_i, t)|^2 = 1. \tag{2.5}$$

Eq. (2.4) means all of the atoms occupy a same single-particle state, in the other word, the system into BECs. In addition, the form of Eq. (2.4) is same with Hartree approximation.

Next, we can use Eq. (2.4) to calculate the energy expectation of the systems,

$$\begin{aligned} E(t) &= \int d\mathbf{r}_1 \cdots \int \mathbf{r}_N \psi^*(\mathbf{r}_1, \cdots, \mathbf{r}_N, t) H\psi(\mathbf{r}_1, \cdots, \mathbf{r}_N, t) \\ &\simeq N\int d\mathbf{r}\frac{\hbar^2}{2m}|\nabla\phi(\mathbf{r}, t)|^2 + N\int d\mathbf{r}U(\mathbf{r}, t)|\phi(\mathbf{r}, t)|^2 \\ &+ \frac{N^2}{2}\int d\mathbf{r}\int d\mathbf{r}'V(\mathbf{r} - \mathbf{r}')|\phi(\mathbf{r}, t)|^2|\phi(\mathbf{r}', t)|^2 \end{aligned} \tag{2.6}$$

where, we have used the normalization condition Eq. (2.5) and assumed $N \gg 1$. Meanwhile, we can define the condensate wave function as

$$\Psi(\mathbf{r},t) \equiv \sqrt{N}\phi(\mathbf{r},t), \tag{2.7}$$

it is also called Order Parameter (OP) of BECs.

Now, we consider the equation of motion for the condensates wave function. To do that, we define the Lagrangian

$$L \equiv \int d\mathbf{r}\mathcal{L}[\Psi, \nabla\Psi, \partial_t\Psi], \tag{2.8}$$

where $\mathcal{L}$ indicate the Lagrangian density with a form as following,

$$\mathcal{L}[\Psi, \nabla\Psi, \partial_t\Psi] \equiv \frac{i\hbar}{2}[\Psi^*(\mathbf{r},t)\frac{\partial}{\partial t}\Psi(\mathbf{r},t) - \Psi(\mathbf{r},t)\frac{\partial}{\partial t}\Psi^*(\mathbf{r},t)] - \mathcal{H}[\Psi, \nabla\Psi, \pi, \nabla\pi], \tag{2.9}$$

where $\pi(\mathbf{r},t)$ is the canonical momentum which have a canonical commutation relation with $\Psi(\mathbf{r},t)$

$$\pi(\mathbf{r},t) \equiv \frac{\delta L}{\delta\partial_t\Psi(\mathbf{r},t)} = i\hbar\Psi^*(\mathbf{r},t), \tag{2.10}$$

and $\mathcal{H}$ is the Hamiltonian density. From Eq. (2.6), we can get

$$\begin{aligned}\mathcal{H}[\Psi, \nabla\Psi, \pi, \nabla\pi] \equiv & \frac{\hbar^2}{2m}|\nabla\Psi(\mathbf{r},t)|^2 + U(\mathbf{r},t)|\Psi(\mathbf{r},t)|^2 \\ & + \frac{1}{2}\int d\mathbf{r}'V(\mathbf{r}-\mathbf{r}')|\Psi(\mathbf{r}',t)|^2|\Psi(\mathbf{r},t)|^2.\end{aligned} \tag{2.11}$$

Then we can take all of above results to Euler-Lagrange equation

$$\frac{\partial}{\partial_t}\left[\frac{\delta L}{\delta\partial_t\Psi^*(\mathbf{r},t)}\right] + \nabla\cdot\left[\frac{\delta L}{\delta\nabla\Psi^*(\mathbf{r},t)}\right] - \frac{\delta L}{\delta\Psi^*(\mathbf{r},t)} = 0, \tag{2.12}$$

and we can get the time-dependent GPE,

$$i\hbar\frac{\partial}{\partial t}\Psi(\mathbf{r},t) = -\frac{\hbar^2}{2m}\nabla^2\Psi(\mathbf{r},t) + U(\mathbf{r},t)\Psi(\mathbf{r},t) + \int d\mathbf{r}'V(\mathbf{r}-\mathbf{r}')|\Psi(\mathbf{r}',t)|^2\Psi(\mathbf{r},t). \tag{2.13}$$

2.1.2 Based on the Second Quantization

In the section, we drive the GPE from the second quantization representation.

The Hamiltonian in second quantization representation is

$$\begin{aligned}\hat{H}(t) = &\int d\mathbf{r}\hat{\psi}^\dagger(\mathbf{r})\left[-\frac{\hbar^2}{2m}\nabla^2 + U(\mathbf{r},t)\right]\hat{\psi}(\mathbf{r}) \\ &+ \frac{1}{2}\int d\mathbf{r}\int d\mathbf{r}'\hat{\psi}^\dagger(\mathbf{r})\hat{\psi}^\dagger(\mathbf{r}')V(\mathbf{r}-\mathbf{r}')\hat{\psi}^\dagger(\mathbf{r}')\hat{\psi}^\dagger(\mathbf{r}),\end{aligned} \tag{2.14}$$

where $\hat{\psi}(\mathbf{r})$ and $\hat{\psi}^\dagger(\mathbf{r})$ are the annihilation and creation operators, which satisfying the canonical communication as follows,

$$[\hat{\psi}(\mathbf{r}), \hat{\psi}^\dagger(\mathbf{r}')] = \delta(\mathbf{r}-\mathbf{r}'), \tag{2.15}$$

$$[\hat{\psi}(\mathbf{r}), \hat{\psi}(\mathbf{r}')] = [\hat{\psi}^\dagger(\mathbf{r}), \hat{\psi}^\dagger(\mathbf{r}')] = 0. \tag{2.16}$$

In Heisenberg representation, the field operators read as

$$\hat{\psi}(\mathbf{r},t) \equiv \hat{U}_T^\dagger(t)\hat{\psi}(\mathbf{r})\hat{U}_T(t), \tag{2.17}$$

$$\hat{U}_T(t) \equiv \hat{T}\exp\left[-\frac{i}{\hbar}\int_0^t d\mathbf{r}'\hat{H}(t')\right], \tag{2.18}$$

where the $\hat{U}_T(t)$ is the time translation operator, and T is related to time. In the case the Hamiltonian is time-independent,

$$\hat{\psi}(\mathbf{r},t) = e^{i\hat{H}t/\hbar}\hat{\psi}(\mathbf{r})e^{-i\hat{H}t/\hbar}, \tag{2.19}$$

Then, we can get the Heisenberg Equation of field operators as

$$i\hbar\frac{\partial}{\partial t}\hat{\psi}(\mathbf{r},t) = -\frac{\hbar^2}{2m}\nabla^2\hat{\psi}(\mathbf{r},t) + U(\mathbf{r},t)\hat{\psi}(\mathbf{r},t) + \int d\mathbf{r}'V(\mathbf{r}-\mathbf{r}')|\hat{\psi}(\mathbf{r}',t)|^2\hat{\psi}(\mathbf{r},t). \tag{2.20}$$

To get the equation of motion of condensates wave function, we assume that the expectation of field operator can be regarded as the condensates wave function, i.e.,

$$\Psi(\mathbf{r},t) \equiv \langle\hat{\psi}(\mathbf{r},t)\rangle. \tag{2.21}$$

So that, we can write down the field operator as

$$\hat{\psi}(\mathbf{r},t) = \langle\hat{\psi}(\mathbf{r},t)\rangle + \left[\hat{\psi}(\mathbf{r},t) - \langle\hat{\psi}(\mathbf{r},t)\rangle\right] \equiv \Psi(\mathbf{r},t) + \hat{\phi}(\mathbf{r},t), \tag{2.22}$$

where $\hat{\phi}(\mathbf{r},t)$ can be explained as the annihilation operator of particles that didn't fall into the condensates, and these operators have same commutation relations

with $\hat{\psi}(\mathbf{r},t)$ because of $\Psi(\mathbf{r},t)$ being a C-number,

$$[\hat{\phi}(\mathbf{r}),\hat{\phi}^{\dagger}(\mathbf{r}')]=\delta(\mathbf{r}-\mathbf{r}'), \tag{2.23}$$

$$[\hat{\phi}(\mathbf{r}),\hat{\phi}(\mathbf{r}')]=[\hat{\phi}^{\dagger}(\mathbf{r}),\hat{\phi}^{\dagger}(\mathbf{r}')]=0. \tag{2.24}$$

At zero–temperature, we assume that the thermal depletion of the system is negligible. Furthermore, for weak interacting systems, the quantum fluctuations will not play a important role, so that we can neglect the thermal contributions, i.e.,

$$\langle\hat{\phi}(\mathbf{r},t)\rangle=0$$

.

Now, we substitute Eq. (2.22) to the Heisenberg Equation of motion Eq. (2.20), and take the expectation values both two sides for the equation, meanwhile ignore the terms with $\hat{\phi}(\mathbf{r},t)$, then we get the time-dependent GPE as follows,

$$i\hbar\frac{\partial}{\partial t}\Psi(\mathbf{r},t)=-\frac{\hbar^2}{2m}\nabla^2\Psi(\mathbf{r},t)+U(\mathbf{r},t)\Psi(\mathbf{r},t)+\int d\mathbf{r}'V(\mathbf{r}-\mathbf{r}')|\Psi(\mathbf{r}',t)|^2\Psi(\mathbf{r},t). \tag{2.25}$$

2.1.3 Effective Interaction Potential

In the time-dependent GPE (Eq. (2.25)), the interaction potential $V(\mathbf{r}-\mathbf{r}')$ includes two kinds of interactions, the first one is a short range repulsive interaction, and the second one is a longer range attractive van der Waals interaction. These two kinds potentials compete with each other and leads to rich physics, for example, molecular bound states. It is unnecessary to solve the Schrödinger equation with $V(\mathbf{r}-\mathbf{r}')$ term for ultracold atomic gases, because it have some disadvantages. Alternatively, using an effective potential can make the problem simplified greatly.

The effective contact interaction potential can be written as

$$V(\mathbf{r}-\mathbf{r}')=g\delta(\mathbf{r}-\mathbf{r}'), \tag{2.26}$$

where

$$g=\frac{4\pi\hbar^2a}{m}, \tag{2.27}$$

is the strength of the interaction for three dimensional system, a is the scatering length.

By substituting Eq. (2.26) to the time-dependent GPE, Eq. (2.25), we can get

the final form of GPE as follows,

$$i\hbar\frac{\partial}{\partial t}\Psi(\mathbf{r},t) = -\frac{\hbar^2}{2m}\nabla^2\Psi(\mathbf{r},t) + U(\mathbf{r},t)\Psi(\mathbf{r},t) + g|\Psi(\mathbf{r},t)|^2\Psi(\mathbf{r},t). \tag{2.28}$$

The equation, Eq. (2.28), is basis for the thesis.

2.1.4 Time-independent GPE

In the section, we consider the case, GPE does not depend on the time. In the case, we can treat the external field as $U(\mathbf{r},t) = U(\mathbf{r})$. The wave function of the condensates can be written as

$$\Psi(\mathbf{r},t) = \Psi(\mathbf{r})e^{-i\mu t/\hbar}, \tag{2.29}$$

because we consider the stationary states here, and μ is the chemical potential. By substituting the Eq. (2.29) to time-dependent GPE (Eq. (2.28)), we can get the time-independent GPE as follows,

$$\left[-\frac{\hbar^2}{2m}\nabla^2 + U(\mathbf{r}) + g|\Psi(\mathbf{r})|^2\right]\Psi(\mathbf{r}) = \mu\Psi(\mathbf{r}). \tag{2.30}$$

From the equation, we can get the stationary states of the system according to the energy μ, we will research the ground states and excited states of the BEC with Spin-Orbit coupling in the later chapters based on the time-independent equation.

2.2 Order Parameter

In this section, we are discussing the physical meaning of the order parameter of the Bose-Einstein condensates by rewriting the GPE in form of the quantum continuity equation.

From Eq. (2.5) and Eq. (2.7), we can find that the total number of particles of the system is

$$N = \int d\mathbf{r}|\Psi(\mathbf{r},t)|^2, \tag{2.31}$$

and, the local density of the Bose-Einstein condensates can be written as

$$n(\mathbf{r},t) \equiv |\Psi(\mathbf{r},t)|^2. \tag{2.32}$$

In the general case, the wave function of the Bose-Einstein condensates have the form of complex number, and can be written as following the separating form of the amplitude and the phase,

$$\psi(\mathbf{r},t) = \sqrt{n(\mathbf{r},t)}e^{i\varphi(\mathbf{r},t)}, \tag{2.33}$$

where φ is a real number, it indicates the phase of the Bose-Einstein condensates. By substituting Eq. (2.33) to the time-dependent GPE (Eq. (2.28)), then we can get two equations according to the real and imaginary parts, respectively.

$$\frac{\partial}{\partial t}n(\mathbf{r},t) = -\nabla\cdot\left[n(\mathbf{r},t)\frac{\hbar}{m}\nabla\varphi(\mathbf{r},t)\right], \tag{2.34}$$

and

$$\begin{aligned}\hbar\frac{\partial}{\partial t}\varphi(\mathbf{r},t) = &-U(\mathbf{r},t) - gn(\mathbf{r},t)\\ &+\frac{\hbar^2}{2m}\frac{1}{\sqrt{n(\mathbf{r},t)}}\nabla^2\sqrt{n(\mathbf{r},t)} - \frac{\hbar^2}{2m}\left[\nabla\varphi(\mathbf{r},t)\right]^2.\end{aligned} \tag{2.35}$$

Where, Eq. (2.34) is the continuity equation that describes the particle conservation. In addition, the particle flux density $J(\mathbf{r},t)$ can be written as,

$$\begin{aligned}J(\mathbf{r},t) &\equiv -\frac{i\hbar}{2m}\left[\Psi^*(\mathbf{r},t)\nabla\Psi(\mathbf{r},t) - \Psi(\mathbf{r},t)\nabla\Psi^*(\mathbf{r},t)\right]\\ &= n(\mathbf{r},t)\frac{\hbar}{m}\nabla\varphi(\mathbf{r},t).\end{aligned} \tag{2.36}$$

Then, the continuity equation Eq. (2.34) can be reduced to

$$\begin{aligned}\frac{\partial}{\partial t}n(\mathbf{r},t) &\equiv -\nabla\cdot\mathbf{J}(\mathbf{r},t)\\ &\equiv -\nabla\cdot\left[n(\mathbf{r},t)\upsilon(\mathbf{r},t)\right],\end{aligned} \tag{2.37}$$

where $\upsilon(\mathbf{r},t)$ denotes the local velocity field of the Bose-Einstein condensates with definition as follows,

$$\upsilon(\mathbf{r},t) \equiv \frac{\hbar}{m}\nabla\varphi(\mathbf{r},t). \tag{2.38}$$

Based on the Eq. (2.32) and Eq. (2.38), we can get the physical meaning of the wave function of the Bose-Einstein condensates. The square modulus of the amplitude of the wave function of the Bose-Einstein condensates indicate the local density of the condensates, and the phase gradient of the wave function of

condensates express the velocity of the Bose-Einstein condensates.

2.3 Solutions in Free Space

In this section, we consider the solutions of ground states of GPE in free space, i.e., the external potential $U(\mathbf{r},t) = 0$. Then the time-independent GPE can be written as,

$$\left[-\frac{\hbar^2}{2m}\nabla^2 - \mu + g|\Psi(\mathbf{r})|^2\right]\Psi(\mathbf{r}) = 0, \tag{2.39}$$

by solving Eq. (2.39), we can get the solutions of the system.

2.3.1 Plane Wave

At first, we consider the simplest case. We take the average density of particle is n_0, then we can find that the plane wave solution satisfies Eq. (2.39).

$$\Psi(\mathbf{r}) = \sqrt{n_0}e^{imv\cdot\mathbf{r}/\hbar}, \tag{2.40}$$

$$\mu = gn_0 + \frac{1}{2}mv^2. \tag{2.41}$$

where v indicates the velocity vector. As a obvious case, we have found that the plane wave is a solution for GPE. In the rest parts, we will try to find other non-obvious solutions.

2.3.2 Topological Defect: Dark Soliton

The soliton and vortices are the important topological defects. In the part, we will show that the dark soliton satisfies Eq. (2.39).

Let us just consider the time-independent GPE with repulsive interactions. Under a boundary condition as below:

$$\begin{aligned} |\Psi(x)| &\to \sqrt{n_0}, \\ \varphi(x) &\to \frac{mvx}{\hbar} \pm const, \end{aligned} \tag{2.42}$$

if,

$$x \to \pm\infty,$$

we can find a solution as follows,

$$\Psi(x) = \sqrt{n_0} e^{imvx/\hbar} \{ \sqrt{1 - (\frac{v}{v_s})^2} \tanh \left[\sqrt{1 - (\frac{v}{v_s})^2} \frac{x - x_0}{\xi} \right] + i \frac{v}{v_s} \}, \tag{2.43}$$

and

$$\mu = g n_0 + \frac{1}{2} m v^2, \tag{2.44}$$

where v is the velocity of soliton in x direction, ξ denotes the system's length scale that is defined as

$$\xi \equiv \frac{\hbar}{\sqrt{m g n_0}}, \tag{2.45}$$

v_s expresses the sound velocity of system,

$$v_s \equiv \sqrt{\frac{g n_0}{m}}, \tag{2.46}$$

and x_0 is a real number that describes the center position of soliton.

For the dark soliton, the center of soliton has rare density, and the part far away from the center of the soliton has a density similar with plane wave. Especially, for a soliton with $v = 0$, the density at center is exactly 0. In the case, we cannot define a phase at origin, because there is not value for wave function. From the view of the topological point, soliton is a kind of topological defect. In addition, it is not necessary for the phase of the soliton to keep the continuity at origin, because there is not definition. Actually, there is a jump for phase of the soliton with $v = 0$ at origin.

For solitons with $v = 0$, we call them Dark Soliton, and for solitons with $v \neq 0$, we call them Gray Soliton, in which the zero point for wave function does not exist. So seriously, gray soliton can not be called topological defect, but, customarily, it also called soliton. Furthermore, soliton solution will change to the plane wave solution when $v = v_s$.

In the section, we have considered the one dimensional infinite system, and found the soliton solution for GPE. Actually, for one-dimensional finite system, we also can find the soliton solution [35].

2.3.3 Bright Soliton

In the above section, we have considered the repulsive interaction situation, and find that the dark soliton exist in the system.

For attractive interaction, the soliton is also exist, but the form of the solution has a little different. In the center, the density is bigger than other part in BECs, we call this kind of soliton Bright Soliton.

2.3.4 Stability

In ultracold atomic gases, the solitons have been realized in experiment [36–40]. However, due to the one-dimensional system can not be made in experiment, therefore, researchers consider generally the one-dimentional soliton in the high-dimensional space. The soliton is stable in one-dimensional space, but, in high-dimensional space, the solutions of soliton has instability because the solutions just depend on the one-direction. The instability called Snake instability [41, 42]. It have been observed in experiment [38, 39]. The snake instability is very important for the research on the quantum vortices [41].

2.3.5 Quantum Vortices

Quantum vortices are the vortices in the superfluid, they are quite different from classical vortices.

As showed in Eq. (2.38), the phase gradient of the wave function of the Bose-Einstein condensates express the velocity of condensates,

$$v(\mathbf{r},t) \equiv \frac{\hbar}{m}\nabla\varphi(\mathbf{r},t). \tag{2.47}$$

To find the difference between the quantum and classical vortices, we can calculate the vorticity that features the property of vortices. The definition of the vorticity is reading as

$$\omega(\mathbf{r},t) \equiv \nabla \times v(\mathbf{r},t). \tag{2.48}$$

By substituting Eq. (2.47) to Eq. (2.48), we find that

$$\omega(\mathbf{r},t) = \nabla \times \frac{\hbar}{m}\nabla\varphi(\mathbf{r},t) = 0. \tag{2.49}$$

It means that the vorticity for the Bose-Einstein condensates is zero.

Then, we consider another quantity that also describes the vortices, circulation Γ,

$$\Gamma(\mathbf{r},t) \equiv \oint_C d\mathbf{r}\cdot v(\mathbf{r},t), \tag{2.50}$$

where C indicates the arbitrary closed curve, the integration is a line integration along the closed curve. It will be zero if the region surrounded by the closed curve C is simply connected. On the other hand, it will be non-zero if the region is multiply connected.

By substituting Eq. (2.47) to Eq. (2.50), we find that

$$\begin{aligned}\Gamma(\mathbf{r},t) &= \frac{\hbar}{m}\oint_C d\mathbf{r}\cdot\nabla\varphi(\mathbf{r},t)\\ &= \frac{\hbar}{m}\oint_C d\varphi(\mathbf{r},t)\\ &= \frac{\hbar}{m}\triangle\varphi,\end{aligned} \tag{2.51}$$

where $\triangle\varphi$ indicate the change of the phase around a vortex. Since the wave function of the Bose-Einstein condensates needs to be single-valued, the change of phase must be integer multiple of 2π, so that the circulation must be

$$\Gamma(\mathbf{r},t) = \frac{2\pi\hbar}{m}n \equiv kn, \tag{2.52}$$

where $n = 0, \pm1, \pm2, \cdots$, and $k = 2\pi\hbar/m$ is the quanta of circulation. When the phase winds round in an anticlockwise direction, the vortex is negatively charged. Furthermore, when it winds in a clockwise direction, it is positively charged.

The difference between the quantum vortices and the classical vortices is that the circulation for the quantum vortices is quantized by integer n while the circulation for the classical vortices are not. It is reduced by the properties of the single-value of the wave function, so it does not exist in classical one.

Under the cylindrical coordinate system (r,θ,z), the wave function of the vortices can be written as

$$\Psi(\mathbf{r}) \equiv \sqrt{n_0}f(r)e^{in\theta}. \tag{2.53}$$

where $f(r)$ is a real function.

2.4 Solution in a Harmonic Trap

Figure 2.1 shows the density profiles of the solutions for the Bose-Einstein condensates with different interacting cases in a 3D harmonic potential. For the non-interacting case, the density profile of the ground state have the Gaussian form. The wave function of the ground state of a Bose-Einstein condensate in an

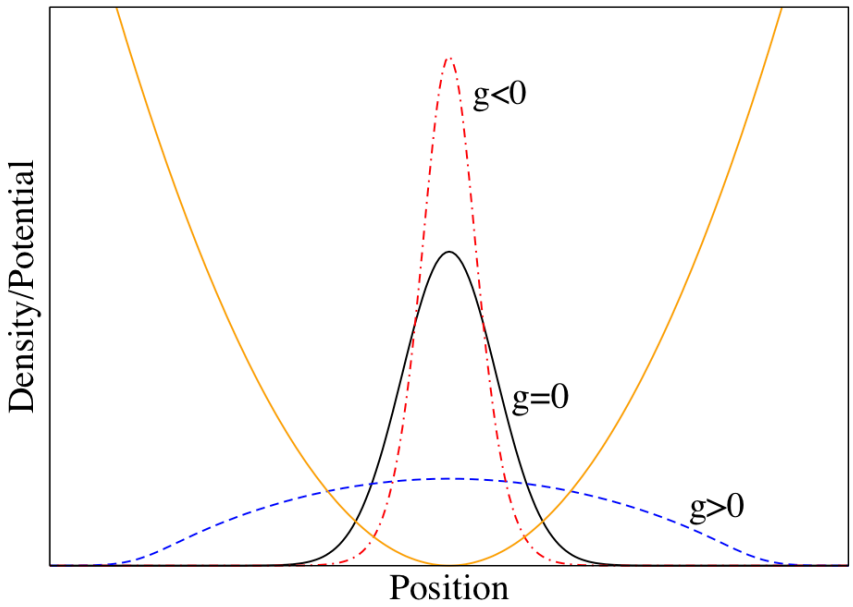

Fig. 2.1 Density profiles of the ground states of a Bose-Einstein condensate in a harmonic potential (orange line). The black solid line indicates the non-interacting case, the red dash-dot line expresses the attractive interacting case, and the blue dash line is the repulsive interacting case. The wave functions appeared here are normalized to the same particle numbers. The figure is cited from Ref. [3].

anisotropic trap can be written as [24]

$$\phi_0(\mathbf{r}) = \frac{\sqrt{N}}{\pi^{3/4}(l_x l_y l_z)^{1/2}} e^{-x^2/2l_x^2 - y^2/2l_y^2 - z^2/2l_z^2}, \tag{2.54}$$

where $l_i (i = x, y, z)$ denotes the width of the wave function in i direction, and

$$l_i = \sqrt{\frac{\hbar}{m\omega_i}}. \tag{2.55}$$

For the case of the attractive or repulsive interaction, the density profile will has some changes than non-interacting case in the height and width.

To identify the different interacting cases, a interaction parameter can be introduced as

$$\chi = \frac{N a_s}{l}, \tag{2.56}$$

where $l = l_x = l_y = l_z$ denotes the length of the harmonic oscillator in an isotropic system, χ indicates the strength of the interactions in the system. In the weak interaction case $\chi \ll 1$, especially, for ideal Bose gas, $\chi = 0$. While in the strong interaction case $\chi \gg 1$, the Thomas-Fermi approximation is a good description for the system.

2.4.1 Thomas-Fermi Approximation

The mail idea for the Thomas-Fermi approximation is that the kinetic energy term can be ignored in the time-independent GPE because the repulsive interaction term is very large in the equation [43]. In the Thomas-Fermi approximation, the solution of the ground state, called Thomas-Fermi solution, can be written as

$$\phi(\mathbf{r}) = \begin{cases} \sqrt{\mu - V_{ext}(\mathbf{r})/g}, & \text{if } \mu \geqslant V_{ext}(\mathbf{r}) \\ 0, & \text{otherwise} \end{cases} \tag{2.57}$$

if the Bose-Einstein condensates is in a harmonic trap,

$$V_{ext}(\mathbf{r}) = \frac{1}{2} m(\omega_x^2 x^2 + \omega_y^2 y^2 + \omega_z^2 z^2), \tag{2.58}$$

where $\omega_i (i = x, y, z)$ is the trapping frequency. Furthermore, the Thomas-Fermi radius that indicates the spatial extension of the Bose-Einstein condensates can

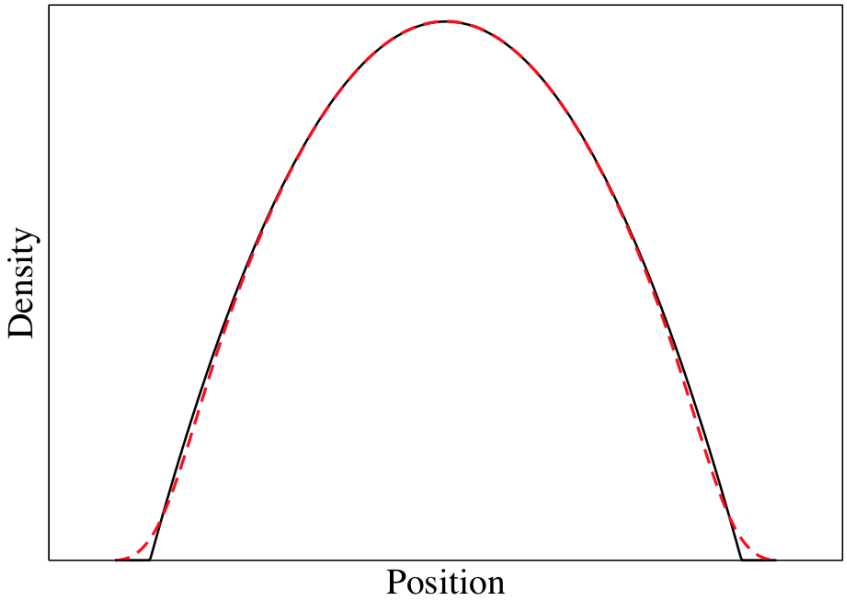

Fig. 2.2 Comparison between the Thomas-Fermi approximation and the numerical result for the density profile of the ground states. The black solid line indicates the Thomas-Fermi approximation, and the red dashed line denotes the numerical result. The figure is cited from Ref. [3].

be written as

$$R_i = \sqrt{\frac{2\mu}{m\omega_i^2}}, i = x, y, z \tag{2.59}$$

Fig. 2.2 shows the difference between the Thomas-Fermi approximation and the numerical result for the density profile of the ground states for a Bose-Einstein condensate in a harmonic trap. We can find that in the centre, the Thomas-Fermi result is agreement with numerical result very well, but in the edge area the agreement is not good. The reason can be understood by considering the relative relations between the harmonic trap and the interaction, in the centre than the edge area, the harmonic trap is deeper so that the interaction is larger.

2.5 Chapter summary

In the chapter, we have reviewed the theory of the Bose-Einstein condensates. At first, we have gave the mean-field theory and Gross-Pitaevskii equation. Next, the physical meaning of the order parameter of the Bose-Einstein condensates

have been considered. Then, we reviewed the solutions of the Bose-Einstein condensates in free space and in a harmonic trap, includes the plane wave solution, bright and dark solitons, and vortices.

Chapter 3

Spin-Orbit Coupled Bose-Einstein Condensates

In the chapter, we review the basic concepts and research progress on the Spin-Orbit (SO) coupled Bose-Einstein Condensates (BECs).

We start with introducing the concept of SO coupling both in solid-state physics and ultracold atomic system. Then, the theory and experiments of the gauge field will be reviewed. Consequently, we focus on the single-particle and interaction physics of the SO coupled BECs, and show the phase diagram of the ground states. The chapter will be ended by a chapter summary.

3.1 Spin-Orbit Coupling

SO coupling describes the interaction of a particle's orbit angular momentum and its spin angular momentum in a way of quantum mechanics. It is essential in a wide of range of condensed matter physics, such as, topological insulators and spintronics.

The movement of electrons in a electric field in various of materials is the origination of SO coupling in solid-state physics, in which, the parameters are determined by materials. On the other hand, the parameters in ultracold atomic gases are tunable by laser-atom interaction. So that, the SO coupling generated in BECs are more easy for people to get deeper understanding of its physics in variety of parameter regions, and research the unique features that are impossible in other solid-state systems.

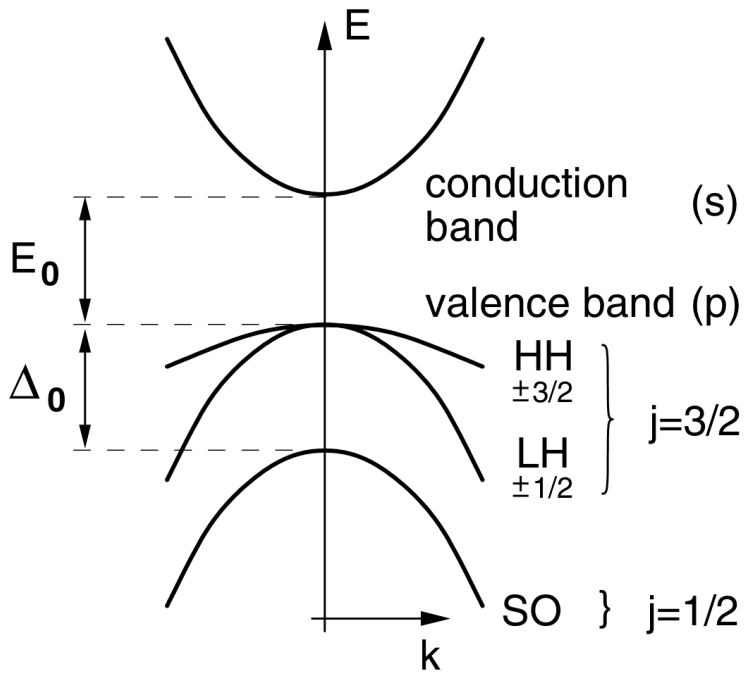

Fig. 3.1 Qualitative illustration of the band structure of GaAs. Here, j indicates the angular momentum. The figure is cited from Ref. [4].

3.1.1 In solid-state physics

In crystals, the behavior of electrons can be described by energy bands $E_n(k)$, here n is the band index, and k is the wave vector. For a system with SO coupling, the structure of the energy bands will be modified significantly.

For instance, SO coupling can split the topmost valence band in GaAs, as showed in Fig. 3.1 (The figure is cited from Ref. [4]). Actually, if we don't consider the spin, the electron states are degenerate at the edge of the valence band. However, if we add the SO coupling into the consideration, we find that the electron states will split to different states with a energy gap $\triangle_0$, which is called SO gap.

3.1.2 In ultracold atomic system

Most researches on the SO coupling are about the fermions, like electrons, in solid-state physics as showed in the last section.

On the other hand, the advantage of ulracold quantum gases, i.e., in which all parameters can be tuned, makes the research of SO coupling in BECs to be pos-

Table 3.1 Experimental realizations of the SO coupled Quantum Gases

Group	Element	Phenomena	Comments
NIST	^{87}Rb	Structure of BEC [7]; Partial wave scattering [44]; Spin hall effect [45]; Zitterbewegung [46]	Harmonic trap
USTC	^{87}Rb	Dipole oscillation [47]; Finite Temp. phase diagram [48]; Collective excitations [49]	Harmonic trap
Shanxi	^{6}Li	ARPES, Fermi surface transition [50]; SO coupled molecule [51]	Fermion; Harmonic trap
MIT	^{6}Li	Inverse ARPES, Zeeman Lattice [52]	Fermion
Purdue	^{87}Rb	Landau-Zener transitions [53]	Harmonic trap
WSU	^{87}Rb	Dynamical instability [54]; Collective excitations [55]	Moving OL

sible. In particular, the experiment realization of SO coupled BECs [7] and generate fermions [50] give us a whole new opportunity to study the novel states of the ultracold quantum gases (Bose-Einstein condensates and degenerate Fermion gases) that are difficult to research in solid-state systems. Up to now, a variety of research groups in the world have realized the SO coupling in different trapping potentials, such as in a harmonic trap or in a moving Optical Lattice (OL), as showed in Table 3.1 (remade based on the Ref. [56]).

Meanwhile, the theoretical research on the SO coupled quantum gases [31–33, 57–64] also make the field to be a research highlight.

3.2 Theory of Gauge Field

In quantum mechanics, the Schrödinger equation can be used to describe a physical system, it reads as

$$i\hbar\frac{\partial\Psi}{\partial t} = H\Psi, \tag{3.1}$$

where Ψ indicates the wave functon of system, and H is the Hamiltonian of systems. It can be shown that the solution of the Schrödinger equation can be written as

$$\Psi(\mathbf{r}, t) = \mathcal{U}(t)\Psi(\mathbf{r}, 0), \tag{3.2}$$

where $\mathcal{U}(t)$ is the time evolution operator

$$\mathcal{U}(t) = \exp(-i\frac{Ht}{\hbar}). \tag{3.3}$$

In the setting, if a charged particle with charge q and mass m undergoes a electromagnetic field, the Hamiltonian of the system will have a change, then it can be written in terms of the scalar potential ϕ and the vector potential $\mathbf{A}$ as [65]

$$H = \frac{1}{2m}(\mathbf{P} - \frac{q\mathbf{A}}{c})^2 + q\phi \tag{3.4}$$

where c is the velocity of light in vacuum, then we can write the electric and magnetic fields down like,

$$\mathbf{E} = -\nabla\phi - \frac{\partial \mathbf{A}}{\partial t}, \tag{3.5}$$

$$\mathbf{B} = -\nabla\mathbf{A}, \tag{3.6}$$

One can find that the gauge potential $\mathbf{A}$ can give rise to the electric and magnetic fields for a charged particle.

3.2.1 Abelian case

The gauge potential $\mathbf{A}$ is a vector, it has three components in three-dimensional co-ordinates. Based on the difference of its commutation relationship, we have two kind of the gauge potential. For a gauge potential $\mathbf{A} = (A_x, A_y, A_z)$, if

$$[A_i, A_j] = 0, \tag{3.7}$$

where, $i, j = x, y, z$, then, we call the potential is abelian one.

3.2.2 Non-Abelian case

In contrast with abelian case, for a gauge potential $\mathbf{A}$, if

$$[A_i, A_j] \neq 0, \tag{3.8}$$

then, we call the potential is non-abelian.

3.3 Experimental Realization of Synthetic Gauge Field

In general, researchers study the Abelian and Non-abelian gauge fields for fermions, like electrons, in solid state physics. However, the ultracold atomic gases with the advantage of all parameters of the system can be tuned, gives us an opportunity to study these problems by using bosons in the system made in laboratory. Owing to this, we call the system with gauge potential, Synthetic Gauge Field.

Actually, up to now, two kinds of gauge field, including abelian [6, 66, 67] and non-abelian one [7] have been realized in boson system. Fig. 3.2 showed the set-ups of experimental realization for different synthetic gauge fields with ultracold atomic gases.

3.3.1 Abelian: Synthetic magnetic field

In the part, we take the synthetic magnetic field as an example to introduce the experimental realization of synthetic abelian gauge field at NIST [6].

Fig. 3.3 shows the details of the experiment, (a) shows the geometry of the system, (b) shows the energy level of atoms, (c) shows the dispersion relation, (d) shows the synthetic vector potential induced by atom-light interaction in (a), (e) and (f) give the spin projection for the dressed states in the case of $\delta = 0$ and not.

Actually, the method described here for creating the synthetic magnetic fields for neutral atoms comes from a fundamental concept in quantum mechanics, i.e., the Berry phase. The method is different with the method by rotating the ultracold atomic gases. Before the experiment of the synthetic magnetic fields, the method of rotating the system is a choice to research the physics of gauge field in quantum gases, even though there are some limitation, such as, adding optical lattices is difficult for the rotating system, the heating issue reduced by the rotation, the difficulty to adding large angular momentum, and it is not easy to fall into the quantum hall region. However, the method of creating the synthetic magnetic fields by Berry phase will taking these advantages. At first, adding an optical lattice is easy for the system, so that the system can be used to research the fractal energy levels of the Hofstadter butterfly. Second, if one adding one-dimentilnal lattice to the system, then the BEC will into an array of two-dimensional systems normal to the field. In addition, by tuning property parameters, the quantum hall regime ca be accessed by the approach.

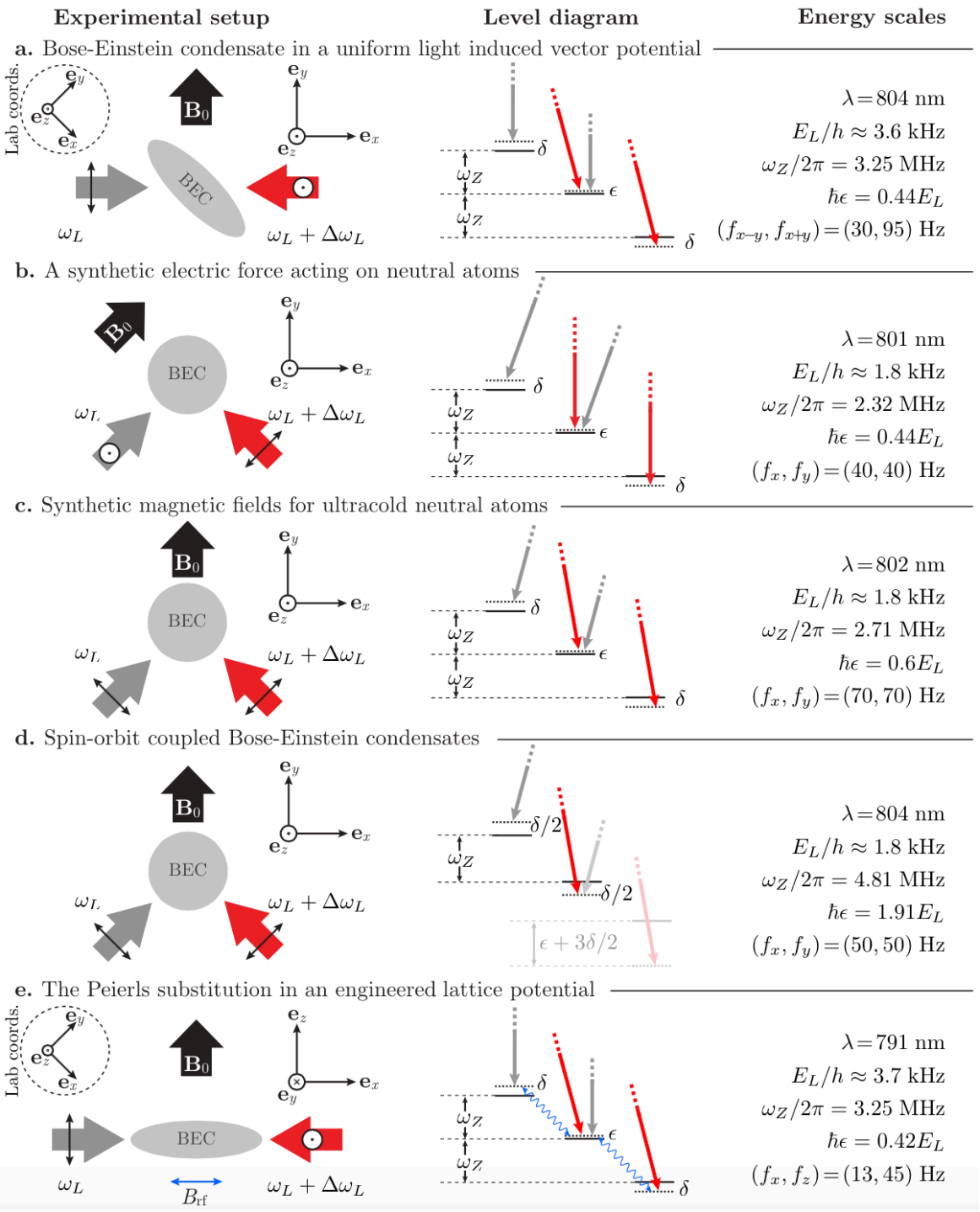

Fig. 3.2 Experimental setups for creating the synthetic gauge fields. The figure is cited from Ref. [5].

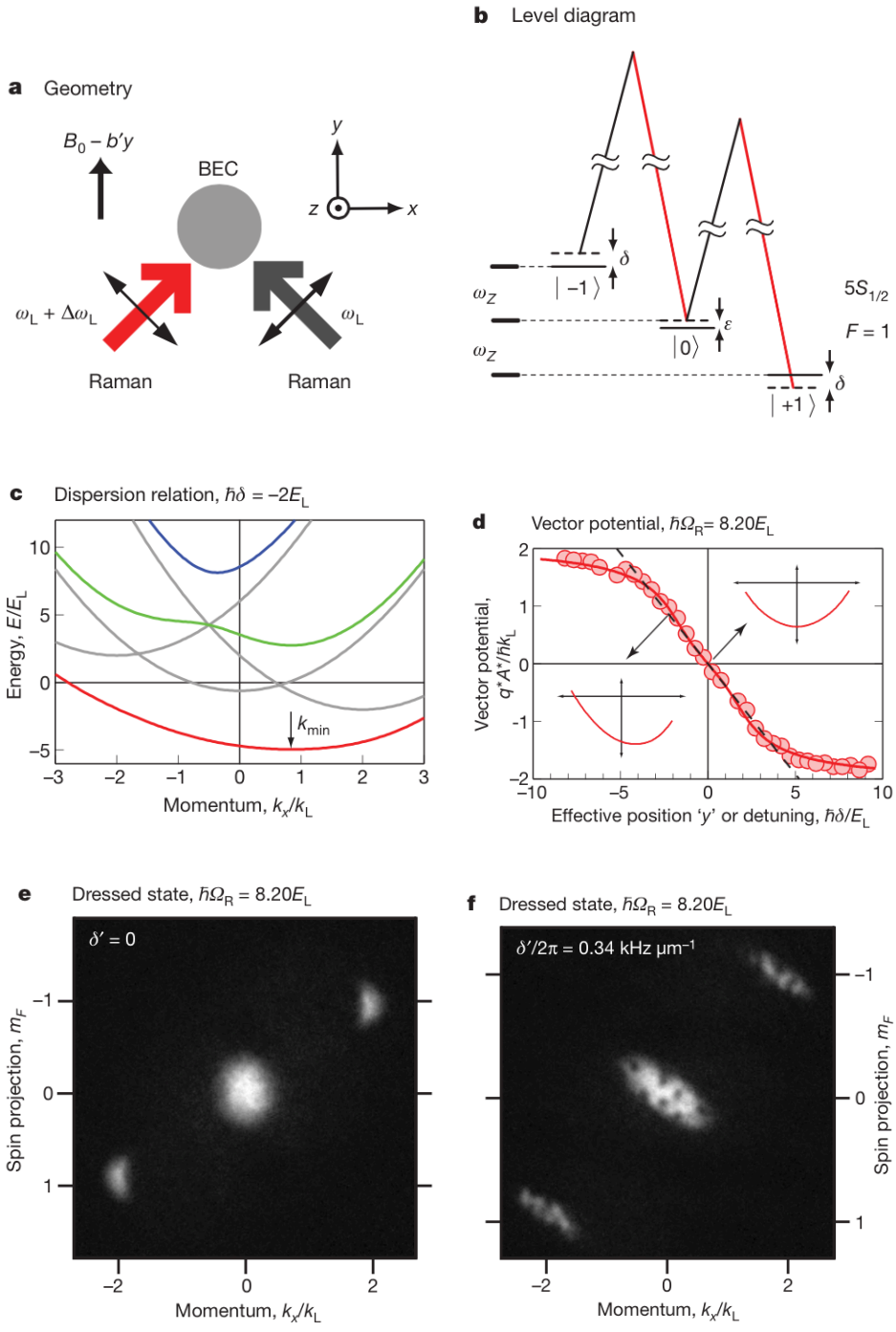

Fig. 3.3 Experiment summary for synthetic magnetic fields for neutral atoms. For the details of the experiment, see the Ref. [6].

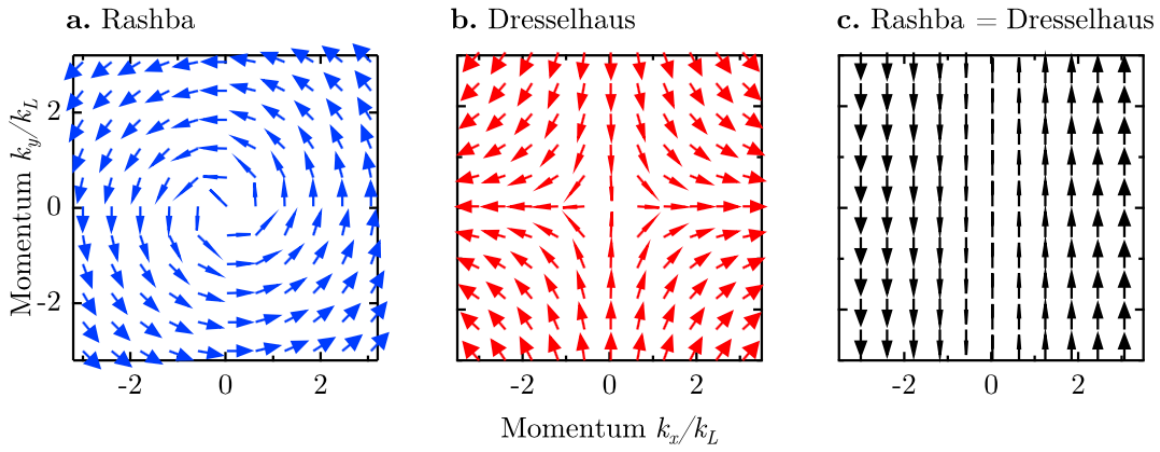

Fig. 3.4 Different kinds of Spin-Orbit coupling in the momentum space of composed of k_x and k_y. **a**. Rashba SO coupling. **b**. The linear Dresselhaus type SO coupling. **c**. A equal sum of Rashba and Dresselhaus SO coupling. The figure is cited from Ref. [5].

3.3.2 Non-Abelian: Synthetic Spin-Orbit Coupling

The experimental realization [7] of another kind of synthetic gauge field, non-abelian one, will be introduced in the part.

The SO coupling expresses the interaction between the spin and the momentum of a quantum particle. It is novel and ubiquitous for quantum systems. In the experiment, researchers engineered a SO coupled BECs with equal Rashba and Dresselhaus strengths by dressing two atomic internal states with a pair of lasers. The realization of the SO coupling BEC is the first time to produces a SO coupling by using bosons. In addition, the interaction of the two dressed states of the system will be changed if the laser coupling takes place, and gives rise to a quantum phase transition between the spin-mixed state and the phase separated state. The realization of the synthetic SO coupling sets the stage for the research of the topological insulators.

In the experiment, researchers use a pair of Raman lasers interacting with BECs of ^{87}Rb to created the synthetic SO coupling for neutral atoms [7]. The SO coupling system we discussed in the part is a superposition of equal strength of the Rashba and Dresselhaus types of the SO coupling.

The details of the experiment is shown in Fig. 3.5 and Fig. 3.6. To do this, two internal states of $F = 1$ ground electronic manifold are selected as the pseudo-spin states, i.e., set the $m_F = 0$ as spin-up and $m_F = -1$ as spin-down in the

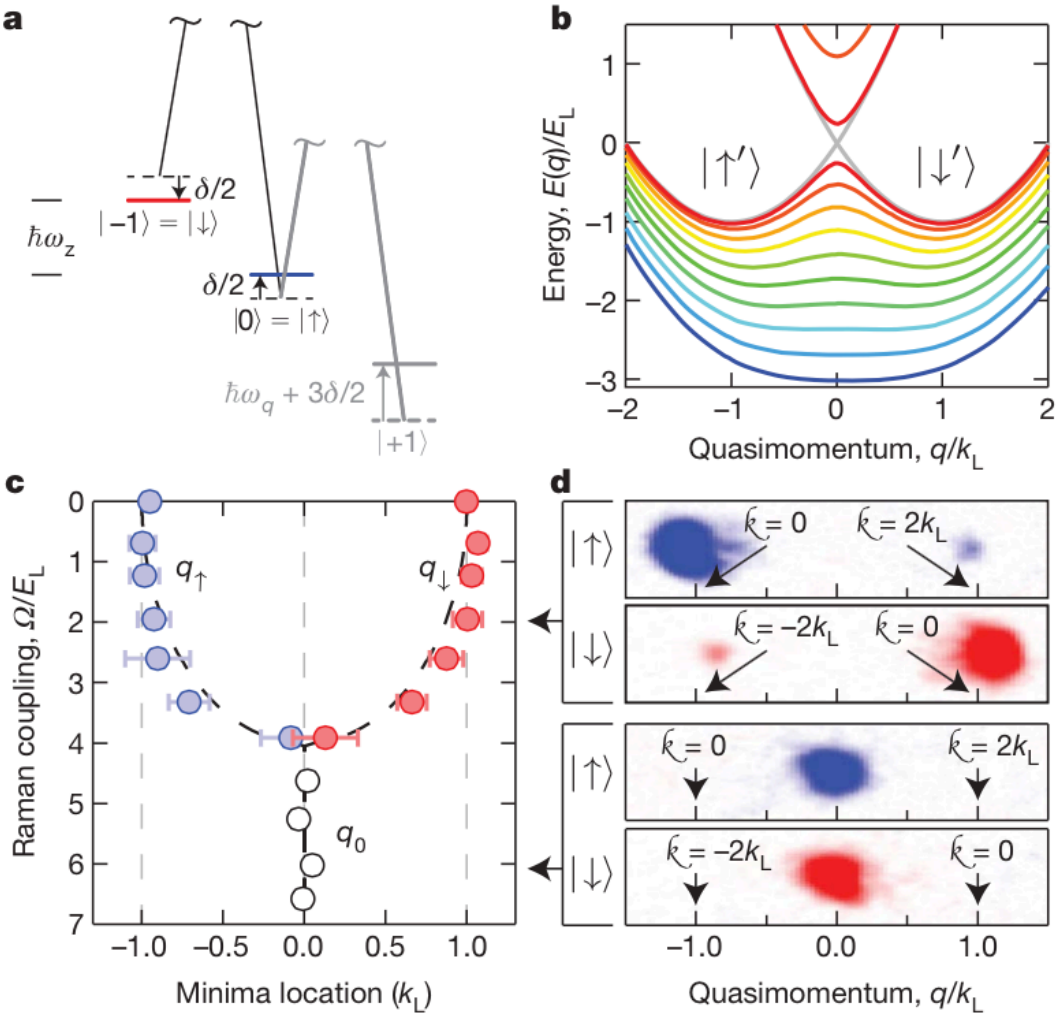

Fig. 3.5 Scheme for creating SO coupling. For the details of the experiment, see the Ref. [7].

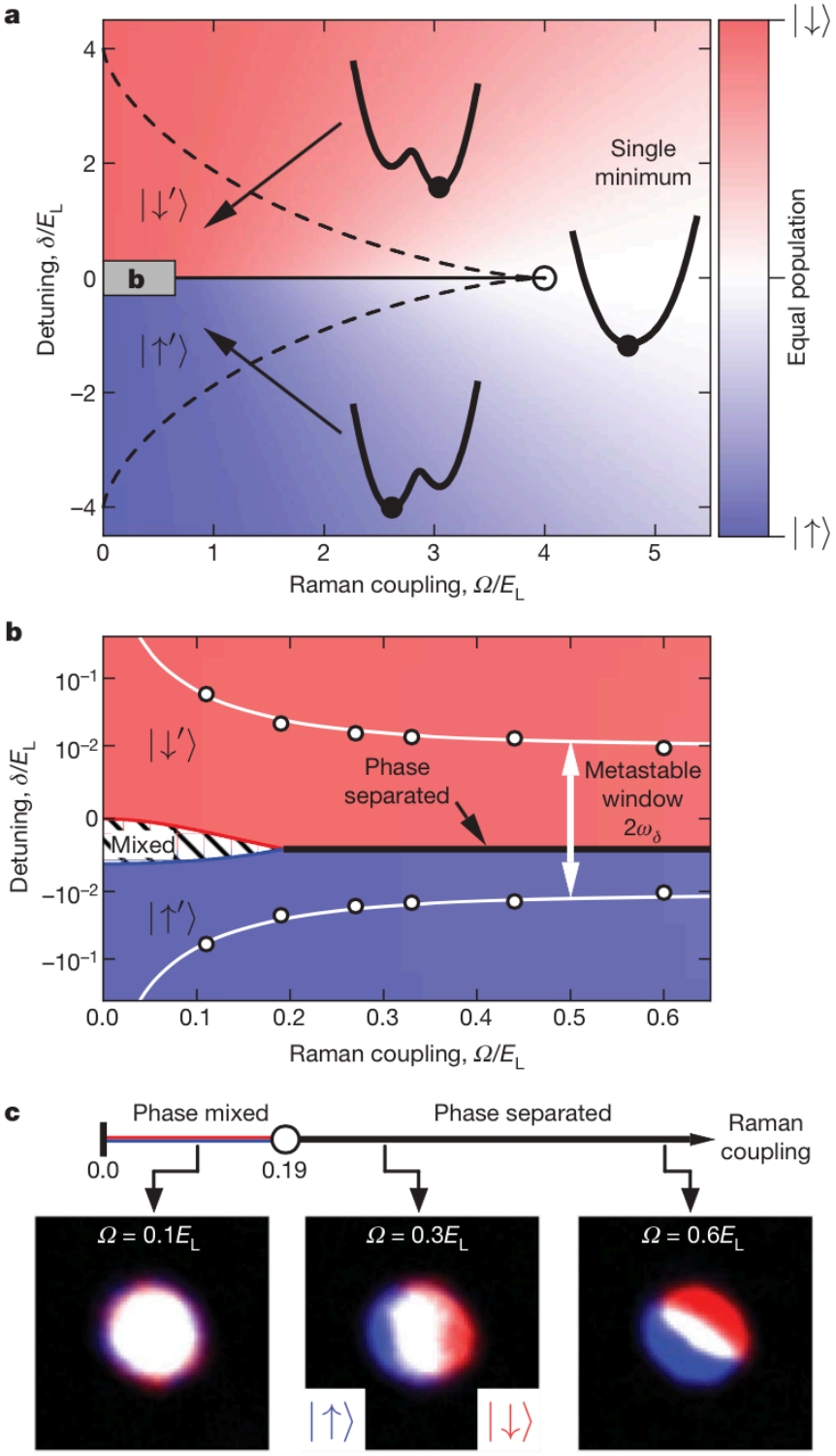

Fig. 3.6 Phases of a SO-coupled BEC. For the details of the experiment, see the Ref. [7].

pseudo-spin basis.

Fig. 3.5 shows the energy level and dispersion relations for (a) and (b), and the relationship between Raman coupling and minima locations in quasi momentum. We found that the energy dispersion relation can be changed by tuning the system's parameters, so that, we can get a deeper understanding about the synthetic quantum atomic system.

Fig. 3.6 indicates the mean-field phase diagram of ground states of the synthetic SO coupling BECs at zero temperature. In the plane of composed of the detuning and Raman coupling, the ground states including single dressed state, the phase mixed state in space and phase separated state. The critical point for the phase transition between the last two phases is 0.19 in the Raman coupling.

3.4 Bose-Einstein Condensates with Synthetic Spin-Orbit Coupling

In the part, we review the theoretical treatment of the SO coupled BECs. At first, we give the physics of single particle states, then the interaction physics of the SO coupled BECs will be considered. In particular, the ground states of the SO coupled BECs with repulsive interaction in free space and in a trap will be addressed.

3.4.1 Single-Particle Physics with Rashba SO Coupling

The single-particle Hamiltonian can be written as [58]

$$\hat{H}_0 = \int d^2\mathbf{r}\Psi^\dagger \frac{1}{2m}(\mathbf{k}^2 + 2\kappa\mathbf{k}\cdot\vec{\sigma})\Psi, \tag{3.9}$$

where $\Psi = (\Psi_\uparrow, \Psi_\downarrow)$ is the wave function for spin-up and spin-down components, For a two-dimensional system, the momentum $\mathbf{k} = \{k_x, k_y\}$ and the Pauli matrix $\vec{\sigma} = \{\vec{\sigma}_x, \vec{\sigma}_y\}$.

The energy dispersion of the single-particle Hamiltonian can be obtained as

$$E_\pm(\mathbf{k}) \propto (|\mathbf{k}| \pm \kappa)^2. \tag{3.10}$$

To confirm the ground states, we just consider the lowest branch of the energy

dispersion E_-. In the case,

$$E_-(\mathbf{k}) \propto (|\mathbf{k}| - \kappa)^2, \tag{3.11}$$

so that, the ground states will degenerate along the ring with radius κ in momentum space, but occupying the origin.

3.4.2 Interaction Physics

The interaction Hamiltonian can be written as

$$H_{int} = \int d\mathbf{r}(g\hat{n}_1^2 + g\hat{n}_2^2 + g_{12}\hat{n}_1\hat{n}_2), \tag{3.12}$$

where we treat the interaction of same series atoms to be g, and the interaction of different series of atoms is g_{12}, and $\hat{n}$ indicates the density of atoms for both components.

As mentioned in the above, the ground states is degenerated as a ring in momentum space for single-particle case, therefore, the interaction part will take a role to select the special state from the ring and to form the ground states in the interaction case. Ref. [58] confirmed that there are two kinds of the ground states: plane wave for the case of $g > g_{12}$ and stripe wave for the case of $g < g_{12}$.

For the plane wave state, the system's density is uniform, and the phase will change periodically for 0 to 2π, the rotation symmetry will be broken. The wave function for the plane wave state can be wrriten as,

$$\Psi(\mathbf{r}) \propto e^{i\kappa x} \begin{pmatrix} 1 \\ 1 \end{pmatrix}. \tag{3.13}$$

On the other hand, the stripe wave state can be seen as a superposition of two plane wave with opposite momentum,

$$\Psi(\mathbf{r}) \propto e^{i\kappa x} \begin{pmatrix} 1 \\ 1 \end{pmatrix} + e^{-i\kappa x} \begin{pmatrix} 1 \\ -1 \end{pmatrix} \propto \begin{pmatrix} \cos\kappa x \\ i\sin\kappa x \end{pmatrix}, \tag{3.14}$$

and the spin density $\rho_s(\mathbf{r})$can be written as,

$$\rho_s(\mathbf{r}) = |\Psi_1(\mathbf{r})|^2 - |\Psi_2(\mathbf{r})|^2 \propto \cos(2\kappa x), \tag{3.15}$$

it means the periodic change in space.

3.5 Spin-Orbit Coupled Bose-Einstein Condensates in a Trap

In general, the ultracold atomic gases trapped in a harmonic potential, in the case, the interplay between the confine potential and SO coupling will give rise to rich phase diagram in ground states.

The Hamiltonian of the SO coupled BECs in a trap acquires the form

$$H(\mathbf{k}) \propto (\hbar\mathbf{k} - \mathbf{A})^2 - \nabla_k^2, \tag{3.16}$$

in the case, some novel phases, such as, half-integer quantum vortices $HV(1/2)$ and $HV(3/2)$ will appear, because of the form of the eigenenergies [8],

$$E_{nl} = \frac{(l + \frac{1}{2})^2}{2\kappa^2} + n + \frac{1}{2}, \tag{3.17}$$

where n indicates the radial excitations. The half-integer quantum vortices solution can be written as

$$\Psi_0(r,\theta) \propto \begin{pmatrix} J_0(\kappa r) \\ e^{i\theta} J_1(\kappa r) \end{pmatrix}, \Psi_{-1}(r,\theta) \propto \begin{pmatrix} e^{-i\theta} J_1(\kappa r) \\ J_0(\kappa r) \end{pmatrix}, \tag{3.18}$$

Fig. 3.7 and Fig. 3.8 (both cited from Ref. [8]) shown the phases and phase diagram of the ground states of SO coupled BEC in a trap.

As shown in Fig. 3.7, the half-integer quantum vortices $HV(1/2)$ will appear when the interaction is small or zero. As increasing the interaction or SO coupling, the system can transit to the second half-integer quantum vortices state, $HV(1/2)$. Further increasing the interaction, the system favors a lattices state with six momentum components, we can found that in Fig. 3.7 (d). Finally, for bigger interactions, the system will fall into a stripe phase like in free space presented in the above part.

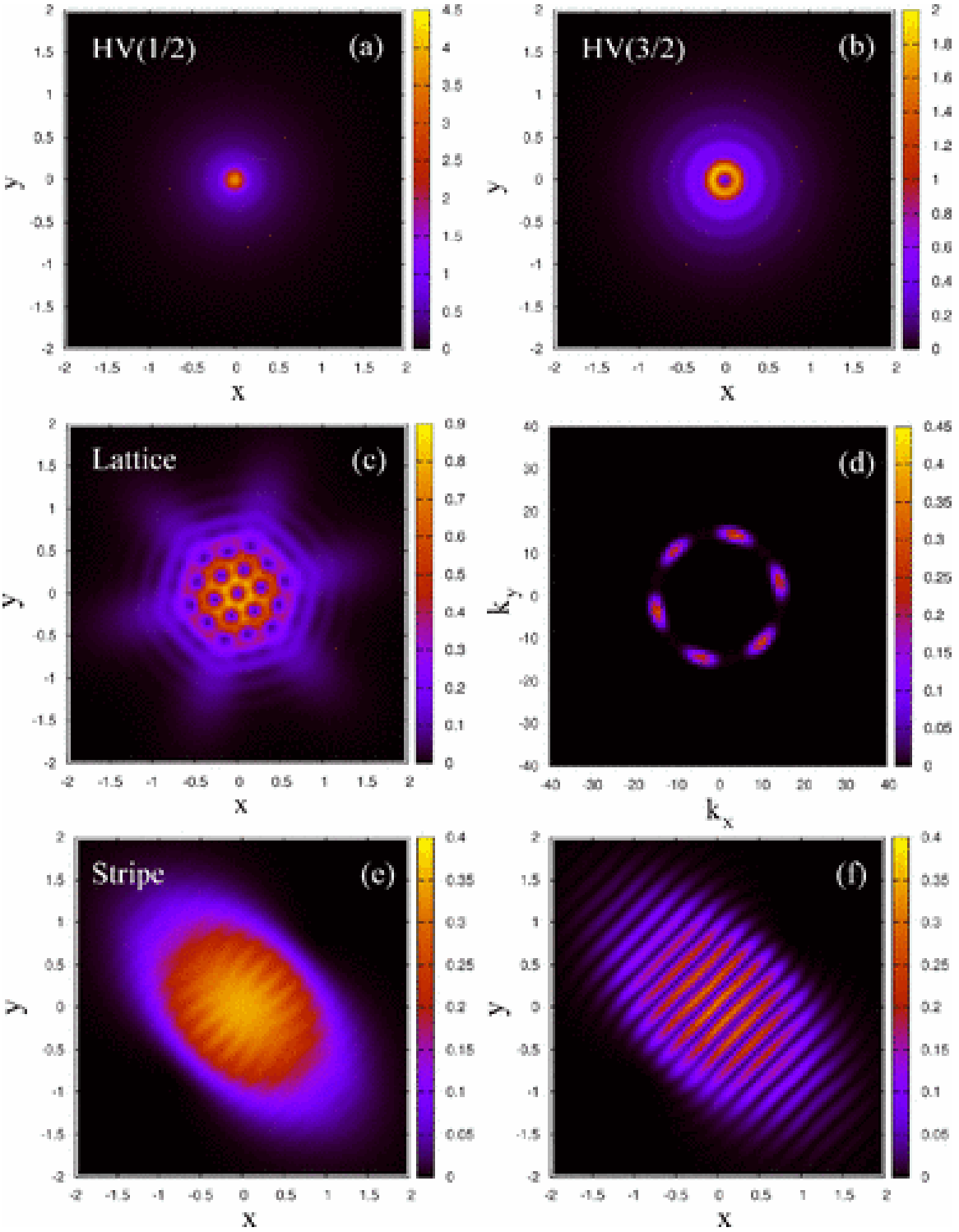

Fig. 3.7 Phases in ground state of SO coupled BECs in a trap. The figure is cited from Ref. [8].

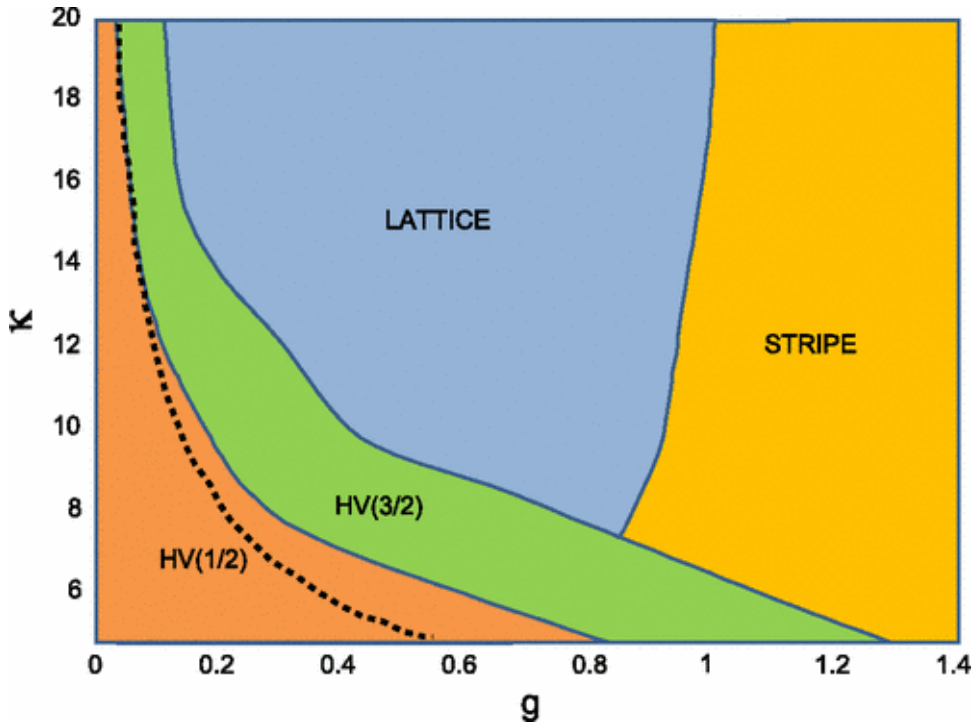

Fig. 3.8 Phases diagram of the ground state of SO coupled BECs in a trap. The figure is cited from Ref. [8].

3.6 Chapter summary

In the chapter, we have reviewed the basics of the SO coupled BECs in a trap, including the experiments and the theory.

Among them, the novel topological defects, such as, the half-quantum vortices, are the important topic. We will find that these topological defects also exist for a SO coupled BECs with attractive interaction in free space.

Chapter 4

Spin-Orbit Coupled Bose-Einstein Condensates in Free Space

In this chapter, we focus on the ground states and dynamics of two-dimensional Spin-Orbit (SO) coupled Bose-Einstein condensates with attractive interaction in free space. Up to now, most of the research on the SO coupled BECs focus on the BECs with repulsive interaction. The research here will give us an opportunity to compare the both side of interaction.

In general, the stable solutions for a two-dimensional (2D) Mean-Field (MF) models with attractive interaction in the context of both of optical fiber and matter waves are not exist, because the collapse of the system will take place. However, we found that the SO coupling can make exception for ultracold quantum gases, in which the stable solution servives. The SO coupled BECs is a good platform to research the stable solution for 2D-BECs with attractive interaction in free space. Furthermore, we found that there are two types of the stable solution in the setting, the first one is half-quantum vortices, and the second stable solution is the superposition of the half-quantum vortices and its partner with time-reversal symmetry, we call it mixed model.

4.1 Introduction

Quantum simulation has been a research highlight, because the advantage of ultracold atomic system in which all the parameters are controllable and tunable. It can be used to address the issues that is difficult to study in condensed matter physics [68]. The realization of synthetic SO coupling [7] with equal weight of the

types of Dresselhaus [69] and Rashba [70] in ultracold boson system is a great breakthrough for quantum simulation of the solid-state physics by using quantum gases. Meanwhile, other type of synthetic gauge fields [6, 66, 67], including uniform vector potential, synthetic magnetic field and synthetic electric field are also realized in NIST. The details of the experiment and theory of these topic can be got from great review papers [57, 62]

The SO coupling BECs holds a lot of important and interesting effects including half-quantum vortices [60], monopoles [71], multi-domain patterns [58, 72], tricritical points [73], solitons [74], and so on. Furthermore, other possibilities can be added by optical lattices in the setting [75], such as, the creation of gap solitons [76].

All the works mentioned above are in the context of BECs with repulsive interaction in external trapping potentials, while the situation of SO coupled BECs with attractive interaction in free space is not studied. In the chapter, we will focus on the issues [31], and address the stable topological defects, especially, vortices and solitons in the system.

4.2 Main Results

Our main results are summarized as follows,

- The ground states of the SO coupled BECs with attractive interaction in free space will fall into the half-quantum vortices state or the mixed model. based on the interplay between the same series and different series interactions. Especially, for two different families of stable vortex solitons, i.e., *half-quantum vortices* with topological charges $m = 0$ and ± 1 in the two components respectively, and the *mixed modes* in which combine $m = 0$ and ± 1 in each component in the 2D BECs with the Rashba type of the synthetic SO coupling in the *free space*.
- Both of the stable solutions will degenerate to Townes soliton which unstable if their norms reach to the critical values.
- In the absence of the Galilean invariance, the stable moving vortex solitons for both of two families are exist under a certain critical velocity.

According to what I have learned, it is the first time to confirm the existence of stable 2D solitons in any system with attractive interaction in free space, based on the interplay between the local attractive interaction and the synthetic SO coupling, although we have known that the 2D solitons can be stabilized by nonlocal

self-attraction terms [77].

4.3 Model

We start with 2D Gross-Pitaevskii equations (GPEs) of the SO coupled BECs in free space with attractive interactions in the dimensionless form,

$$\begin{aligned} i\frac{\partial\phi_+}{\partial t} &= -\frac{1}{2}\nabla^2\phi_+ - (|\phi_+|^2+\gamma|\phi_-|^2)\phi_+ + \lambda\left(\frac{\partial\phi_-}{\partial x} - i\frac{\partial\phi_-}{\partial y}\right), \\ i\frac{\partial\phi_-}{\partial t} &= -\frac{1}{2}\nabla^2\phi_- - (|\phi_-|^2+\gamma|\phi_+|^2)\phi_- - \lambda\left(\frac{\partial\phi_+}{\partial x} + i\frac{\partial\phi_+}{\partial y}\right), \end{aligned} \tag{4.1}$$

where $\boldsymbol{\phi} = (\phi_+, \phi_-)$ are the spinor wave function of the synthetic Rashba type SO coupled BEC system, λ is the strength of SO coupling, γ is the strength of the interaction of the different spin series.

In the rest part, the stationary solutions of Eq. (4.1) will be constructed by methods of the variational approximation (VA) and numerical simulation of the imaginary-time propagation method, and the dynamics of the system can be obtained by numerical simulation of the real-time propagation method.

4.4 Ground states

In the system, the ground states of the SO coupled BEC will include two types of half-quantum vortices and the mixed models.

4.4.1 Half-quantum vortices

It is easy to known that Eq. (4.1) allows a type of the stationary solutions in the following form:

$$\phi_+(x,y,t) = e^{-i\mu t} f_1(r^2),\ \phi_-(x,y,t) = e^{-i\mu t+i\theta} r f_2(r^2), \tag{4.2}$$

where μ is the chemical potential of the system, (r,θ) are polar coordinates in the plane of (x,y), and real functions $f_{1,2}(r^2)$ obey the following equations:

$$\begin{aligned} \mu f_1 + 2\left(r^2 f_1'' + f_1'\right) + \left(f_1^2 + \gamma r^2 f_2^2\right) f_1 - 2\lambda\left(r^2 f_2' + f_2\right) = 0, \\ \mu f_2 + 2\left(r^2 f_2'' + 2f_2'\right) + \left(r^2 f_2^2 + \gamma f_1^2\right) f_2 + 2\lambda f_1' = 0, \end{aligned} \tag{4.3}$$

where $f'_{1,2} \equiv df_{1,2}/d\left(r^2\right)$. These solutions are built as bound states of a fundamental soliton in component ϕ_+ (with zero topological charge, $m_+ = 0$), and a solitary vortex, with $m_- = 1$, in ϕ_- component. Accordingly, composite modes of this type may be called *half-quantum vortices*. The invariance of Eq. (4.1) with respect to the transformation,

$$\phi_\pm\left(r,\theta\right) \to \phi_\mp\left(r,\pi-\theta\right), \tag{4.4}$$

gives rise to another half-quantum vortices which is a mirror image of (4.2), with the pair of $(m_+ = 0, m_- = 1)$ replaced by $(m_+ = -1, m_- = 0)$:

$$\phi_+\left(x,y,t\right) = -re^{-i\mu t-i\theta} f_2(r^2),\ \phi_- = e^{-i\mu t} f_1(r^2). \tag{4.5}$$

The analysis of Eq. (4.3) at $r \to \infty$ shows that the respective asymptotic form of the solution written in terms of r, rather than r^2 is

$$f_1 \approx Fr^{-1/2} e^{-\sqrt{-2\mu-\lambda^2}r} \cos\left(\lambda r+\delta\right),\ f_2 \approx -Fr^{-3/2} e^{-\sqrt{-2\mu-\lambda^2}r} \sin\left(\lambda r+\delta\right), \tag{4.6}$$

where F and δ are arbitrary real constants, in terms of the asymptotic approximation. Thus, the localized modes exist at values of the chemical potential

$$\mu < -\lambda^2/2. \tag{4.7}$$

In fact, Eq. (4.6) gives the asymptotic form of the solitons not only for the half-quantum vortices, but in the general case too.

As shown below (see Fig. 4.3(c) where the half-quantum vortices branch is labeled “0", which implies that ϕ_+ contains solely the zero vorticity), the half-quantum vortices represent the ground state of the system at $\gamma \leq 1$. In fact, the coexistence of the half-quantum vortices in the two mutually symmetric forms, (4.2) and (4.5), implies the degeneracy of the ground state, which is possible in nonlinear systems.

In the past, the composite solitons consists of vortical and fundamental components were considered in a system of coupled nonlinear Schrödinger equations [78, 79]. However, the usual system cannot produces stable solitons in the free space.

The stable half-quantum vortices were generated, as solutions of Eq. (4.1) with $\gamma = 0$, by method of the imaginary-time propagation [80, 81], starting from

the following input

$$\phi_{+}^{(0)} = A_1 \exp\left(-\alpha_1 r^2\right), \ \phi_{-}^{(0)} = A_2 r \exp\left(i\theta - \alpha_2 r^2\right), \tag{4.8}$$

where $A_{1,2}$ and $\alpha_{1,2}(>0)$ are real constants. Obviously, this input conforms to the general ansatz (4.2) for the half-quantum vortices. Figure 4.1(a) displays profiles $|\phi_{+}(x,0)|$ and $|\phi_{-}(x,0)|$ of a typical stable half-quantum vortices, in the cross section of $y=0$, produced by the numerical solution for value $N=5$ of the total norm,

$$N = \int\int (|\phi_{+}|^2 + |\phi_{-}|^2) dxdy \equiv N_{+} + N_{-}. \tag{4.9}$$

Further, Fig. 4.1(b) represents the entire family of half-quantum vortices by showing their chemical potential μ as a function of N. Note that the $\mu(N)$ dependence satisfies the Vakhitov-Kolokolov (VK) criterion [82–84], $d\mu/dN < 0$, which is a necessary condition for the stability of solitary modes supported by the attractive interaction, although it does not secure stability of vortex solitons against splitting. We stress that, as clearly seen in Fig. 4.1(b), there is no finite threshold value of N necessary for the existence of the half-quantum vortices.

The wave form (4.8) can be used not only as the input for the imaginary-time simulations, but also as a variational ansatz. Its substitution in the expression for the total energy corresponding to Eqs. (4.1),

$$\begin{aligned} E = \int\int \Bigg\{ & \frac{1}{2}\left(|\nabla\phi_{+}|^2 + |\nabla\phi_{-}|^2\right) - \frac{1}{2}\left(|\phi_{+}|^4 + |\phi_{-}|^4\right) - \gamma|\phi_{+}|^2|\phi_{-}|^2 \\ & + \frac{\lambda}{2}\left[\phi_{+}^{*}\left(\frac{\partial\phi_{-}}{\partial x} - i\frac{\partial\phi_{-}}{\partial y}\right) + \phi_{-}^{*}\left(-\frac{\partial\phi_{+}}{\partial x} - i\frac{\partial\phi_{+}}{\partial y}\right)\right] + \text{c.c.}\Bigg\} dxdy, \end{aligned} \tag{4.10}$$

where c.c. stands for the complex conjugate, yields

$$E_{\text{semi}} = \pi\left[\frac{A_1^2}{2} - \frac{A_1^4}{8\alpha_1} + \frac{A_2^2}{2\alpha_2} - \frac{A_2^4}{64\alpha_2^3} - \frac{\gamma A_1^2 A_2^2}{4(\alpha_1+\alpha_2)^2} + \frac{4\lambda A_1 A_2 \alpha_1}{(\alpha_1+\alpha_2)^2}\right], \tag{4.11}$$

while the total norm (4.9) of the ansatz is

$$N = \pi\left[A_1^2/\left(2\alpha_1\right) + A_2^2/\left(4\alpha_2^2\right)\right]. \tag{4.12}$$

Then, values of amplitudes A_1, A_2 and inverse squared widths α_1,α_2 of the ansatz are predicted by the minimization of E with respect to the variational parameters, $\partial E_{\text{semi}}/\partial\left(A_{1,2}, \alpha_{1,2}\right) = 0$. These equations can be easily solved numerically.

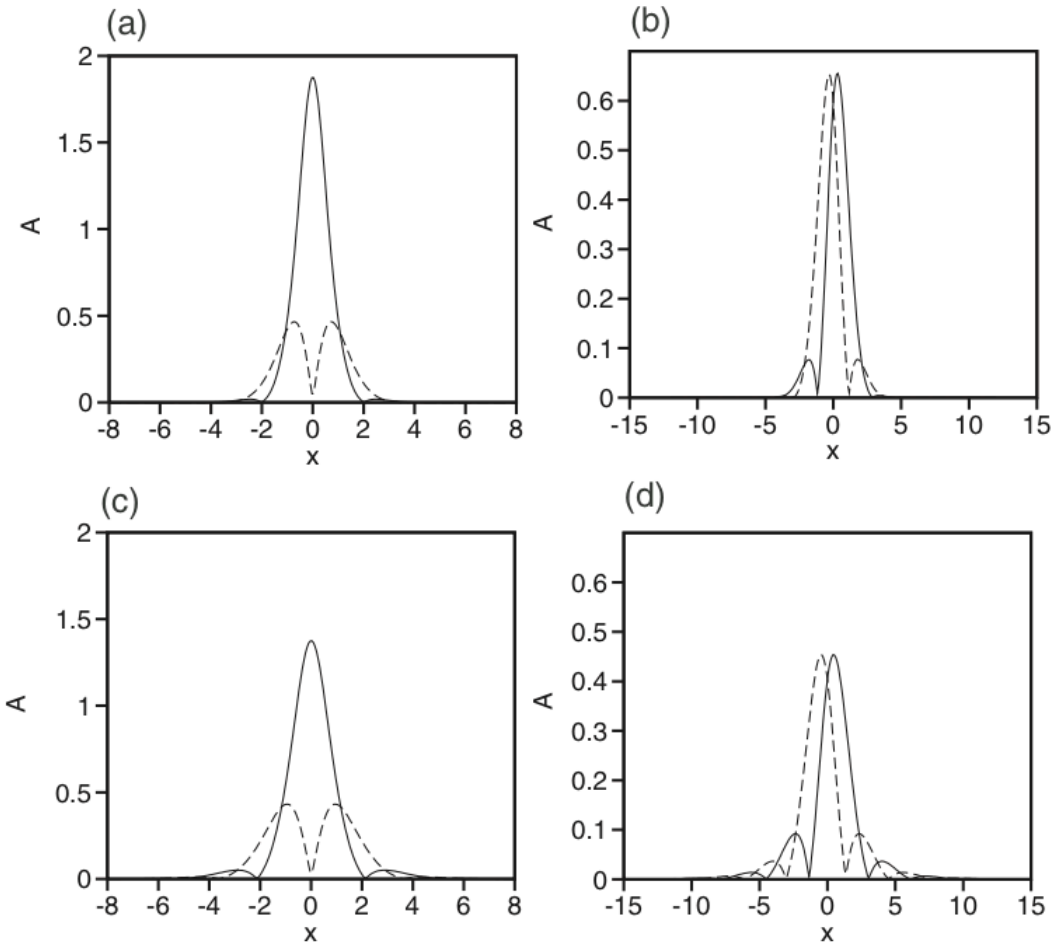

Fig. 4.1 Amplitudes of the SO coupled BEC. (a) Two components of a stable half-quantum vortices initiated by input (4.8), $|\phi_+(x,0)|$ (the solid curve) and $|\phi_-(x,0)|$ (the dashed curve) at $\gamma = 0, \lambda = 1$ and $N = 5$. (b) The same for a mixed mode with norm $N = 2$, initiated by input (4.13), with $\gamma = 2, \lambda = 1$. Both solutions were generated by imaginary-time simulations. (c) and (d) Shapes into which the modes from panels (a) and (b) relax, adiabatically following the decrease of the trap's strength from $\Omega = 0.5$ to 0.

Figure 4.1(c) displays the comparison of the so predicted amplitude A_1 and the maximum value of $|\phi_+|$ obtained from the imaginary-time-generated solution at $\gamma = 0$. The family of the half-quantum vortices exists at $N < N_c \approx 5.85$, the latter value being the well-known collapse threshold for fundamental (Townes) solitons in the free 2D space [85, 86]. Indeed, Fig. 4.1(d) shows, by means of the dependence of ratio N_+/N on N, that the vortical component ϕ_- vanishes at $N \to N_c$, hence in this limit the half-quantum vortices degenerates into the usual unstable Townes soliton, which is subject to the collapse.

In the opposite limit of $N \to 0$, the nonlinear terms in Eqs. (4.1) become vanishingly small, and the ground-state solution degenerates into a quasi-plane-wave with vanishing amplitudes, radial wavenumber λ and chemical potential $\mu_0 = -\lambda^2/2$, see Eqs. (4.6) and (4.7) [57]. In accordance with this expectation, Fig. 4.1(d) shows that $N_+/N \to 1/2$ at $N \to 0$. The comparison with the full numerical solutions demonstrates that Gaussian ansatz (4.8) is inaccurate for small N, therefore Fig. 4.1(c) shows a large relative discrepancy between the variational and numerical results at very small N.

4.4.2 Mixed modes

Another type of 2D self-trapped vortical states supported by the SO coupling model (4.1) can be initiated by the following input for the imaginary-time simulations, which may also serve as the variational ansatz:

$$\begin{aligned} \phi_+^{(0)} &= A_1 \exp\left(-\alpha_1 r^2\right) - A_2 r \exp\left(-i\theta - \alpha_2 r^2\right), \\ \phi_-^{(0)} &= A_1 \exp\left(-\alpha_1 r^2\right) + A_2 r \exp\left(i\theta - \alpha_2 r^2\right). \end{aligned} \tag{4.13}$$

Modes generated by this input may be called mixed ones, as they are built as superpositions of states with topological charges $(0, -1)$ and $(0, +1)$ in the two components. Unlike the half-quantum vortices, it is not possible to find an exact representation for these modes similar to that given by Eqs. (4.2) and (4.3), but the numerical and variational results clearly demonstrate that they exist. Moreover, they play the role of the ground state of the system at $\gamma \geq 1$, see Fig. 4.3(c) below, where the mixed-mode branch is labeled “01", as vorticities 0 and ± 1 are combined in these modes. In accordance with the form of ansatz (4.13), the mixed mode is transformed into itself by symmetry reflection (4.4).

A typical example of cross sections of a stable mixed mode in shown in Fig. 4.2(a) for $\gamma = 2$ and $N = 2$. The $\mu(N)$ dependence for the family of these modes is

displayed in Fig. 4.2(b), which shows that the VK criterion holds in this case too, as well as in the case of half-quantum vortices, the mixed modes do not require any finite threshold value of N necessary for their existence. The family exists in the interval of

$$N < N_c' = 2N_c/(1+\gamma), \tag{4.14}$$

where N_c is the above-mentioned critical norm corresponding to the Townes solitons. Indeed, in the limit of $N \to N_c'$ the vortical components in the mixed mode vanish, and it degenerates into the two-component Townes soliton, similar to the degeneration of the half-quantum vortices, see Figs. 4.1(b) and (c). In the opposite limit of $N \to 0$, the mixed mode degenerates into a quasi-plane-wave with chemical potential $-\lambda^2/2$, which is also similar to the behavior of the half-quantum vortices, in the same limit.

The insertion of input (4.13), as the variational ansatz, into energy functional (4.10) yields

$$E_{\rm mixed} = \pi \left[A_1^2 + \frac{A_2^2}{\alpha_2} - (1+\gamma)\left(\frac{A_1^4}{4\alpha_1} + \frac{A_2^4}{32\alpha_2^3} \right) - \frac{A_1^2 A_2^2}{(\alpha_1+\alpha_2)^2} + \frac{8\lambda A_1 A_2 \alpha_1}{(\alpha_1+\alpha_2)^2} \right], \tag{4.15}$$

the total norm of the ansatz being

$$N = \pi \left[\frac{A_1^2}{\alpha_1} + \frac{A_2^2}{(2\alpha_2^2)} \right]. \tag{4.16}$$

Numerical solution of the respective energy-minimization equations,

$$\frac{\partial E_{\rm mixed}}{\partial \left(A_{1,2}, \alpha_{1,2} \right)} = 0, \tag{4.17}$$

produces values of the parameters of the variational ansatz. Figure 4.2(c) compares the absolute value of the fields at the central point, $|\phi_+(0,0)|$ and its variational counterpart, $|A_1|$, as a function of the total norm.

As seen in Fig. 4.2(a), peak positions of components $|\phi_+(x,y)|$ and $|\phi_-(x,y)|$ are separated along x, Fig. 4.2(d) showing the separation (DX) as a function of the norm. For a small amplitude of the vortex component, A_2, Eq. (4.13) yields

$$\mathrm{DX} \approx \frac{A_2}{\alpha_1 A_1}. \tag{4.18}$$

The separation vanishes as N approaches the aforementioned critical value N_c', at which the mixed mode degenerates into the two-component Townes solitons. This

is explained by the fact that, as said above, the vortical components of the wave functions, which cause the shift of the peaks from the center, vanish in this limit.

4.5 Excited states

In addition to two types of the ground states, half-quantum vortices and mixed modes, numerical analysis reveals their excited versions. First, a set of exciting states can be constructed following the pattern of the half-quantum vortices (4.2):

$$\begin{aligned} \phi_+(x,y,t) &= e^{-i\mu t+iS\theta} r^S f_1(r^2), \\ \phi_-(x,y,t) &= e^{-i\mu t+i(S+1)\theta} r^{S+1} f_2(r^2), \end{aligned} \tag{4.19}$$

with integer $S \geq 1$. The substitution of this ansatz into Eq. (4.1) leads to a system of equations for $f_{1,2}(r^2)$:

$$\begin{aligned} \mu f_1 + 2r^2 f_1'' + 2(1+S) f_1' + r^{2S}({f_1}^2 + \gamma r^2 {f_2}^2) f_1 - 2\lambda \left[r^2 f_2' + (1+S) f_2 \right] = 0, \\ \mu f_2 + 2r^2 f_2'' + 2(2+S) f_2' + r^{2S}(r^2 {f_2}^2 + \gamma {f_1}^2) f_2 + 2\lambda f_1' = 0. \end{aligned} \tag{4.20}$$

In the case of $S = 0$, Eq. (4.20) is tantamount to Eq. (4.3) for the half-quantum vortices. Of course, mirror-image counterparts of excited states (4.19), generated by transformation (4.4), exist too.

In the numerical form, the excited state corresponding to $S = 1$ in Eq. (4.19) was found by means of the imaginary-time integration starting with the following input:

$$\begin{aligned} \phi_+ &= A_1 r e^{i\theta} e^{-\alpha_1 r^2 - i\mu t}, \\ \phi_- &= A_2 r^2 e^{2i\theta} e^{-\alpha_2 r^2 - i\mu t}. \end{aligned} \tag{4.21}$$

Figure 4.3(a) shows cross-section profiles for an example of this excited state, obtained with $N = 5$ and $\gamma = 0$. In Figs. 4.3(c,d), the branch of these excited-state solutions is labeled “1", as it contains vorticity $m_+ = 1$ in component ϕ_+.

Another type of excited states was generated by the input with combined vorticities, $m_+ = 1, -2$ and $m_- = -1, 2$, therefore it is labeled “12" in Figs. 4.3(c,d):

$$\begin{aligned} \phi_+ &= A_1 r e^{i\theta} e^{-\alpha_1 r^2 - i\mu t} - A_2 r^2 e^{-2i\theta} e^{-\alpha_2 r^2 - i\mu t}, \\ \phi_- &= A_1 r e^{-i\theta} e^{-\alpha_1 r^2 - i\mu t} + A_2 r e^{2i\theta} e^{-\alpha_2 r^2 - i\mu t}. \end{aligned} \tag{4.22}$$

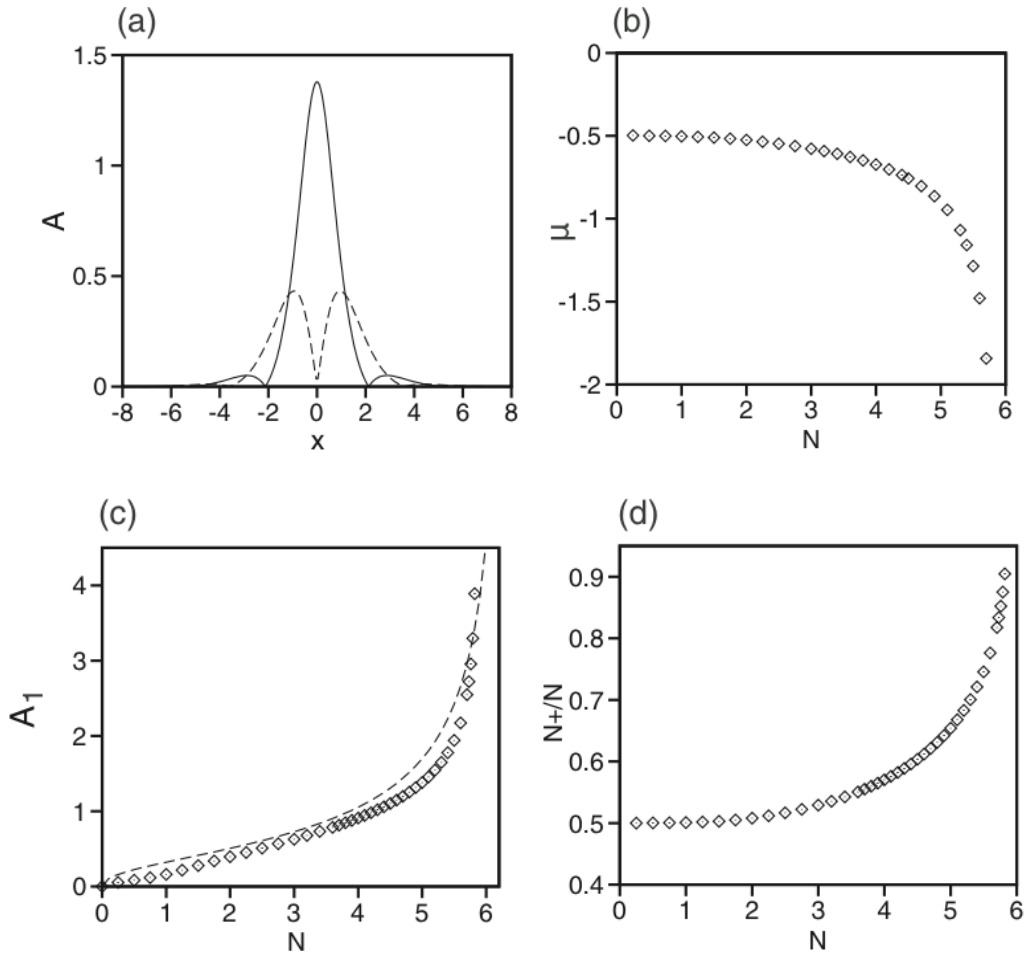

Fig. 4.2 Half-quantum vortices in free space. (a) The same as in Fig. 4.1(a), but for the stable half-quantum vortices without trapping potential. (b) Chemical potential as a function of norm for the family of the localized half-quantum vortices. (c) Comparison of the numerically found amplitude (the chain of rhombuses), and A1, as predicted by the variational approximation (the dashed curve). (d) Ratio N_+/N as a function of N, for the family of the half-quantum vortices.

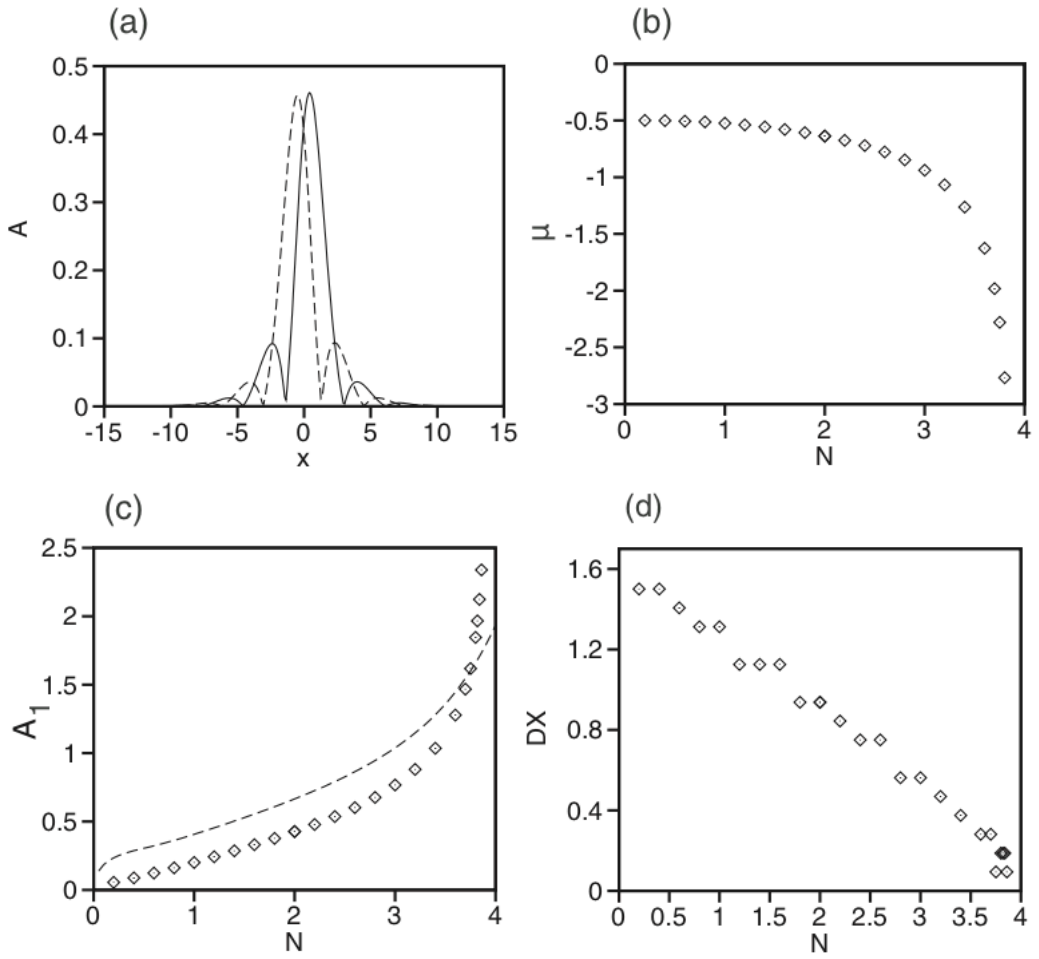

Fig. 4.3 Mixed modes of the ground states of SO coupled BECs in free space. (a) The amplitude of the stable mixed mode in free space, other parameters are same with Fig. 4.1 b. (b) The chemical potential as a function of norm of condensates, for $\gamma = 2$ and $\lambda = 1$. (c) The comparison of the central amplitude of the mixed mode in free space by numerical simulation (the chain of the rhombuses) and the variational analysis (the dashed curve) as a function of the norm N. (d) The separation DX between peak positions of the amplitude of spin-up and spin-down components as a function of the norm N.

This input can be also cast into the form of

$$\phi_+ = re^{i\theta}(A_1 e^{-\alpha_1 r^2 - i\mu t} - A_2 r^2 e^{-3i\theta} e^{-\alpha_2 r^2 - i\mu t}),$$
$$\phi_- = e^{-i\theta}(A_1 e^{-\alpha_1 r^2 - i\mu t} + A_2 r^2 e^{3i\theta} e^{-\alpha_2 r^2 - i\mu t}), \tag{4.23}$$

which implies that it includes a vortex with topological charge 1 set at $(x, y) = (0, 0)$, and three vortices with charges -1 surrounding the origin. Figure 4.3(b) corroborates this interpretation by means of a contour plot of $|\phi_+(x, y)|$, which features three peaks and three holes around the origin. The holes are pivots of the three above-mentioned vortices with charges -1. The pattern is symmetric with respect to rotation by angle $2\pi/3$. The respective contour map of $|\phi_-(x, y)|$ (not shown here) is a mirror image of $|\phi_+(x, y)|$, generated by transformation (4.4). This solution resembles a lattice state found in Ref. [87] for the SO-coupled BEC with the self-repulsive interactions, trapped in a harmonic-oscillator potential.

4.6 Dynamics

4.6.1 The identification of the ground state, and dynamical stability of the vortical modes

The four types of the vorticity-carrying self-trapped modes, generated by inputs (4.2), (4.13), (4.21), and (4.22), respectively, can be produced by the imaginary-time integration of Eq. (4.1) for any value of the interaction constant, γ, in addition to the two latter modes, excited states of still higher orders can be found too, e.g., those given by Eq. (4.19) with $S > 1$, but they all are unstable. To identify the system's ground state, the total energies of the four species of the vortical modes, calculated as per Eq. (4.10), and denoted as E_0 (for the half-quantum vortices), E_{01} (for the mixed mode), and E_1, E_{12} for the excited states (4.21) and (4.22), respectively, are displayed vs. γ in Figs. 4.3(c,d), for two fixed values of the total norm, $N = 3.7$ and $N = 3$. It is found that the energies satisfy relations $E_0 < E_{01} < E_{12} < E_1$ at $\gamma < 1$ and $E_{01} < E_0 < E_1 < E_{12}$ at $\gamma > 1$. It is seen that the half-quantum vortices and mixed state realize the ground state at $\gamma < 1$ and $\gamma > 1$, respectively, while the states labeled “1" and “12" are indeed excited states, separated by a wide energy gap from the competing ground-state modes. The fact that the switch of the ground states occurs at $\gamma = 1$ is not surprising, as it corresponds to the Manakov's nonlinearity, with equal interaction coefficients,

which is known to feature various degeneracies in nonlinear systems, see, e.g., Ref. [88, 89]. It is relevant to mention that the value of γ, which is the ratio of the strengths of the different types of interactions, may be readily altered by means of the Feshbach resonance [90], hence the type of the ground state may be controlled by means of this technique.

The stability of the four species of 2D self-trapped modes constructed above was studied by means of systematic numerical simulations of their perturbed evolution in the framework of Eq. (4.1). The results are reported here for the generic case, represented by two values of the interaction coefficient, $\gamma = 0$ and 2, and a fixed norm, $N = 3.7$. The first result is that the half-quantum vortices, which is the ground state at $\gamma = 0$, and the mixed mode, which plays the same role at $\gamma = 2$, are stable against perturbations.

Next, it is obviously interesting to test the stability of the same two species in the cases when they are *not* ground states, i.e., the half-quantum vortices at $\gamma = 2$, and the mixed mode at $\gamma = 0$. In the former case, we observe in Fig. 4.4(a) that the profile of the half-quantum vortices keeps the initial shape from $t = 0$ till $t = 500$, which exceeds 50 diffraction times for the present mode. However, an instability manifests itself in spontaneous motion of the soliton with a nearly constant velocity, as seen in Fig. 4.4(b), where coordinates of the peak position of the ϕ_+ component, (X, Y), are shown as a function of time. On top of the mean velocity, the peak features oscillatory motion (a cycloid) with a small amplitude, see Fig. 4.4(c).

The evolution of the mixed mode at $\gamma = 0$, when it is not the ground state either, is shown in Fig. 4.5. Panels (a) and (b), pertaining to $t = 50$ and $t = 750$ (the latter can be estimated to be $\simeq 100$ diffraction times of the present mode), demonstrate that this state is unstable, starting spontaneous motion and losing the original symmetry between $|\phi_+|$ and $|\phi_-|$ with respect to to transformation (4.4). By $t = 750$, the mixed mode rearranges into a state close to a half-quantum vortices. Further, Fig. 4.5(c) shows the time evolution of amplitudes of the ϕ_+ and ϕ_- components (the solid and dashed curves, respectively). Breaking the original symmetry, the amplitude of $|\phi_+|$ increases toward the value of the amplitude of the $|\phi_+|$ component of the half-quantum vortices state for the same $N = 3.7$ (that amplitude is ≈ 0.81), while the amplitude of $|\phi_-|$ falls to become nearly equal to the amplitude of the $|\phi_-|$ component of the same half-quantum vortices (the latter amplitude is ≈ 0.34). Figure 4.5(d) shows a trajectory of the peak position of the $|\phi_+|$ component. The localized state moves spontaneously, featuring oscillations

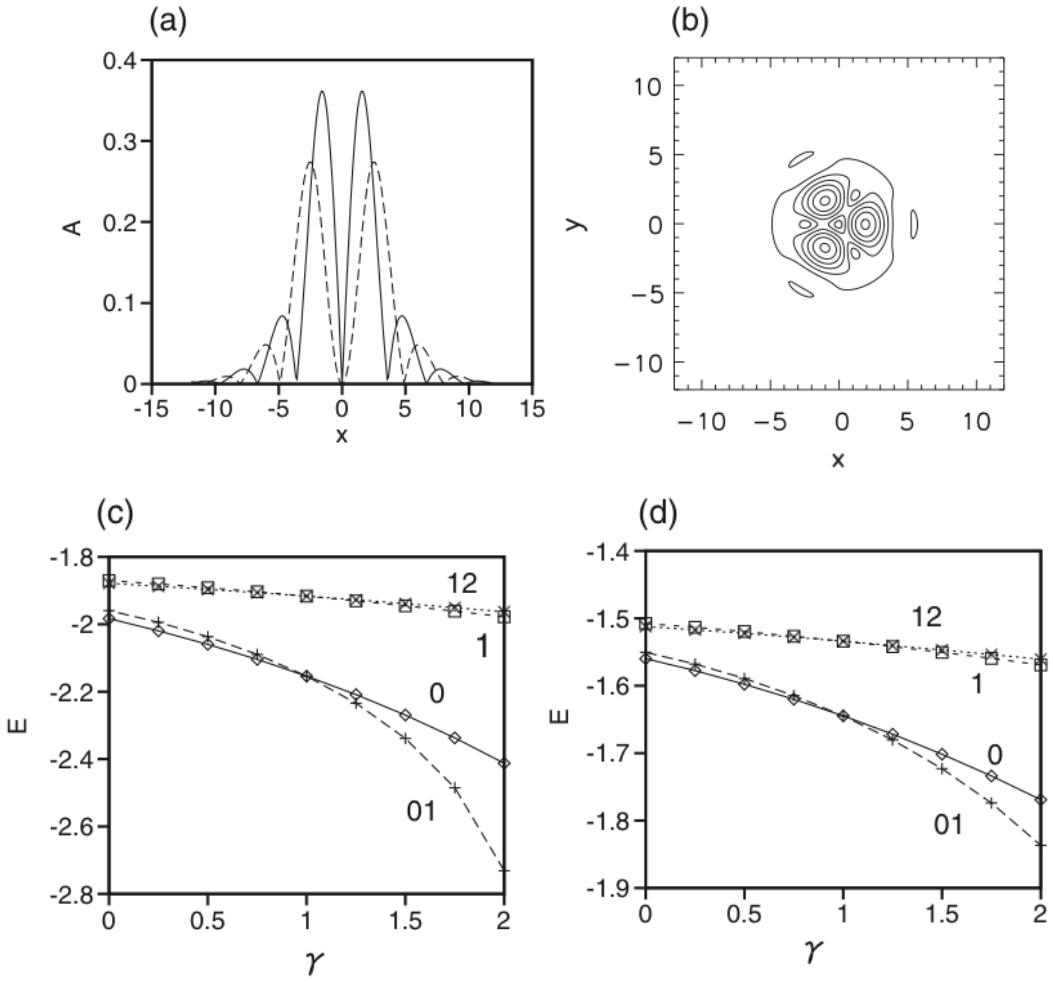

Fig. 4.4 Excited state of the SO coupled BECs in free space. (a) The amplitude of the spin-up (solid curve) and the spin-down (dashed curve) components for $N = 5$, $\lambda = 1$ and $\gamma = 0$. (b) Contour plot of the spin-up component for $N = 3$, $\lambda = 1$ and $\gamma = 2$. (c) Total energies for the four free-space stationary states, the half-quantum vortices (labeled as 0), mixed state (labeled as 01), excited states generated by inputs 4.21 and 4.22 (labeled as 1 and 12) for $N = 3.7$. (d) The same with (c), and only difference is for $N = 3$.

in the x direction, while the average velocity in the y - direction is $v_y = -0.0175$.

The excited states generated by inputs (4.21) and (4.22) are unstable both at $\gamma = 0$ and $g = 2$. In particular, the ring structure of the former vortical state splits in the course of the evolution, as shown in Fig. 4.6 for $\gamma = 0$. Similar splitting is observed much earlier (already at $t = 100$) for $\gamma = 2$.

Figure 4.7 illustrates the evolution of the excited state obtained from input (4.22) at $\gamma = 2$. The original vortex complex gets broken by the instability, evolving into an apparently chaotic pattern. This instability develops quickly, as $t = 250$ (Fig. 4.7 (c)) corresponds to $\lesssim 5$ diffraction times of the original structure.

4.6.2 Mobility and collisions of vortex modes

The numerical results displayed in Figs. 4.4 and 4.5 suggest that propagating modes may exist in the present system. Localized states which move steadily at velocity $\mathbf{v} = (v_x, v_y)$ can be looked for in the form of $\phi_+ = \phi_+(x - v_x t, y - v_y t, t)$ and $\phi_- = \phi_-(x - v_x t, y - v_y t, t)$. The substitution of this into Eq. (4.1) leads to the equations written in the moving reference frame,

$$\begin{aligned} i\frac{\partial \phi_+}{\partial t} - i\left(\mathbf{v}\cdot\nabla\right)\phi_+ &= -\frac{1}{2}\nabla^2\phi_+ - (|\phi_+|^2 + \gamma|\phi_-|^2)\phi'_+ + \lambda\left(\frac{\partial \phi_-}{\partial x} - i\frac{\partial \phi_-}{\partial y}\right), \\ i\frac{\partial \phi'_-}{\partial t} - i\left(\mathbf{v}\cdot\nabla\right)\phi_- &= -\frac{1}{2}\nabla^2\phi_- - (|\phi_-|^2 + \gamma|\phi_+|^2)\phi_- + \lambda\left(-\frac{\partial \phi_+}{\partial x} - i\frac{\partial \phi_+}{\partial y}\right), \end{aligned} \tag{4.24}$$

where x and y actually stand for $x - v_x t$ and $y - v_y t$. Note that Eq. (4.1) has no Galilean invariance, hence steadily propagating solutions cannot by generated by a straightforward transformation, such as

$$\phi_\pm(\mathbf{r}) \equiv \tilde{\phi}_\pm(\mathbf{r}) \exp\left(i\mathbf{v}\cdot\mathbf{r} - \frac{i}{2}v^2 t\right). \tag{4.25}$$

In particular, in the case of $v_x = 0$, the quasi-Galilean transformation (4.25) casts Eq. (4.24) into a form which differs from underlying equations (4.1) by the presence of terms causing for linear mixing of the two components:

$$\begin{aligned} i\frac{\partial \phi_+}{\partial t} &= -\frac{1}{2}\nabla^2\phi_+ - (|\phi_+|^2 + \gamma|\phi_-|^2)\phi'_+ + \lambda\left(\frac{\partial \phi_-}{\partial x} - i\frac{\partial \phi_-}{\partial y}\right) + \lambda v_y \phi_-, \\ i\frac{\partial \phi'_-}{\partial t} &= -\frac{1}{2}\nabla^2\phi_- - (|\phi_-|^2 + \gamma|\phi_+|^2)\phi_- + \lambda\left(-\frac{\partial \phi_+}{\partial x} - i\frac{\partial \phi_+}{\partial y}\right) + \lambda v_y \phi_+. \end{aligned} \tag{4.26}$$

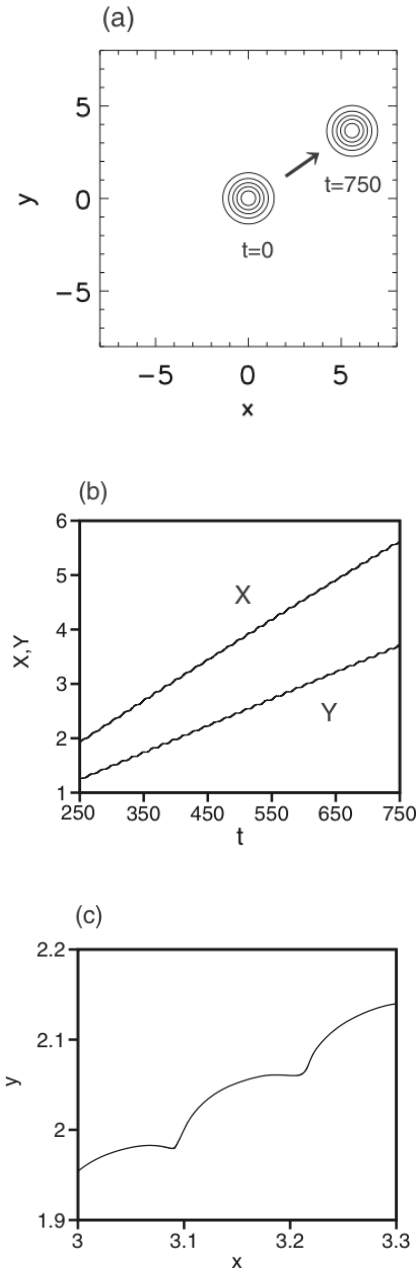

Fig. 4.5 Evolution of excited states with type of the half-quantum vortices (according to Fig. 4.4 (c)) in free space. The parameters used in here includes, $N = 3.7$ and $\gamma = 2$. (a) The contour plots of $|\phi_+(x, y)|$ at $t = 0$ and $t = 750$. (b) The time dependence of the coordinates of the peak position, (X, Y), of $|\phi_+(x, y)|$. (c) A zoom of a segment of the trajectory $(X(t), Y(t))$, which demonstrates a small oscillatory component of the motion.

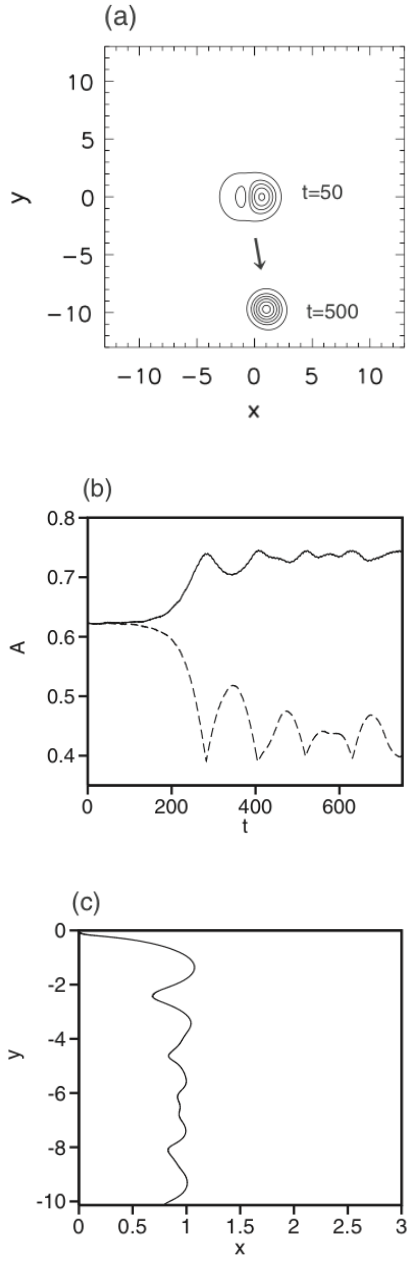

Fig. 4.6 Dynamics of the mixed mode in free space. (a) Contour plots of $|\phi_+(x,y)|$ at $t = 50$ and $t = 500$ for the mixed mode with $N = 3.7$ at $\gamma = 0$, when this mode is not a ground state. (b) The evolution of amplitudes of the ϕ_+ and ϕ_- components (solid and dashed curves, respectively). (c) The trajectory of the peak position of $|\phi_+(x,y)|$.

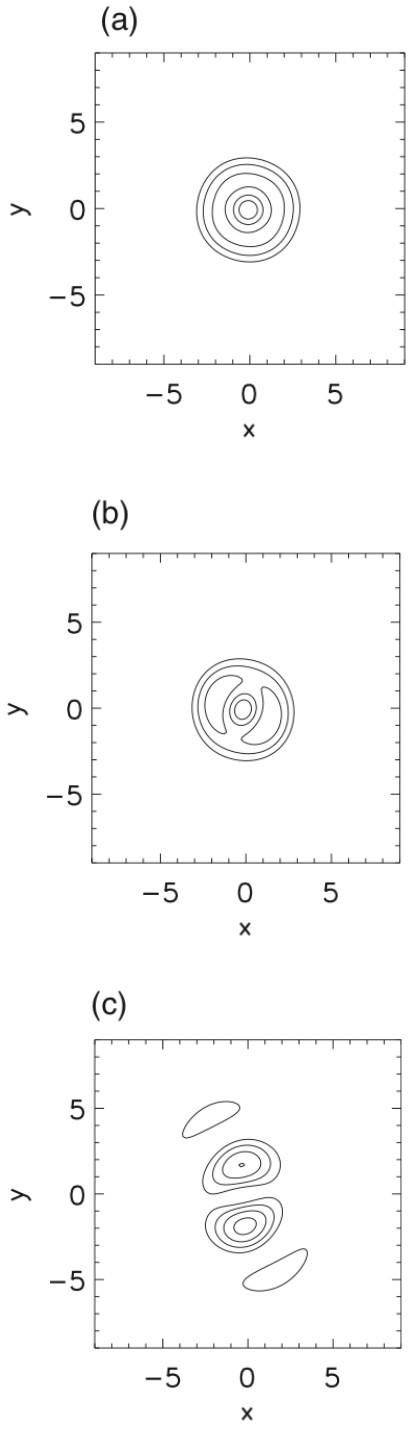

Fig. 4.7 Dynamics of the spin-up component of the excited vortical state in free space. Here $\gamma = 0$ and $N = 3.7$. (a) $t = 500$, (b) $t = 950$, (c) $t = 1200$. For the case of $\gamma = 2$, the instability of the excited state is stronger.

The same linear mixing can be imposed, in diverse 1D [91–93] and 2D [94, 95] settings, by a GHz wave coupling the two underlying atomic states, i.e., the mixing by itself represents a physically relevant addition to the basic model. A straightforward impact of the addition of the mixing terms in Eq. (4.26) is a shift of the edge of the *semi-infinite gap* (4.7) in which solitons may exist, from $\mu = -\lambda^2/2$ to $\mu < -\left(\lambda^2/2 + |\lambda v_y|\right)$.

Coming back to equations (4.24) written in the moving reference frame, stationary solutions to them can be obtained, as well as in the case of underlying equations (4.1), by means of the imaginary-time evolution method for $v_y \neq 0$, but the procedure produces results solely for $v_x = 0$ (this situation is possible, as the present 2D system is not isotropic). In particular, at $\gamma = 2$, when the quiescent mixed mode is the ground state, its moving version, which is displayed in Figs. 4.8(a,b) for $N = 3.1$ and $v_y = 0.5$, exists and is stable too. As well as its quiescent counterpart, this mode features the mirror symmetry between the profiles of $|\phi_+(x,y)|$ and $|\phi_-(x,y)|$. Figure 4.8(c) shows the amplitude of the moving mixed mode,

$$A = \sqrt{|\phi_+(x=0,y=0)|^2 + |\phi_-(x=0,y=0)|^2}, \tag{4.27}$$

as a function of v_y. The amplitude monotonously decreases with the growth of the velocity, and the mode vanishes at

$$v_y = (v_y)_{\max}^{(\mathrm{mixed})} \approx 1.8. \tag{4.28}$$

The availability of the stably moving mixed modes suggests to consider collisions between them. In particular, we have performed simulations of Eq. (4.1) for the head-on collision between two solitons displayed in Figs. 4.8(a,b), moving at velocities $v_y = \pm 0.5$. Figures 4.9(a), (b), and (c) display snapshot patterns of $\sqrt{|\phi_+(x,y)|^2 + |\phi_-(x,y)|^2}$ at $t = 4$, $t = 24$, and $t = 64$, respectively. The collision results in fusion of the two solitons into a single one, of the same mixed-mode type, which is spontaneously shifted along direction x. The shift may be understood as manifestation of spontaneous symmetry breaking caused by the collision. The fusion is accompanied by emission of small-amplitude radiation waves.

At $\gamma = 0$, the half-quantum vortices, which, as shown above, is the ground state in the class of quiescent modes, can also move stably, but only in a small interval of velocities,

$$|v_y| < (v_y)_{\max}^{(\mathrm{semi})} \approx 0.03 \tag{4.29}$$

Figures 4.10(a) and (b) show the profiles of $|\phi_+(x,y)|$ and $|\phi_-(x,y)|$ for the half-

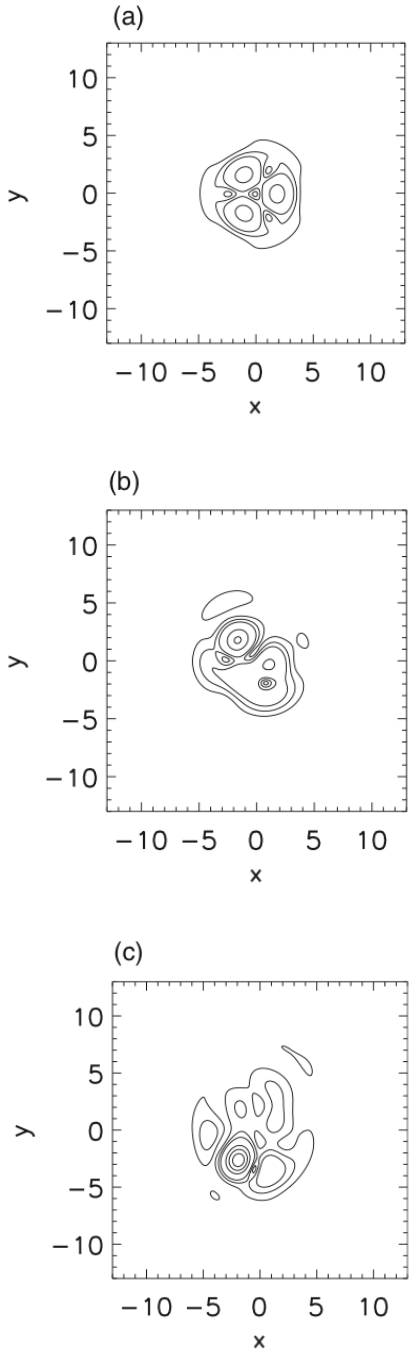

Fig. 4.8 Dynamics of spin-up component of the excited state genreated by input 4.22, here $N = 3.7$ and $\gamma = 2$. (a) $t = 50$, (b) $t = 150$, (c) $t = 250$. For the case of $\gamma = 0$, this mode is also unstable.

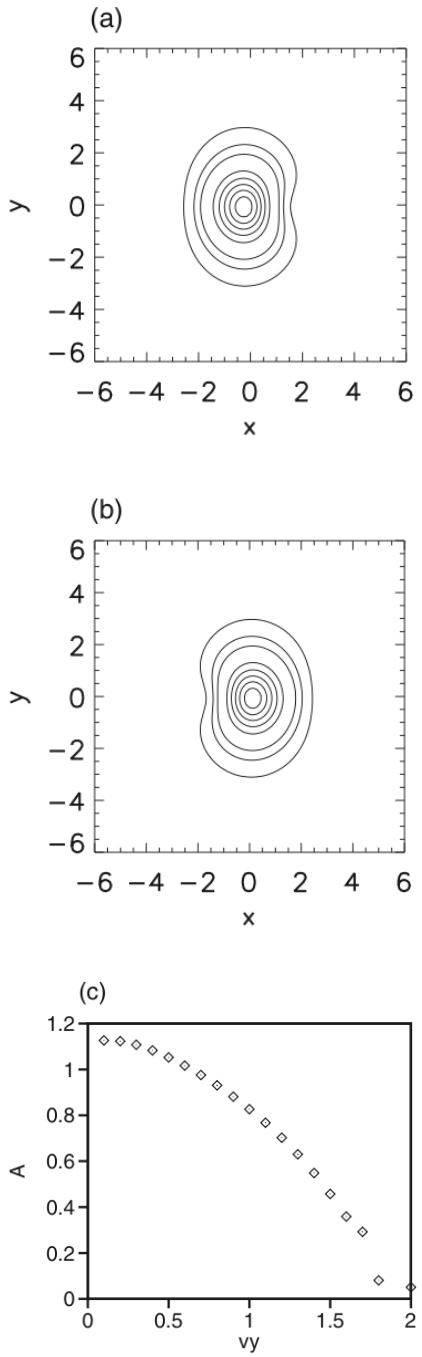

Fig. 4.9 Contour plot of the moving stable mixed mode. (a) Spin-up component, (b) spin-down component, (c) the amplitude of the moving mixed mode as a function of v_y. Here, $N = 3.1$, $v_x = 0$, $v_y = 0.5$, $\gamma = 2$, $\lambda = 1$.

quantum vortices with norm $N = 3.7$ moving at velocity $v_y = -0.02$. In addition, Fig. 4.10(c) displays the evolution of $\sqrt{|\phi_+|^2 + |\phi_-|^2}$ in the cross section of $x = 0$, produced by direct simulations of Eq. (4.1), starting from the initial conditions corresponding to Figs. 4.10(a,b). The localized solution is stably moving at velocity $v_y = -0.02$. In fact, this moving state is similar to the one generated by the spontaneous onset of motion of the unstable quiescent mixed mode at $\gamma = 0$ and the same norm, which rearranges into a state close to the half-quantum vortices, as shown above in Fig. 4.5.

At $|v_y| > 0.03$ (see Eq. (4.29)), the solution to Eq. (4.24) produced by means of the imaginary time propagation method converges not to a half-quantum vortices, but rather to a mixed-mode state, which turns to be stable in real-time simulations. Thus, the moving half-quantum vortices are rather fragile objects, while the mixed modes are, on the contrary, very robust ones in the state of motion.

4.7 Chapter Summary

In conclusion,

- We have confirmed the existence of two types of vortex-solitons in a 2D SO coupled BECs with attractive interactions in free space. These stable solutions, including half-quantum vortex state and a mixed model state, holds the ground states based on the interaction relationship of same and different spin series components, respectively. The half-quantum vortices state is important for modern physics, especially, in condensed matter physics. The experimental realization of synthetic gauge field enables us to research the half-quantum vortices in ultracold atomic gases. The mixed state can be seen as a superposition of the half-quantum vortices and its time reversal symmetry partner. The half-quantum vortices and mixed models will turn into unstable Townes solitons if the state's norm reaches to the critical values.
- Meanwhile, we also addressed the excited state in the BECs with synthetic SO couping by numerical simulation and analytical approximation. These solitons have similar structures with ground states.
- Finally, we also found that the stable moving solitons exist for the non-Galilean invariant system. The dynamics of two moving mixed models is also studied.

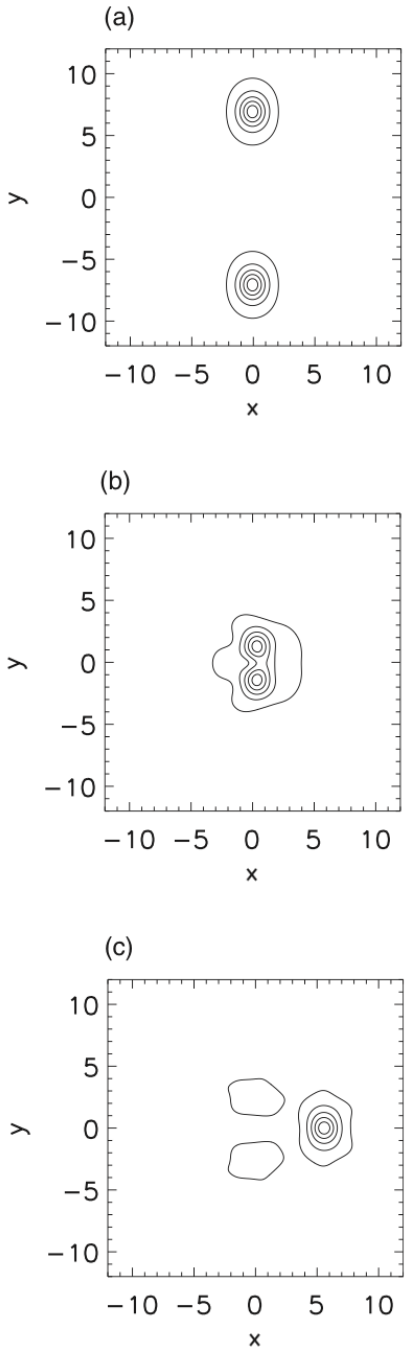

Fig. 4.10 Dynamics of the collision of two mixed-mode solitons. (a) $t = 4$, (b) $t = 24$, (c) $t = 64$. Here, $N = 3.1$, $v_y = \pm 0.5$.

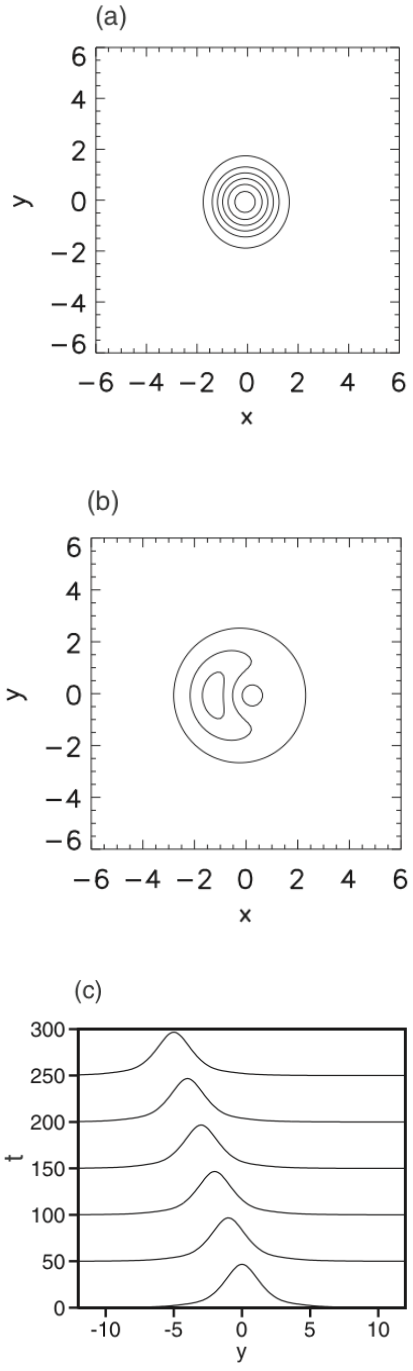

Fig. 4.11 Moving stable half-quantum vortices state. (a) Contour plot of the pin-up component, (b) contour plot of the spin-down component, (c) the time evolution of $\sqrt{|\phi_+(0,y)|^2+|\phi_-(0,y)|^2}$ for $x=0$. Here, $N=3.7$ and $v_y=-0.02$.

Chapter 5

Spin-Orbit Coupled Bose-Einstein Condensates in Optical Lattices

In the chapter, we focus on the theoretical research of the ground states of Bose-Einstein condensates with Rashba type of the Spin-Orbit (SO) coupling in optical lattices reduced by laser beam based on the mean-field theory.

We address the Bloch states of the wave function and energy spectrum for the single particle Hamiltonian of the SO coupled Bose-Einstein condensates in optical lattices by ***numerical simulation*** method at first. On the other hand, the Bloch states of the wave function and the energy spectrum for the non-interacting Hamiltonian is also searched in series expansion by the ***analytical method***. Then, we consider the effect of a weak interaction on a spin-orbit coupled Bose-Einstein condensate. In particular, we show the existence of the vortex structures, such as, vortex-antivortex-pair lattices state on the ground states of the SO coupled Bose-Einstein condensates in optical lattices by simulating the Gross-Pitaevskii equation. In addition, we also studied the spin structures of the ground states in the SO coupled Bose-Einstein condensates.

5.1 Introduction

Spin-orbit coupling describes the interaction of spin and momentum degrees of freedom of quantum particles, such as, the election and atoms [6]. It takes a key role for understanding the mechanism of the spin-Hall effec [96] and topological insulators [97] in condensed matter physics. As a great breakthrough, in most recently, Bose-Einstein condensates and fermionic degenerated gases with

synthetic SO coupling were realized experimently in ultracold atom systems by engineering atom-light interaction [7, 50]. It opens up a new research area for ultracold atoms gases under the synthetic gauge fields in both of theory and experiment. Specially, because the bosonic systems with half-integer spin degrees of freedom are absent in nature, the research about Bose-Einstein condensates with SO coupling attracts more interests and attention from scientists.

Up to now, some works concerning SO coupled Bose-Einstein condensates *in free space and trap potential by using Gross-Pitaevskii equation* have been done theoretically [57]. Among them, Wang et al. found that the mean-field ground state has two different phases, i.e., plane-wave and stripe phases, depending on the intra- and inter-series interactions [58]. Half-quantum vortex states were found in a spin-orbit-coupled Bose-Einstein condensates in free space or confined in a harmonic potential [59–61]. On the other hand, some researches on the SO coupled Bose-Einstein condensates *in optical lattices by using the Bose-Hubbard model* have also been done, such as, Exotic spin textures were predicted in Bose-Hubbard models corresponding to SO coupled Bose-Einstein condensates in the Mott-insulator phase [62–64].

In this work, however, we will focus on the SO coupled Bose-Einstein condensates *in optical lattices potential by using Gross-Pitaevskii equation*, because of the presence of the space period, the ground states will have different pattens with one in free space or trap. In the present system, a vortex-antivortex-pair lattices state will be found by numerical simulation directly.

5.2 Model and method

The SO coupled Bose-Einstein condensates in optical lattice can be described by Gross-Pitaevskii equation in mean-field approximation. The dimensionless model equation can be expressed as

$$\begin{aligned} i\frac{\partial\psi_+}{\partial t} = &-\frac{1}{2}\nabla^2\psi_+ + \lambda\left(\frac{\partial\psi_-}{\partial x} - i\frac{\partial\psi_-}{\partial y}\right) - V_0\{\cos(2\pi x)+\cos(2\pi y)\}\psi_+ \\ &+\left(g|\psi_+|^2+\gamma|\psi_-|^2\right)\psi_+ \end{aligned} \tag{5.1}$$

and

$$
\begin{aligned}
i\frac{\partial\psi_-}{\partial t} =& -\frac{1}{2}\nabla^2\psi_- + \lambda\left(-\frac{\partial\psi_+}{\partial x} - i\frac{\partial\psi_+}{\partial y}\right) - V_0\{\cos(2\pi x)+\cos(2\pi y)\}\psi_- \\
&+ \left(g|\psi_-|^2 + \gamma|\psi_+|^2\right)\psi_-
\end{aligned}
\tag{5.2}
$$

where $\psi_\pm$ denote the wave function for the spin-up and spin-down components of the spinor Bose-Einstein condensates, V_0 is the strength of the optical lattice, g and γ express the intra- and inter-series interactions respectively, λ denotes the strength of the Rashba spin-orbit coupling, and the wavelength of the optical lattice is 1 in this dimensionless model.

5.3 Single particle energy spectrum

5.3.1 Numerical solution

We consider the single particle situation at first. In the case, both of g and γ are zero in the above dimensionless Gross-Pitaevskii equation, then the equation become linear one with a spatially periodic potential. On the other hand, the Bloch states are stationary solutions to the linear equations. Therefore, we can express the solutions for the linear case as

$$\psi_+(x,y,t) = \phi_+(x,y)\exp(ik_x x + ik_y y - i\mu t), \tag{5.3}$$

$$\psi_-(x,y,t) = \phi_-(x,y)\exp(ik_x x + ik_y y - i\mu t), \tag{5.4}$$

where $\phi_\pm$ are the wave functions with period of the optical lattice potential for spin-up and spin-down components, k_x and k_y are the wave numbers in x and y directions, and μ is the chemical potential. Substituting the solutions to Eq. (5.1) and Eq. (5.2) in linear case, then we can find that $\phi_\pm$ satisfy

$$
\begin{aligned}
\mu\phi_\pm =& -\frac{1}{2}\nabla^2\phi_\pm + \frac{1}{2}(k_x^2+k_y^2)\phi_\pm - ik_x\frac{\partial\phi_\pm}{\partial x} - ik_y\frac{\partial\phi_\pm}{\partial y} \\
&+ \lambda\left(\pm\frac{\partial\phi_\mp}{\partial x} - i\frac{\partial\phi_\mp}{\partial y} \pm ik_x\phi_\mp + k_y\phi_\mp\right) \\
&- V_0\{\cos(2\pi x)+\cos(2\pi y)\}\phi_\pm
\end{aligned}
\tag{5.5}
$$

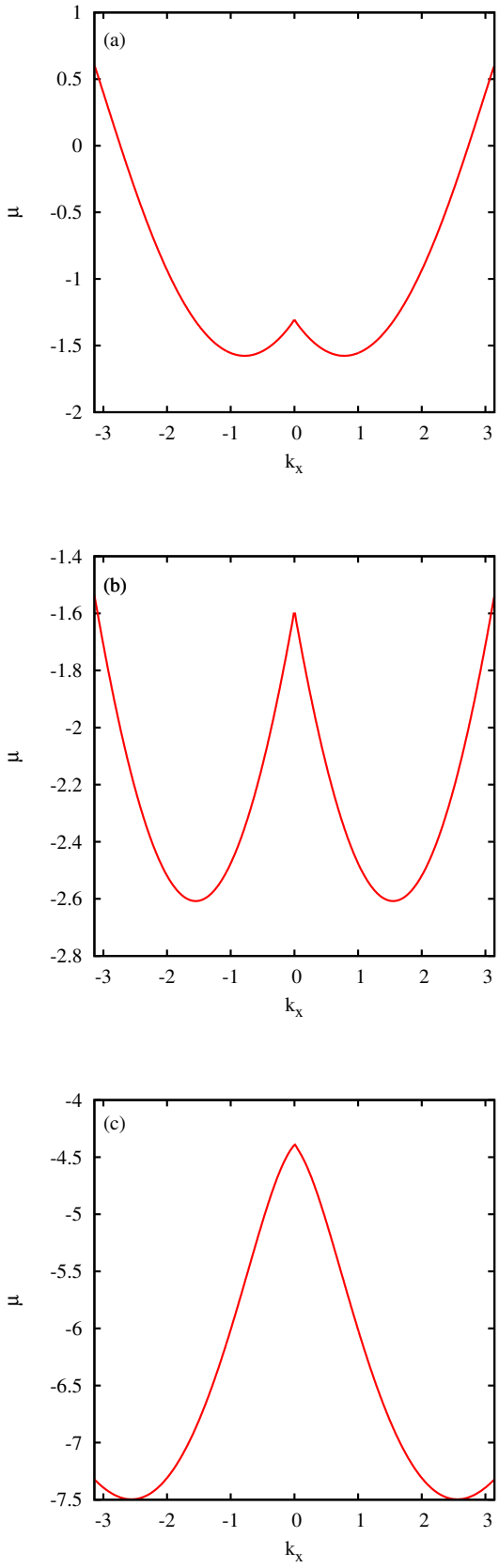

Fig. 5.1 Single particle energy spectrum of SO coupled Bose-Einstein condensates in an optical lattice. (a) $\lambda = \pi/4$, $k_y = 0$. (b) $\lambda = \pi/2$, $k_y = 0$. (c) $\lambda = \pi$, $k_x = k_y$.

The eigenvalue μ and the eigenfunctions $\phi_\pm$ can be numerically obtained from the stationary solution of the linear equation [98]:

$$\begin{aligned}\frac{\partial\phi_+}{\partial t} =&\frac{1}{2}\nabla^2\phi_+ - \frac{1}{2}(k_x^2+k_y^2)\phi_+ + ik_x\frac{\partial\phi_+}{\partial x} + ik_y\frac{\partial\phi_+}{\partial y}\\ &+ V_0\{\cos(2\pi x)+\cos(2\pi y)\}\phi_+\\ &- \lambda\left(\frac{\partial\phi_-}{\partial x} - i\frac{\partial\phi_-}{\partial y} + ik_x\phi_- + k_y\phi_-\right) + \mu'\phi_+,\end{aligned} \tag{5.6}$$

$$\begin{aligned}\frac{\partial\phi_-}{\partial t} =&\frac{1}{2}\nabla^2\phi_- - \frac{1}{2}(k_x^2+k_y^2)\phi_- + ik_x\frac{\partial\phi_-}{\partial x} + ik_y\frac{\partial\phi_-}{\partial y}\\ &+ V_0\{\cos(2\pi x)+\cos(2\pi y)\}\phi_-\\ &- \lambda\left(-\frac{\partial\phi_+}{\partial x} - i\frac{\partial\phi_+}{\partial y} - ik_x\phi_+ + k_y\phi_+\right) + \mu'\phi_-,\end{aligned} \tag{5.7}$$

$$\frac{d\mu'}{dt} = \alpha(N_0 - N), \tag{5.8}$$

where $\alpha > 0$ is a parameter in our numerical simulation,

$$N = \int\int(|\phi_+(x,y)|^2 + |\phi_-(x,y)|^2)dxdy \tag{5.9}$$

is the total norm, and N_0 is fixed by the normalization condition. The time evolution of the dissipative equation leads to a stationary state and the total norm N approaches N_0, and μ' will to be eigenvalue for the stationary state.

In our numerical method, the stationary state of the Bloch wave function is obtained by simulating the Gross-Pitaevski Equation with k_x and k_y terms as the time evolution by proper selection of initial wave function. That is based on a fact that the system's energy will decrease during the process of imaginary-time evolution.

Figure 5.1 shows the energy spectrum $\mu(k_x)$ of SO coupled Bose-Einstein condensates in an optical lattice as a function of k_x for $k_y = 0$ or $k_y = k_x$, $V_0 = 5$, for different strengths of spin-orbit coupling. As a result of present of the optical lattices, $\mu(k_x)$ is a periodic function of k_x with same period with external periodic potential. We can find that the energy spectrum shape will be determined by the strength of SO coupling. There are three situations shown in this figure, for (a) the strength of SO coupling is $\lambda = \pi/4$, and $k_y = 0$, for (b) $\lambda = \pi/2$ and $k_y = 0$, for (c) $\lambda = \pi$ and $k_x = k_y$. We find that the momentum value according to the

minimum in the energy spectrum increase with the increase of the strength of SO coupling, and the energy minimum will reduce with the increase of the SO coupling.

In addition, we found an interesting result. For the single particle situation of Spin-Orbit coupled Bose-Einstein Condensates in free space or trap,

$$\lambda = \sqrt{k_x^2 + k_y^2}, \tag{5.10}$$

it is well know, for one-dimensional Spin-Orbit coupling, the minimum of the energy spectrum in momentum space are $k_x = \pm\lambda$. And, for two-dimensional Spin-Orbit coupling, the minimum of the energy spectrum in momentum space forms a ring with $\lambda = \sqrt{k_x^2 + k_y^2}$. However, for the situation of adding optical lattices to the Spin-Orbit coupled Bose-Einstein Condensates, the energy spectrum is changed extremely by optical lattices strength. We can find the values of k_x according to the minimum of energy is shifted with λ. If the strength of Spin-Orbit coupling is small, such as, for $\lambda = \pi/4$, the value of λ is almost same with the value of momentum according to the minimum energy. However, if the strength of Spin-Orbit coupling is strong, the difference of λ and the value of momentum according to the minimum energy is also larger.

5.3.2 Analytical solution

On the other side, the analytical solution of the linear equations can be obtained. Because $\phi_\pm(x, y)$ are the functions with period of optical lattices, we can expand $\phi_\pm(x, y)$ in the simplest approximation as:

$$\phi_\pm(x, y) = C_{0\pm} + C_{1\pm}e^{2\pi ix} + C_{2\pm}e^{-2\pi ix} + C_{3\pm}e^{2\pi iy} + C_{4\pm}e^{-2\pi iy}. \tag{5.11}$$

Substituting the ansatz into eigen-equations with k_x and k_y terms, for $k_y = 0$ and $\phi_- = i\phi_+$, we find

$$\begin{aligned}\mu =& \frac{k_x^2}{2} - \lambda k_x + \frac{V_0^2/4}{\mu - (k_x + 2\pi)^2/2 + \lambda(k_x + 2\pi)} + \frac{V_0^2/4}{\mu - (k_x - 2\pi)^2/2 + \lambda(k_x - 2\pi)} \\ &+ \frac{V_0^2}{4}\frac{2\mu - (k_x^2 + 4\pi^2) - 2\lambda k_x}{\{\mu - (k_x^2 + 4\pi^2)/2\}^2 - \lambda^2(k_x^2 + 4\pi^2)}.\end{aligned} \tag{5.12}$$

Furthermore, for a uniform system in where $V_0 = 0$, we can see

$$\mu = \frac{1}{2}(k_x - \lambda)^2 - \frac{\lambda^2}{2}. \tag{5.13}$$

The system will be in the ground states when $k = \lambda$ [57, 58], here $k = \sqrt{k_x^2 + k_y^2}$. Obviously, the present of optical lattices modifies the energy spectrum of SO coupled Bose-Einstein condensates, this result is consistent with results based on the Bose-Hubbard Model for weak coupling superfluid [64].

The analytical results are also consistent with numerical simulation by using Gross-Pitaevskii equation for small SO coupling, but for the large SO coupling, there is a little inconsistent [32]. The problem can be solved by adding more higher harmonic terms in the procedure of expanding the wave functions.

5.3.3 Vortex-antivortex-pair state

In this section, we address the ground states of the Spin-Orbit coupled Bose-Einstein condensates in a optical lattice by numerical simulation. We found that the ground state is not a simple plane wave phase, but have a complex structure. In the main part of the Spin-Orbit coupled Bose-Einstein condensates, there is a plane wave, but in their edge, a vortex-antivortex-pair will appear. The density of the Bose-Einstein condensates surrounded the vortex-antivortex-pair is very small, so that it is difficult to find the vortex-antivortex-pair from the density distribution. However, we can find them from the phase distribution.

Figure 5.2 shows (a) the density and (b) the phase distribution for the spin-up component of the Spin-Orbit coupled Bose-Einstein condensates in a optical lattice for $\lambda = 3\pi/2, k_x = 3\pi/2, k_y = 0$ and $V_0 = 5$. To find the vortex-antivortex-pair, we make a counter plot in the fig (a).The results for the spin-down component of the Spin-Orbit coupled Bose-Einstein condensates is similar to the spin-up component, the only different is that the ground state of the spin-up and spin-down components have a symmetry about y axes, the symmetry can be understood by substituting x to $-x$ in Gross-Pitaevskii equation.

5.4 Interaction system

In the section, we consider the non-linear Gross-Pitaevskii equation. At fist, we consider the case of $g > \gamma$.

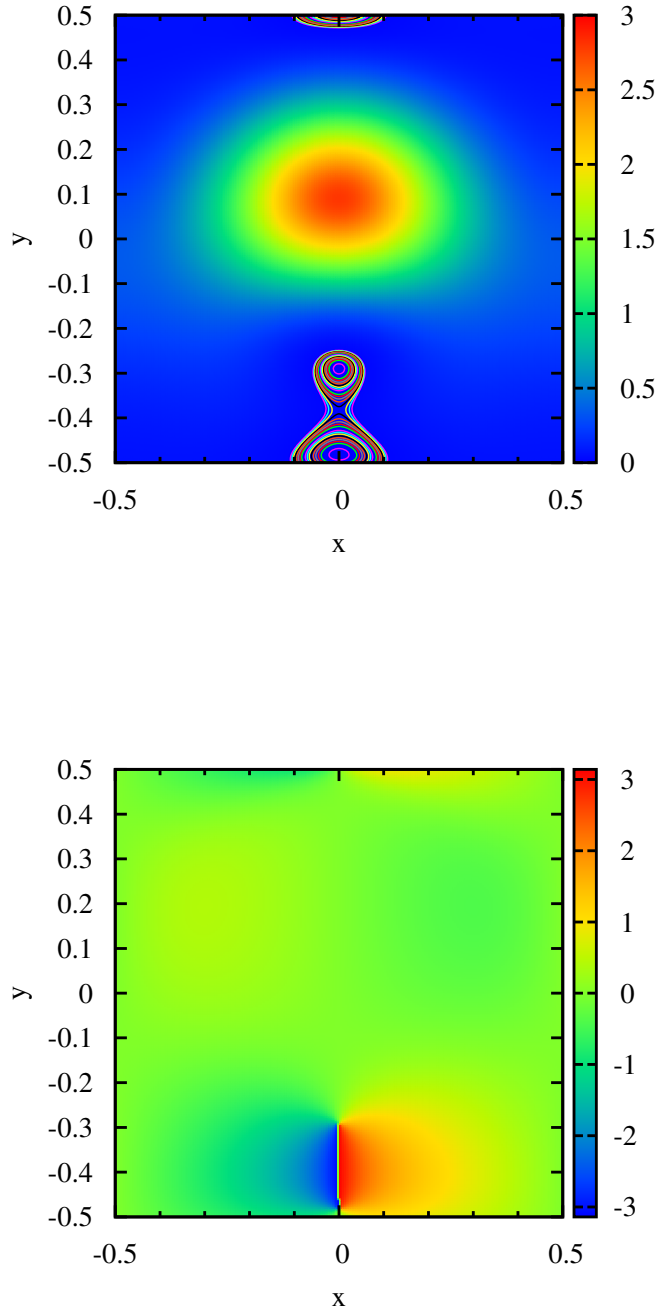

Fig. 5.2 Density (top) and phase (bottom) of spin-up component of the spin-orbit coupled Bose-Einstein condensates in an optical lattice for $\lambda = 3\pi/2, k_x = 3\pi/2,$ and $k_y = 0$.

5.4.1 Vortex-antivortex-pair lattices

In case of $g > \gamma$, for an uniform system, the Spin-Orbit coupled Bose-Einstein condensates will be in the plane wave phase. In the present system, however, a vortex-antivortex-pair lattice is expected, because a vortex-antivortex-pair have appeared in an optical lattice. The numerical simulation from Gross-Pitaevskii equation verified my expect. Concerning the details of the numerical simulation, the system size is $L \times L$. In addition, we take the periodic boundary conditions and the optical lattices is shifted as

$$V = V_0[\cos\{2\pi(x - 1/2)\} + \cos\{2\pi(y - 1/2)\}], \tag{5.14}$$

by (1/2, 1/2) to confine the Spin-Orbit coupled Bose-Einstein condensates in the space of $[0, L] \times [0, L]$.

Figure 5.3 (a) and (b) show the contour plot of the spin-up and spin-down components of Spin-Orbit coupled Bose-Einstein condensates in optical lattices for $\lambda = \pi$, $g = 1$, $\gamma = 0.5$, $L = 8$, and $V_0 = 5$. It is easy to find that vortex-antivortex pair exist in every lattice, and for the whole lattices, the ground states carrying a vortex-antivortex-pair lattice. Actually, vortex lattices can be created by rotating trap potential for ultracold atomic gases. However, in the present work, the vortex-antivortex-pair lattice has spontaneously appeared in the present of Spin-Orbit coupling.

The wave vector (k_x, k_y) can be evaluated from the results of the linear equation. Fig. 5.3(c) shows the vortex-antivortex-pair lattices structure of spin-up component from linear equation for $\lambda = \pi$ and $k_x = k_y = 3\pi/4$. The eigenvalue of the Spin-Orbit coupled Bose-Einstein condensates in optical lattices μ has a minimum at $k_x = k_y = 3\pi/4$ in the finite-size system, here $L = 8$. The results is almost same with Fig. 5.3(a), it suggest that the Black wave can be a good approximation for the solution of the Gross-Pitaevskii euation. Fig. 5.3(d) shows the minimum values of spin-up component of Spin-Orbit coupled Bose-Einstein condensates in optical lattices for the linear equation as a function of λ for $k_x = k_y = \lambda/\sqrt{2}$ at $V_0 = 5$. We can find that the minimum will take zero if $\lambda > 2.9$, it means that there is a vortex.

Similarly, we find that two components of the Spin-Orbit coupled Bose-Einstein condensates in optical lattices have also a symmetry about $y = x$ axes, but have a little different with the case of the Spin-Orbit coupled Bose-Einstein condensates in an optical lattice, where the symmetry axes is y. Actually, the reason is that,

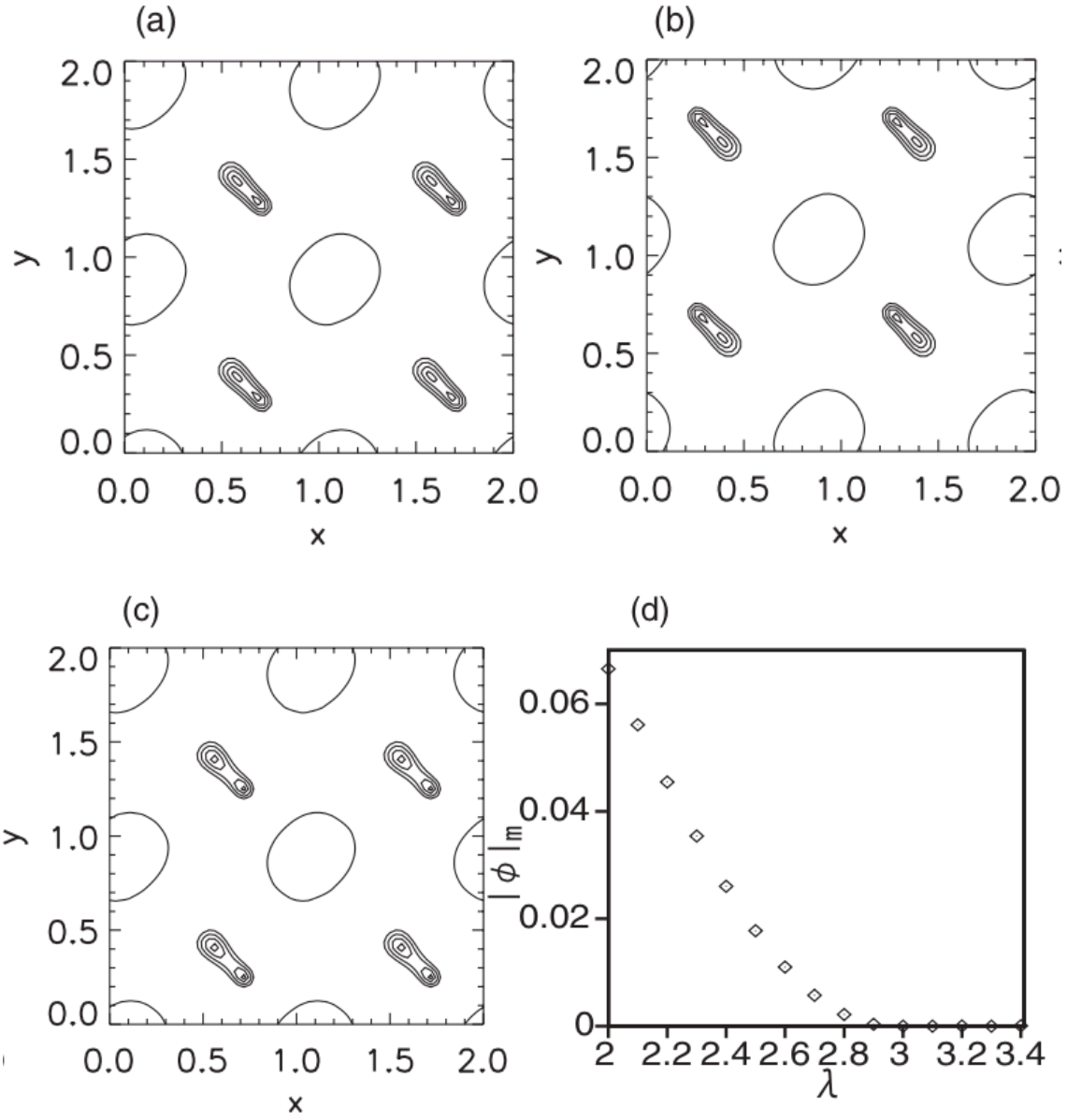

Fig. 5.3 Vortex-antivortex-pair lattices structure of spin-up component (a) and spin-down component (b) the Spin-Orbit coupled Bose-Einstein condensates in optical lattices for $\lambda = \pi$, $g = 1$ and $\gamma = 0.5$. (c) Vortex-antivortex-pair lattices structure of spin-up component from linear equation for $\lambda = \pi$ and $k_x = k_y = 3\pi/4$. (d) Minimum value of $|\phi|_+$ as a function of λ for $k_x = k_y = \pi/2$.

for the linear case, we have taken the $k_y = 0$, but for the Gross-Pitaevskii equation (Eq. (5.1) and Eq. (5.2)), we can not control the k_x and k_y.

5.4.2 Vortices lattice

In the present part, we discuss the situation of $g < \gamma$. Actually, for a uniform system, the Spin-Orbit coupled Bose-Einstein condensates will be in the stripe phase in this situation. Therefore, the result of $g < \gamma$ is more complex than $g > \gamma$ in optical lattices.

As a simple approximation for $\gamma > g$, we consider the superposition of Bloch waves of (k_x, k_y) and $(-k_x, -k_y)$. Figures 5.4 (a) and (b) show contour plots of $|\Psi_+|$ and $|\Psi_-|$ at $g = 1$, $\gamma = 2$, $L = 8$, and $\lambda = \pi$. The wave vector is evaluated as $(k_x, k_y) = (3\pi/4, 3\pi/4)$ in this case, too. The contour lines are drawn for $|\Psi|$ = 0.025, 0.05, 0.075, 0.1, 1, and 1.5. Vortex cores exist in the regions with dark points. The vortex lattice structure is rather complicated. The circular contour lines correspond to peak regions of $|\Psi|$. The peak regions stand in a line in the direction of angle $-\pi/4$ and the peak lines for ψ_+ and ψ_- alternate in the diagonal direction of angle $\pi/4$. Figure 5.4 (c) shows a contour plot of a linear combination $|(\phi_{++} + \phi_{+-})/\sqrt{2}|$ of two Bloch waves ϕ_{++} and ϕ_{+-} with $(k_x, k_y) = (3\pi/4, 3\pi/4)$ and $(-3\pi/4, -3\pi/4)$ for the spin-up component at $\lambda = \pi$. The superposition of the Bloch waves is a good approximation for the stationary solution to the GP equation. The superposition of two Bloch waves with opposite wave vectors generates a standing wave. For plane waves, the amplitude becomes zero at the nodal lines. The nodal lines are perturbed by the optical lattice and vortices are generated. A vortex lattice structure therefore appears even for small Spin-Orbit coupling in the case of $\gamma > g$. Figure 5.4 (d) shows a vortex lattice pattern with $k_x = k_y = \pi/4$ at $\lambda = 1$ and $V_0 = 5$. For large Spin-Orbit coupling, a vortex pair is created in a single Bloch wave and the superposition of the two Bloch waves makes the vortex lattice structure more complicated as shown in Fig. 5.4 (c).

5.5 Spin texture

The complicated patterns might be simplified, if a spin representation is used, as in the Bose-Hubbard model [99, 100]. The spin vector are defined as

$$\vec{s} = \frac{\psi^\dagger \vec{\sigma} \psi}{2|\psi|^2} \tag{5.15}$$

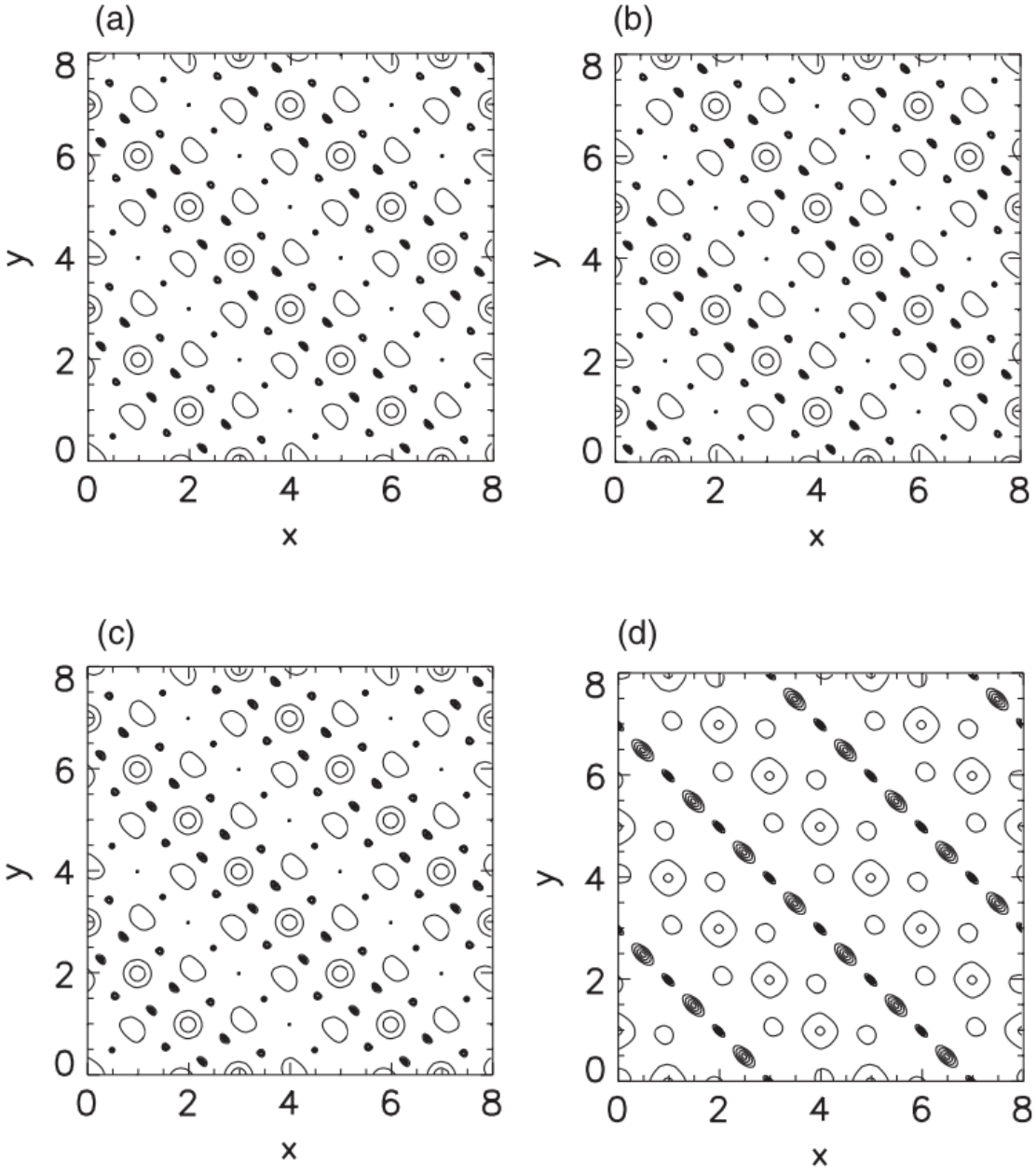

Fig. 5.4 Countour plot of the SO coupled BEC in optical lattices. (a) spin-up component for $\lambda = \pi$, $g = 1$, $\gamma = 2$, and $L = 8$. Here $k_x = k_y$ are evaluated as $3\pi/4$, (b) spin-down component, (c) the superposition of $|(\phi_{++} + \phi_{+-})/\sqrt{2}|$ on the linear equation for $\lambda = \pi$ and $k_x = k_y = \pm 3\pi/4$, (d) the superposition of $|(\phi_{++} + \phi_{+-})/\sqrt{2}|$ on the linear equation for $\lambda = 1$ and $k_x = k_y = \pm\pi/4$.

where $\vec{\sigma}$ is Pauli matrix. Figure 5.5 (a) shows (s_x, s_y) corresponding to the pattern in Figures 5.5 (a) and (b) for $g = 1$, $\gamma = 0.5$, $\lambda = \pi$, and $V_0 = 5$. The vector (s_x, s_y) is expressed as an arrow on each lattice point. The pattern is interpreted as a ferromagnetic state in the (x, y) plane in this spin representation. The spin s_z is zero for this pattern. Figures 5.5 (b) and (c) show spin configurations respectively for (s_x, s_y) and s_z for the pattern at $g = 1$ and $\gamma = 2$ shown in Figures 5.4 (a) and (b). The spin configuration is also rather complicated. An antiferromagnetic order is seen in the diagonal direction of angle $\pi/4$ and a ferromagnetic order appears in its orthogonal direction of angle $-\pi/4$ for both the (s_x, s_y) and s_z patterns. The (s_x, s_y) component appears at the sites where the s_z component vanishes, and the s_z component appears at the sites where the (s_x, s_y) component vanishes.

5.6 Chapter Summary

We have investigated the Spin-Orbit coupled Bose-Einstein condensates in optical lattices by using the Gross-Pitaevskii equation, and found that a vortex-antivortex-pair lattice structure appears for large Spin-Orbit coupling in the case of $\gamma < g$. Meanwhile, a vortex lattice structure appears even for small Spin-Orbit coupling in the case of $\gamma > g$, because the nodal lines in the stripe wave pattern are perturbed by the optical lattice. The complicated patterns can be qualitatively understood using the corresponding Bloch waves. The Bloch waves are further approximated by a Fourier series expansion with five modes to understand the formation of the vortices. Furthermore, we found that these two components of the Spin-Orbit coupled Bose-Einstein condensates have a symmetry, it can be understood from the Gross-Pitaevskii equation directly. Finally, we have also found a complicated spin configuration in the case of $\gamma > g$, and we have obtained various spin configurations by changing the parameter Spin-Orbit coupling.

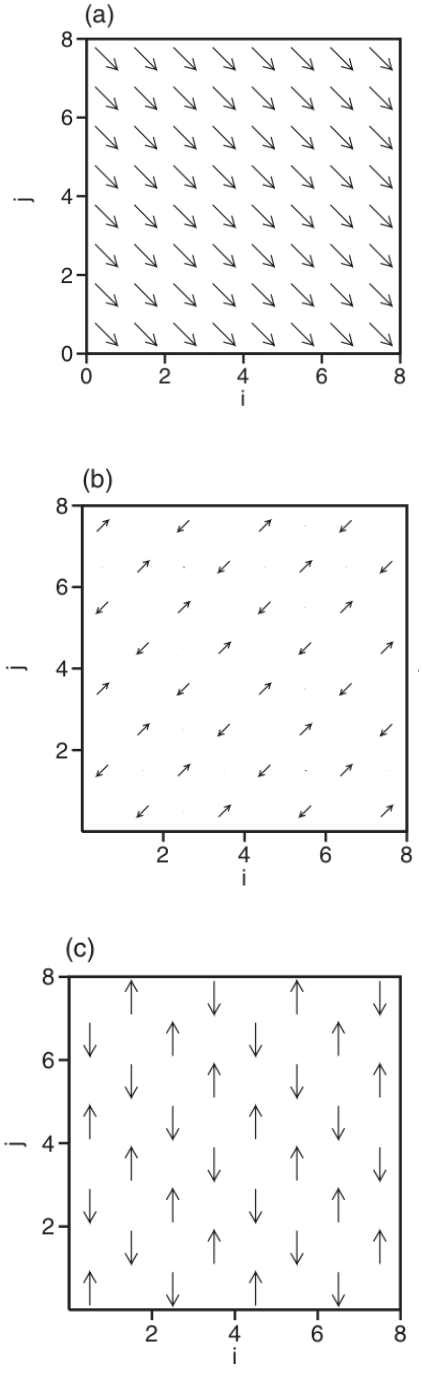

Fig. 5.5 Spin textures of Spin-Orbit coupled Bose-Einstein condensates in optical lattices. (a) (s_x, s_y), $\lambda = \pi$, $g = 1$, $\gamma = 0.5$. (b) (s_x, s_y), $\lambda = \pi$, $g = 1$, $\gamma = 2$. (c) s_z, $\lambda = \pi$, $g = 1$, $\gamma = 2$.

Chapter 6

Conclusions

6.1 Spin-Orbit Coupled Bose-Einstein Condensates

In the thesis, we have payed our attention to the Spin-Orbit (SO) Coupling Bose-Einstein Condensates (BECs), the different aspects of the system have been studied, especially

- **Spin-Orbit Coupled Bose-Einstein Condensates in Optical Lattices.** The energy dispersion, the numerical methods, the ground states [32] and vortex-antivortex pair lattices [33] of SO coupled BECs with repulsive interaction in optical lattices, and
- **Spin-Orbit Coupled Bose-Einstein Condensates in free space.** The ground states and dynamical properties of the SO coupled BECs with attractive interaction in free space [31] have been studied by analytical and numerical methods during my PhD course.

6.2 Spin-Orbit Coupled Bose-Einstein Condensates in Free Space

We predicted a new phenomenon that a stable soliton can be created in free space in two-dimensional SO coupled BECs with cubic self-attraction, which was impossible in general fiber or matter wave systems because of the occurrence of collapse. Furthermore, by numerical simulating and variational calculating, we shown that the solitons include two types, the Semi-Vortices in which the ground states will to be a vortex and soliton in different components and the Mixed Modes of two Semi-Vortices with different topological charges. These stable solitons can

be realized in a trap, and keep stable in free space if we remove the trap gradually. In addition, these solitons will possess the ground states of the SO coupled BECs system based on the ratio between the intra- and inter-series interactions. On the other hand, the Semi-Vortices and Mixed Modes in exited state will have drift instability, and they degenerate into unstable Townes solitons when their norms reach the critical values in free space. Meanwhile, moving stable solitons also can be realized in the present non-Galilean-invariant system in free space under a critical velocity, and collisions between two moving solitons will result their mixture and finally to be a single one.

6.3 Spin-Orbit Coupled Bose-Einstein Condensates in Optical Lattices

We researched the SO coupled BECs with repulsive interaction in optical lattices by numerical simulating the Gross-Pitaevskii equation and analytical expansion of Bloch functions, and showed some important results that is quite different with one in a trap as following. (1) The optical lattices will change the energy dispersion. For a two-dimensional SO coupled BECs in a trap, the ground states will form a ring in momentum space, and the radius will be the SO coupling strength. However, for a SO coupled BECs in optical lattices, there is a separation between the SO coupling strength and the momentum values in where the system fall into the ground states. (2) Higher harmonic terms are necessary for analytical calculations. By comparing the analytical results with limited harmonic terms in Bloch function with numerical one, we showed that the higher harmonic terms involved in the expansion function will affect dramatically the precision of analytical calculations. (3) Vortex-antivortex pair lattices appear in the plane wave phase of ground states. We found the interesting Vortex-antivortex pair lattices by watching the contour plots of the density and phase distribution, and the pairs will correspond to the optical lattices strictly.

References

[1] Dallin Durfee and Wolfgang Ketterle. Experimental studies of bose-einstein condensation. *Opt. Express*, 2(8):299–313, Apr 1998.

[2] Wikipedia. Bose-einstein condensate, 2015.

[3] Robert William Pattinson. *Two-Component Bose-Einstein Condensates: Equilibria and Dynamics at Zero Temperature and Beyond*. PhD thesis, School of Mathematics & Statistics, Newcastle University, Newcastle upon Tyne, United Kingdom, 2014.

[4] Roland Winkler. *Spin-Orbit Coupling Effects in Two-Dimensional Electron and Hole Systems*. Springer-Verlag, Berlin Heidelberg, 2003.

[5] Karina Jiménez-García. *Artificial Gauge Fields for Ultracold Neutral Atoms*. PhD thesis, Joint Quantum Institute, National Institute of Standards and Technology, and the University of Maryland, Gaithersburg, Maryland, 2012.

[6] Y-J Lin, Rob L Compton, K Jimenez-Garcia, James V Porto, and Ian B Spielman. Synthetic magnetic fields for ultracold neutral atoms. *Nature*, 462(7273):628–632, Dec 2009.

[7] Y-J Lin, K Jimenez-Garcia, and IB Spielman. Spin-orbit-coupled bose-einstein condensates. *Nature*, 471(7336):83–86, 2011.

[8] Subhasis Sinha, Rejish Nath, and Luis Santos. Trapped two-dimensional condensates with synthetic spin-orbit coupling. *Phys. Rev. Lett.*, 107:270401, Dec 2011.

[9] Ronald W. Clark. *Einstein: The Life and Times*. William Morrow, 1st edition, 2007.

[10] F. London. The λ-phenomenon of liquid helium and the bose-einstein degeneracy. *Nature*, 141:643, 1938.

[11] F. London. On the bose-einstein condensation. *Phys. Rev.*, 54:947–954, Dec 1938.

[12] M. H. Anderson, J. R. Ensher, M. R. Matthews, C. E. Wieman, and E. A. Cornell. Observation of bose-einstein condensation in a dilute atomic vapor. *Science*, 269(5221):198–201, 1995.

[13] K. B. Davis, M. O. Mewes, M. R. Andrews, N. J. van Druten, D. S. Durfee, D. M. Kurn, and W. Ketterle. Bose-einstein condensation in a gas of sodium atoms. *Phys. Rev. Lett.*, 75:3969–3973, Nov 1995.

[14] C. C. Bradley, C. A. Sackett, J. J. Tollett, and R. G. Hulet. Evidence of bose-einstein condensation in an atomic gas with attractive interactions. *Phys. Rev. Lett.*, 75:1687–1690, Aug 1995.

[15] C. C. Bradley, C. A. Sackett, and R. G. Hulet. Bose-einstein condensation of lithium: Observation of limited condensate number. *Phys. Rev. Lett.*, 78:985–989, Feb 1997.

[16] Steven Chu. Nobel lecture: The manipulation of neutral particles. *Rev. Mod. Phys.*, 70:685–706, Jul 1998.

[17] William D. Phillips. Nobel lecture: Laser cooling and trapping of neutral atoms. *Rev. Mod. Phys.*, 70:721–741, Jul 1998.

[18] Claude N. Cohen-Tannoudji. Nobel lecture: Manipulating atoms with photons. *Rev. Mod. Phys.*, 70:707–719, Jul 1998.

[19] E. A. Cornell and C. E. Wieman. Nobel lecture: Bose-einstein condensation in a dilute gas, the first 70 years and some recent experiments. *Rev. Mod. Phys.*, 74:875–893, Aug 2002.

[20] Wolfgang Ketterle. Nobel lecture: When atoms behave as waves: Bose-einstein condensation and the atom laser. *Rev. Mod. Phys.*, 74:1131–1151, Nov 2002.

[21] P. Kapitza. Viscosity of liquid helium below the l-point. *Nature*, 141:74, 1938.

[22] J. F. Allen and A. D. Misener. Flow of liquid helium ii. *Nature*, 141:75, 1938.

[23] L. D. Landau. The theory of superfluidity of helium ii. *J. Phys. (USSR)*, 5:71, 1941.

[24] C. Pethick and H. Smith. *Bose-Einstein condensation in dilute gases*. Cambridge University Press, 2002.

[25] A. Robert, O. Sirjean, A. Browaeys, J. Poupard, S. Nowak, D. Boiron, C. I. Westbrook, and A. Aspect. A bose-einstein condensate of metastable atoms. *Science*, 292(5516):461–464, 2001.

[26] Yosuke Takasu, Kenichi Maki, Kaduki Komori, Tetsushi Takano, Kazuhito Honda, Mitsutaka Kumakura, Tsutomu Yabuzaki, and Yoshiro Takahashi. Spin-singlet bose-einstein condensation of two-electron atoms. *Phys. Rev. Lett.*, 91:040404, Jul 2003.

[27] Tino Weber, Jens Herbig, Michael Mark, Hanns-Christoph Nägerl, and Rudolf Grimm. Bose-einstein condensation of cesium. *Science*, 299(5604):232–235, 2003.

[28] Axel Griesmaier, Jörg Werner, Sven Hensler, Jürgen Stuhler, and Tilman Pfau. Bose-einstein condensation of chromium. *Phys. Rev. Lett.*, 94:160401, Apr 2005.

[29] Simon Stellmer, Meng Khoon Tey, Bo Huang, Rudolf Grimm, and Florian Schreck. Bose-einstein condensation of strontium. *Phys. Rev. Lett.*, 103:200401, Nov 2009.

[30] Y. N. Martinez de Escobar, P. G. Mickelson, M. Yan, B. J. DeSalvo, S. B. Nagel, and T. C. Killian. Bose-einstein condensation of ^{84}Sr. *Phys. Rev. Lett.*, 103:200402, Nov 2009.

[31] Hidetsugu Sakaguchi, Ben Li, and Boris A. Malomed. Creation of two-dimensional composite solitons in spin-orbit-coupled self-attractive bose-einstein condensates in free space. *Phys. Rev. E*, 89:032920, Mar 2014.

[32] Hidetsugu Sakaguchi and Ben Li. Vortex lattice solutions to the gross-pitaevskii equation with spin-orbit coupling in optical lattices. *Phys. Rev. A*, 87:015602, Jan 2013.

[33] Ben Li and Hidetsugu Sakaguchi. Vortex-antivortex-pair lattices in spin-orbit coupled bose-einstein condensates. *Journal of Low Temperature Physics*, 175(1-2):243–249, 2014.

[34] Yuki Kawaguchi and Masahito Ueda. Spinor bose-einstein condensates. *Physics Reports*, 520(5):253 – 381, 2012. Spinor Bose-Einstein condensates.

[35] R. Kanamoto, L. D. Carr, and M. Ueda. Metastable quantum phase transitions in a periodic one-dimensional bose gas: Mean-field and bogoliubov analyses. *Phys. Rev. A*, 79:063616, Jun 2009.

[36] S. Burger, K. Bongs, S. Dettmer, W. Ertmer, K. Sengstock, A. Sanpera, G. V. Shlyapnikov, and M. Lewenstein. Dark solitons in bose-einstein condensates. *Phys. Rev. Lett.*, 83:5198–5201, Dec 1999.

[37] J. Denschlag, J. E. Simsarian, D. L. Feder, Charles W. Clark, L. A. Collins, J. Cubizolles, L. Deng, E. W. Hagley, K. Helmerson, W. P. Reinhardt, S. L. Rolston, B. I. Schneider, and W. D. Phillips. Generating solitons by phase engineering of a bose-einstein condensate. *Science*, 287(5450):97–101, 2000.

[38] Zachary Dutton, Michael Budde, Christopher Slowe, and Lene Vestergaard Hau. Observation of quantum shock waves created with ultra- compressed slow light pulses in a bose-einstein condensate. *Science*, 293(5530):663–668, 2001.

[39] B. P. Anderson, P. C. Haljan, C. A. Regal, D. L. Feder, L. A. Collins, C. W. Clark, and E. A. Cornell. Watching dark solitons decay into vortex rings in a bose-einstein condensate. *Phys. Rev. Lett.*, 86:2926–2929, Apr 2001.

[40] P. Engels and C. Atherton. Stationary and nonstationary fluid flow of a bose-einstein condensate through a penetrable barrier. *Phys. Rev. Lett.*, 99:160405, Oct 2007.

[41] C. Josserand and Y. Pomeau. Generation of vortices in a model of superfluid 4 he by the kadomtsev-petviashvili instability. *EPL (Europhysics Letters)*, 30(1):43, 1995.

[42] Joachim Brand and William P. Reinhardt. Solitonic vortices and the fundamental modes of the "snake instability": Possibility of observation in the gaseous bose-einstein condensate. *Phys. Rev. A*, 65:043612, Apr 2002.

[43] Gordon Baym and C. J. Pethick. Ground-state properties of magnetically trapped bose-condensed rubidium gas. *Phys. Rev. Lett.*, 76:6–9, Jan 1996.

[44] R. A. Williams, L. J. LeBlanc, K. Jiménez-García, M. C. Beeler, A. R. Perry, W. D. Phillips, and I. B. Spielman. Synthetic partial waves in ultracold atomic collisions. *Science*, 335(6066):314–317, 2012.

[45] M. C. Beeler, R. A. Williams, K. Jimenez-Garcia, L. J. LeBlanc, A. R. Perry, and I. B. Spielman. The spin hall effect in a quantum gas. *Nature*, 498(7453):201–204, 06 2013.

[46] Lindsay J LeBlanc, Matthew C Beeler, Karina Jiménez-García, Abigail R Perry, Seiji Sugawa, Ross A Williams, and Ian B Spielman. Direct observation of zitterbewegung in a bose-einstein condensate. *New J. Phys.*, 15:073011, jul 2013.

[47] Jin-Yi Zhang, Si-Cong Ji, Zhu Chen, Long Zhang, Zhi-Dong Du, Bo Yan, Ge-Sheng Pan, Bo Zhao, You-Jin Deng, Hui Zhai, Shuai Chen, and Jian-Wei Pan. Collective dipole oscillations of a spin-orbit coupled bose-einstein condensate. *Phys. Rev. Lett.*, 109:115301, Sep 2012.

[48] Si-Cong Ji, Jin-Yi Zhang, Long Zhang, Zhi-Dong Du, Wei Zheng, You-Jin Deng, Hui Zhai, Shuai Chen, and Jian-Wei Pan. Experimental determination of the finite-temperature phase diagram of a spin-orbit coupled bose gas. *Nat Phys*, 10(4):314–320, 04 2014.

[49] S.-C. Ji, L. Zhang, X.-T. Xu, Z. Wu, Y. Deng, S. Chen, and J.-W. Pan. Softening of Roton and Phonon Modes in a Bose-Einstein Condensate with Spin-Orbit Coupling. *ArXiv e-prints*, August 2014.

[50] Pengjun Wang, Zeng-Qiang Yu, Zhengkun Fu, Jiao Miao, Lianghui Huang, Shijie Chai, Hui Zhai, and Jing Zhang. Spin-orbit coupled degenerate fermi gases. *Phys. Rev. Lett.*, 109:095301, Aug 2012.

[51] Zhengkun Fu, Lianghui Huang, Zengming Meng, Pengjun Wang, Long Zhang, Shizhong Zhang, Hui Zhai, Peng Zhang, and Jing Zhang. Production of feshbach molecules induced by spin-orbit coupling in fermi gases. *Nat Phys*, 10(2):110–115, 02 2014.

[52] Lawrence Cheuk, Ariel Sommer, Zoran Hadzibabic, Tarik Yefsah, Waseem Bakr, and Martin Zwierlein. Spin-injection spectroscopy of a spin-orbit coupled fermi gas. *Phys. Rev. Lett.*, 109:095302, Aug 2012.

[53] Abraham J. Olson, Su-Ju Wang, Robert J. Niffenegger, Chuan-Hsun Li, Chris H. Greene, and Yong P. Chen. Tunable landau-zener transitions in a spin-orbit-coupled bose-einstein condensate. *Phys. Rev. A*, 90:013616, Jul 2014.

[54] C Hamner, Yongping Zhang, MA Khamehchi, Matthew J Davis, and P Engels. Spin-orbit coupled bose-einstein condensates in a one-dimensional optical lattice. *arXiv:1405.4048*, 2014.

[55] M. A. Khamehchi, Y. Zhang, C. Hamner, T. Busch, and P. Engels. Long-range interactions and roton minimum softening in a spin-orbit coupled Bose-Einstein condensate. *ArXiv e-prints*, September 2014.

[56] S. Zhang, W. S. Cole, A. Paramekanti, and N. Trivedi. Spin-orbit Coupling in Optical lattices. *ArXiv e-prints*, November 2014.

[57] Hui Zhai. Spin-orbit coupled quantum gases. *International Journal of Modern Physics B*, 26(01), 2012.

[58] Chunji Wang, Chao Gao, Chao-Ming Jian, and Hui Zhai. Spin-orbit coupled spinor bose-einstein condensates. *Phys. Rev. Lett.*, 105:160403, Oct 2010.

[59] Wu Cong-Jun, Ian Mondragon-Shem, and Zhou Xiang-Fa. Unconventional bose-einstein condensations from spin-orbit coupling. *Chinese Physics Letters*, 28(9):097102, 2011.

[60] B. Ramachandhran, Bogdan Opanchuk, Xia-Ji Liu, Han Pu, Peter D. Drummond, and Hui Hu. Half-quantum vortex state in a spin-orbit-coupled bose-einstein condensate. *Phys. Rev. A*, 85:023606, Feb 2012.

[61] Yongping Zhang, Li Mao, and Chuanwei Zhang. Mean-field dynamics of spin-orbit coupled bose-einstein condensates. *Phys. Rev. Lett.*, 108:035302, Jan 2012.

[62] Xiangfa Zhou, Yi Li, Zi Cai, and Congjun Wu. Unconventional states of bosons with the synthetic spin-orbit coupling. *Journal of Physics B: Atomic, Molecular and Optical Physics*, 46(13):134001, 2013.

[63] J. Radić, A. Di Ciolo, K. Sun, and V. Galitski. Exotic quantum spin models in spin-orbit-coupled mott insulators. *Phys. Rev. Lett.*, 109:085303, Aug 2012.

[64] William S. Cole, Shizhong Zhang, Arun Paramekanti, and Nandini Trivedi. Bose-hubbard models with synthetic spin-orbit coupling: Mott insulators, spin textures, and superfluidity. *Phys. Rev. Lett.*, 109:085302, Aug 2012.

[65] J. D. Jackson. *Classical Electrodynamics*. Wiley, USA, third edition, 1998.

[66] Y.-J. Lin, R. Compton, A. Perry, W. Phillips, J. Porto, and I. Spielman. Bose-einstein condensate in a uniform light-induced vector potential. *Phys. Rev. Lett.*, 102:130401, Mar 2009.

[67] Y-J. Lin, R. L. Compton, K. Jimenez-Garcia, W. D. Phillips, J. V. Porto, and I. B. Spielman. A synthetic electric force acting on neutral atoms. *Nat Phys*, 7(7):531–534, 07 2011.

[68] Philipp Hauke, Fernando M Cucchietti, Luca Tagliacozzo, Ivan Deutsch, and Maciej Lewenstein. Can one trust quantum simulators? *Reports on Progress in Physics*, 75(8):082401, 2012.

[69] G. Dresselhaus. Spin-orbit coupling effects in zinc blende structures. *Phys. Rev.*, 100:580–586, Oct 1955.

[70] Yu A Bychkov and E I Rashba. Oscillatory effects and the magnetic susceptibility of carriers in inversion layers. *Journal of Physics C: Solid State Physics*, 17(33):6039, 1984.

[71] G. J. Conduit. Line of dirac monopoles embedded in a bose-einstein condensate. *Phys. Rev. A*, 86:021605, Aug 2012.

[72] D. A. Zezyulin, R. Driben, V. V Konotop, and B. A. Malomed. Nonlinear modes in binary bosonic condensates with pseudo-spin-orbital coupling. *Phys. Rev. A*, 88:013607, Jul 2013.

[73] Yun Li, Lev P. Pitaevskii, and Sandro Stringari. Quantum tricriticality and phase transitions in spin-orbit coupled bose-einstein condensates. *Phys. Rev. Lett.*, 108:225301, May 2012.

[74] V. Achilleos, D. J. Frantzeskakis, P. G. Kevrekidis, and D. E. Pelinovsky. Matter-wave bright solitons in spin-orbit coupled bose-einstein condensates. *Phys. Rev. Lett.*, 110:264101, Jun 2013.

[75] Wei Han, Suying Zhang, and Wu-Ming Liu. Spin-orbit coupled bose-einstein condensates in spin-dependent optical lattices. *arXiv preprint arXiv:1211.2097v3*, 2013.

[76] Yaroslav V. Kartashov, Vladimir V. Konotop, and Fatkhulla Kh. Abdullaev. Gap solitons in a spin-orbit-coupled bose-einstein condensate. *Phys. Rev. Lett.*, 111:060402, Aug 2013.

[77] S. Skupin, O. Bang, D. Edmundson, and W. Krolikowski. Stability of two-dimensional spatial solitons in nonlocal nonlinear media. *Phys. Rev. E*, 73:066603, Jun 2006.

[78] Ziad H. Musslimani, Mordechai Segev, Demetrios N. Christodoulides, and Marin Soljačić. Composite multihump vector solitons carrying topological charge. *Phys. Rev. Lett.*, 84:1164–1167, Feb 2000.

[79] Ziad H. Musslimani, Marin Soljačić, Mordechai Segev, and Demetrios N. Christodoulides. Interactions between two-dimensional composite vector solitons carrying topological charges. *Phys. Rev. E*, 63:066608, May 2001.

[80] M. L. Chiofalo, S. Succi, and M. P. Tosi. Ground state of trapped interacting bose-einstein condensates by an explicit imaginary-time algorithm. *Phys. Rev. E*, 62:7438–7444, Nov 2000.

[81] D. L. Feder, M. S. Pindzola, L. A. Collins, B. I. Schneider, and C. W. Clark. Dark-soliton states of bose-einstein condensates in anisotropic traps. *Phys. Rev. A*, 62:053606, Oct 2000.

[82] N.G. Vakhitov and A.A. Kolokolov. Stationary solutions of the wave equation in a medium with nonlinearity saturation. *Radiophysics and Quantum Electronics*, 16(7):783–789, 1973.

[83] Luc Bergé. Wave collapse in physics: principles and applications to light and plasma waves. *Physics Reports*, 303(5–6):259 – 370, 1998.

[84] E.A. Kuznetsov and F. Dias. Bifurcations of solitons and their stability. *Physics Reports*, 507(2–3):43 – 105, 2011.

[85] Luc Bergé. Wave collapse in physics: principles and applications to light and plasma waves. *Physics Reports*, 303(5–6):259 – 370, 1998.

[86] E.A. Kuznetsov and F. Dias. Bifurcations of solitons and their stability. *Physics Reports*, 507(2–3):43 – 105, 2011.

[87] Hui Hu, B. Ramachandhran, Han Pu, and Xia-Ji Liu. Spin-orbit coupled weakly interacting bose-einstein condensates in harmonic traps. *Phys. Rev. Lett.*, 108:010402, Jan 2012.

[88] T Kanna, M Vijayajayanthi, and M Lakshmanan. Coherently coupled bright optical solitons and their collisions. *Journal of Physics A: Mathematical and Theoretical*, 43(43):434018, 2010.

[89] Antonio Mecozzi, Cristian Antonelli, and Mark Shtaif. Nonlinear propagation in multi-mode fibers in the strong coupling regime. *Opt. Express*, 20(11):11673–11678, May 2012.

[90] Cheng Chin, Rudolf Grimm, Paul Julienne, and Eite Tiesinga. Feshbach resonances in ultracold gases. *Rev. Mod. Phys.*, 82:1225–1286, Apr 2010.

[91] R. Ballagh, K. Burnett, and T. Scott. Theory of an output coupler for bose-einstein condensed atoms. *Phys. Rev. Lett.*, 78:1607–1611, Mar 1997.

[92] J. Williams, R. Walser, J. Cooper, E. Cornell, and M. Holland. Nonlinear josephson-type oscillations of a driven, two-component bose-einstein condensate. *Phys. Rev. A*, 59:R31–R34, Jan 1999.

[93] Sadhan Adhikari and Boris Malomed. Two-component gap solitons with linear interconversion. *Phys. Rev. A*, 79:015602, Jan 2009.

[94] Hiroki Saito, Randall G. Hulet, and Masahito Ueda. Stabilization of a bose-einstein droplet by hyperfine rabi oscillations. *Phys. Rev. A*, 76:053619, Nov 2007.

[95] H Susanto, PG Kevrekidis, BA Malomed, and F Kh Abdullaev. Effects of time-periodic linear coupling on two-component bose-einstein condensates in two dimensions. *Physics Letters A*, 372(10):1631–1638, 2008.

[96] Y. K. Kato, R. C. Myers, A. C. Gossard, and D. D. Awschalom. Observation of the spin hall effect in semiconductors. *Science*, 306(5703):1910–1913, 2004.

[97] David Hsieh, Dong Qian, Lewis Wray, YuQi Xia, Yew San Hor, RJ Cava, and M Zahid Hasan. A topological dirac insulator in a quantum spin hall phase. *Nature*, 452(7190):970–974, 2008.

[98] Hidetsugu Sakaguchi and Hironobu Takeshita. Symmetry breaking of vortex patterns in a rotating harmonic potential. *Journal of the Physical Society of Japan*, 77(5):054003, 2008.

[99] J. Radić, A. Di Ciolo, K. Sun, and V. Galitski. Exotic quantum spin models in spin-orbit-coupled mott insulators. *Phys. Rev. Lett.*, 109:085303, Aug 2012.

[100] William Cole, Shizhong Zhang, Arun Paramekanti, and Nandini Trivedi. Bose-hubbard models with synthetic spin-orbit coupling: Mott insulators, spin textures, and superfluidity. *Phys. Rev. Lett.*, 109:085302, Aug 2012.